THE UNIVERSITY
of EDINBURGH

Impairing hepatocyte regeneration to determine the regenerative capacity of the biliary epithelium

Alexander Philip Raven

Doctor of Philosophy

University of Edinburgh

2017

Declaration

I declare that this thesis was composed by myself, that the work contained herein is my own except where explicitly stated otherwise in the text.

The data included in this text has not been submitted for any other degree or professional qualification, and does not exceed the word limit of 100,000 words set by the College of Medicine and Veterinary Medicine.

Parts of this work have been published as a collaborative project in the journal Nature, Raven et al, 2017.

Alexander Raven

Abstract

Liver injury stimulates hepatocyte proliferation, regenerating the liver through self-replication. In cases where there is severe, repetitive, parenchymal damage, as seen in human chronic liver disease, hepatocyte mediated regeneration becomes impaired. In this setting it is currently unclear whether endogenous biliary epithelial cells can repopulate the hepatocyte compartment. This thesis therefore aimed to address this point by lineage tracing the main two liver epithelia populations on a background of impaired hepatocyte regeneration.

To impair regeneration, an *Itgb1* transgene was specifically deleted, conditionally, from the hepatocyte epithelium. Long-term loss of β1-Integrin alone or with additional injury caused an epithelial ductular reaction of biliary origin. Alongside β1-Integrin ablation, the hepatocyte epithelium was also labelled with a heritable *ROSA26*^{LSL}*tdTomato* reporter. Impaired hepatocyte regeneration mediated by β1-integrin ablation resulted in 25% of hepatocytes becoming tdTomato negative (non-hepatocyte derived). To verify that the non-hepatocyte mediated regeneration was originating from the biliary epithelium, anti-*Itgb1* RNAi was administrated to *K19*$^{CreERT\ LSL}$*tdTomato* mice. Resulting in tdTomato positive hepatocytes that had differentiated from the labelled tdTomato positive biliary epithelial cells.

In summary, this thesis demonstrates that hepatocyte β1-Integrin ablation combined with toxic damage causes marked ductular reactions and results in a substantial regeneration of functional hepatocytes from the biliary epithelium.

Lay abstract

The liver is capable of repair after injury, normally this occurs through self-duplication of the resident liver cells. These liver cells are comprised from either the major functional cells of the liver, the hepatocytes, or the cells that form the liver bile ducts, the cholangiocytes. During human chronic liver disease, the hepatocytes lose the ability to divide to replace lost cells. When this occurs, it is unknown if the cholangiocytes in the bile ducts can become hepatocytes, acting as an alternative cell source for liver repair.

In this thesis, I describe experiments performed in the mouse which confirm that cholangiocytes can become hepatocytes. I show this using genetic tools that allowed me to specifically label the distinct cell populations in the liver and track their fate after injury. Using this method, I found that cholangiocytes can significantly contribute to the formation of new hepatocytes when the original hepatocytes fail to replace themselves.

This finding builds upon previous work that showed cholangiocytes have a therapeutic potential in chronic liver disease. By understanding the environment needed for cholangiocytes to become hepatocytes we can now develop therapies that could enhance cholangiocyte derived repair of the liver.

Acknowledgements

Firstly, I would like to thank my supervisor Stuart Forbes, I am deeply grateful for his guidance and support during this PhD project. I feel extremely privileged to have had the opportunity to work with Stuart; he has given me the freedom to explore exciting ideas and provided me with the tools to perform important and novel experiments. Essentially, he is responsible for the decent parts of this half-decent scientist and PhD candidate. I would also like to thank Luke Boulter, his support and advice have been invaluable, I learnt a lot from our chats together.

A large thankyou to every member of the Forbes lab, both past and present. Individually, I extend a special thank you to Davina Wojtacha, who nursed me through my first year and taught me many useful skills. I would like to thank the harassed post docs; Wei Yu Lu, Ben Dwyer, Philip Starkey Lewis, Eoghan O'Duibhir and Baukje Schotanus, who have all patiently answered my many questions over the years and listened to my crazy ideas. Especially Wei, thank you for your unlimited patience and advice throughout this project. Thank you, Janet Man for always coming to my aid and teaching me how to cut a respectable tissue section. I would also like to thank Sofia Ferreira-Gonzalez for her friendship and advice throughout our PhDs.

Personally, I would like to thank my parents who have supported and encouraged me throughout every stage of my education, you have been incredible. Finally, I would like to thank Zaniah Gonzalez, the last few years would have been a lot harder without you and your encouragement.

Contents

Declaration i

Abstract ii

Lay abstract iii

Acknowledgements iv

Contents v

Abbreviations ix

Chapter 1: Introduction 1

- Liver anatomy and physiology 2
- Liver disease 4
  - Epidemiology and aetiology 4
  - Hepatocytes in diseased livers have a defective regenerative capacity 5
  - The ductular reaction 6
  - Organ failure and potential treatments 8
- Liver regeneration 11
  - Adult regeneration 11
  - Hepatocyte mediated regeneration 12
  - A liver stem cell and Hepatic progenitor cell theory, contradictions and uncertainty 14
- Animal models of liver disease and hepatic progenitor mediated regeneration 16
  - Rat models 16
  - Mouse models 17
  - Zebrafish models 17
- Cell fate and differentiation in the liver 18
  - Development 18
  - In vitro studies 20
  - In vivo studies 21
- β1-Integrin and liver regeneration 23
  - Extracellular matrix and cell adhesion 23
  - β1-Integrin: an important promiscuous protein 24

- ECM and Integrin expression in the liver 24
- Role of hepatocyte β1-Integrin 25
- Loss of β1-Integrin from hepatocytes: lessons from cancer and an acute liver injury model 26

- Summary 27
- Hypothesis and aims 27

Chapter 2: Materials and Methods 28

- Liver injury models 29
  - 3,5-Diethoxycarbonyl-1,4-dihydrocollidine (DDC) diet 29
  - Methionine and choline deficient (MCD) diet 29
  - Thioacetamide (TAA) 29
  - Choline deficient ethionine supplemented (CDE) diet 30
- Transgenic mouse models 30
  - Adeno Associated Virus 8 (AAV8) Cre induction 30
  - *Itgβ1*$^{fl/fl}$ and *R26R*^{LSL}*tdTomato* mice 31
  - Tamoxifen induction 31
  - *K19*$^{CreERT\ LSL}$*tdTomato* mice 32
  - Tissue harvest 33
- siRNA nanoparticles 33
- Histology 33
  - Immuno-histochemistry 33
  - Immuno-fluorescence 34
  - Histochemistry 34
- Histological analysis 36
  - Microscopy 36
  - Fluorescent cell quantification and analysis 36
- Quantative PCR analysis 40
- Protein homogenates and western blots 40
- Serum analysis 41
- Isolation of biliary ducts and hepatocytes, and FACS 41
- RNA sequencing analysis 41
- Statistical analysis 43

Chapter 3: AAV8.TBG.Cre labels the hepatocyte epithelium and deletes β1-Integrin, inducing liver injury and ductular reaction 44

- Introduction 45
- Results 46
  - AAV8.TBG.Cre labelled 99.5% of the hepatocytes in the liver 46
  - AAV8.TBG.Cre ablated β1-Integrin from hepatocytes 48
  - Hepatocyte β1-Integrin ablation caused liver injury 51
  - Aberrant bile canaliculi structure in β1-Integrin ablated livers 51
  - β1-Integrin ablated livers had prominent ductular reactions 57
  - Hepatocyte β1-Integrin ablation reduced tdTom labelling in hepatocytes, leading to periportal patches of $tdTom^{neg}$ hepatocytes 59
- Discussion 61

Chapter 4: Liver injury diets combined with hepatocyte β1-Integrin deletion results in a delayed regenerative response from a non-hepatocyte origin 64

- Introduction 65
- Results 66
  - Hepatocyte β1-Integrin loss delayed recovery after DDC induced liver injury 66
  - Ki67 and p21 expression was altered after DDC injury in livers with hepatocyte β1-Integrin ablation 71
  - Hepatocyte β1-Integrin ablation and DDC injury resulted in a highly necrotic event early in recovery 73
  - DDC induced ductular reaction 76
  - β1-integrin ablation and DDC injury resulted in liver fibrosis 78
  - DDC injury and subsequent regeneration reduced hepatocyte labelling in the $\beta1\text{-}Integrin^{fl/fl}$ liver 81
  - DR and loss of labelled hepatocytes also occurred with other liver injury models 85
  - tdTomato negative hepatocytes were adjacent to the DR 87
  - At Day 14 of recovery tdTomato positive hepatocytes were mainly distributed around the central vein 89
  - tdTomato negative hepatocytes were more proliferative and had smaller nuclei when compared to neighbouring tdTomato positive hepatocytes 91
  - Whole liver RNA sequencing at day 7 of recovery 94

- Wnt expression increased early in recovering β1-Integrin$^{fl/fl}$ livers 100
- Discussion 102

Chapter 5: Biliary ductular cells regenerate the liver when hepatocyte regeneration is impaired by β1-Integrin loss 106

- Introduction 107
- Results 109
  - Validation of the nanoparticle formulated RNAi and the inducible *K19*^{CreERT} ^{LSL}*tdTomato* transgene 109
  - Conventional murine liver injury models do not induce biliary derived regeneration 111
  - *Itgb1* knock down in hepatocytes provokes biliary derived regeneration of the hepatocyte epithelium 113
  - Transcriptome comparison of hepatocyte derived hepatocytes and ductal derived hepatocytes 115
- Discussion 122

Chapter 6: Conclusions and future perspectives 124

References 133

Abbreviations

AAF	2-acetylaminofluorene
AAV8	Adeno-associated virus 8
AAV8.TBG.Cre	AAV8. Thyroid binding globulin. Cre
AhCre	Rat Cyp1A1 promoter Cre
AKT	Protein kinase B
ALP	Alkaline phosphatase
ALT	Alanine transaminase
ANOVA	Analysis of variance
APC	Adenomatous polyposis coli
AST	Aspartate transaminase
AWERB	Animal welfare and ethical review body
BDhepatocytes	Biliary derived hepatocytes
BEC	Biliary epithelial cell
BIRC5	Baculoviral inhibitor of apoptosis repeat-containing 5
BM	Basement membrane
BMP	Bone morphogenetic protein
BrdU	Bromodeoxyuridine
C/EBP	CCAAT-enhancer-binding proteins
CCL4	Carbon tetrachloride
CCO	Cytochrome C oxidase
CD	Cluster of differentiation
CDE	Choline deficient ethionine supplemented
cDNA	complementary DNA
CK19	Cytokeratin 19
cMET	MET Proto-Oncogene, Receptor Tyrosine Kinase

CNS	Central nervous system
Cre	Cre recombinase
Cre^{ERT}	Cre estrogen receptor
CV	Central vein
CYP2D	Cytochrome P450 2D6
DAAM	Dishevelled associated activator of morphogenesis
DAB	Diaminobenzidine
DAMP	Damage associated molecular pattern
DDC	3,5-Diethoxycarbonyl-1,4-dihydrocollidine
DMSO	Dimethyl sulfoxide
DNA	Deoxyribonucleic acid
DNMT1	DNA (cytosine-5)-methyltransferase 1
DR	Ductular reaction
ECM	Extracellular matrix
EDTA	Ethylenediaminetetraacetic acid
EdU	5-Ethynyl-2´-deoxyuridine
EGF	Epidermal growth factor
EGRR	EGF receptor
EGTA	Egtazic acid
EpCAM	Epithelial cell adhesion molecule
ERK	Extracellular signal-regulated kinase
ESC	Embryonic stem cell
FABP10A	Fatty acid binding protein 10a
FACS	Fluorescence activated cell sorting
FAH	Fumarylacetoacetate hydrolase
FGF	Fibroblast growth factor

FOXA	Forkhead box A
FOXL1	Forkhead box L-1
FZD	Frizzled receptor
GATA	GATA binding factor
GC	Genome copies
GRHL2	Grainyhead like transcription factor 2
GS	Glutamine synthetase
H&E	Haematoxylin and eosin
HAV	Hepatitis A virus
HBV	Hepatitis B virus
HCC	Hepatocellular carcinoma
HCV	Hepatitis C virus
HDV	Hepatitis D virus
HEV	Hepatitis E virus
HGF	Hepatocyte growth factor
HH	Hedgehog
HMGB1	High mobility group box 1 protein
HNF	Hepatocyte nuclear factor
HPC	Hepatic progenitor cell
HRP	Horseradish peroxidase
HSC	Hepatic stellate cell
IFABP	Intestinal fatty acid binding protein
IL	Interleukin
ILK	Integrin linked kinase
IP	Intraperitoneal
iPSC	Induced pluripotent stem cell

ITG	Integrin
JAK	Janus kinase
K19	Keratin 19
KGF	Keratinocyte growth factor
KO	Knock out
LFT	Liver function test
LGR	Leucine-rich repeat-containing G-protein coupled receptor
LN	Laminin
LPS	Lipopolysaccharide
MAP	Mitogen activated protein
MCD	Methionine and choline deficient
MDM2	Mouse double minute 2 homolog
MDR1	Multi-drug resistance protein 1
MFSD2A	Major facilitator super family domain containing 2a
MIR	Micro RNA
MSigDB	Molecular signature database
NASH	Non-alcoholic steatohepatitis
NCAM	Neural cell adhesion molecule
NEG	Negative
NKD	Naked Cuticle Homolog
NTB	2-(2-nitro-4-trifluoro-methylbenzyol)-1,3-cyclohexanedione
NTR	Nitroreductase
OPN	Osteopontin
OSM	Oncostatin M
PAMP	Pathogen associated molecular pattern
PAR1b	Partitioning-defective 1b

PBS	Phosphate buffered saline
PCA	Principle component analysis
PCNA	Proliferating cell nuclear antigen
PCP	Planar cell polarity
PH	Partial hepatectomy
POS	Positive
PPIA	Peptidylprolyl isomerase A
PROX1	Prospero homeobox 1
PSR	Picrosirius red
PT	Portal tract
qPCR	Quantitative polymerase chain reaction
RFP	Red fluorescent protein
RHOU	Ras homolog family member U
RIN	RNA integrity number
RM1	Rat & mouse No1 maintenance diet
RNA	Ribonucleic acid
RNA-Seq	RNA-Sequencing
ROS	Reactive oxygen species
SASP	Senescence associated secretory phenotype
SCA	Stem cells antigen
SDS	Sodium dodecyl sulfate
SFRP	Secreted frizzled related protein
siRNA	Small interfering RNA
SOX9	Sex determining region Y-box 9
STAT	Signal transducer and activator of transcription
STM	Septum transversum mesenchyme

TAA	Thioacetamide
TBX3	T-Box transcription factor TBX3
tdTom	tdTomato
TGF	Transforming growth factor
TNF	Tumour necrosis factor
TWEAK	TNF-like weak inducer of apoptosis
UV	Ultraviolet
VEGFR	Vascular endothelial growth factor receptor
WIF	WNT inhibitory factor
WT	Wildtype
YAP	Yes associated protein
αSMA	α-Smooth muscle actin

Chapter 1

Introduction

Liver Anatomy and Physiology

The liver is a vital organ, performing multiple functions in the body including: glucose and lipid metabolism, hormone secretion, bile synthesis, and detoxification of ammonia or xenobiotic agents. To execute these various functions, the cells of the liver are organised around a unique vasculature structure that has a dense fenestrated capillary network supplied with blood from both the portal vein and hepatic artery. These afferent vessels branch to smaller vessels forming portal tracts (PT) throughout the liver. Blood drains out of the liver through efferent central veins (CV) that tribute the hepatic vein. On a microstructural scale, blood flows along a portal tract to central vein axis, through the fenestrated capillaries, termed sinusoids (Figure 1.1a,b). Adjacent to the sinusoids are the major epithelial cells of the liver, the hepatocytes[1]. Polarised hepatocytes form an epithelial sheet between the sinusoids, with the basal surface of the cells exposed to blood flow via the fenestrated sinusoids[2] (Figure 1.1c). Exposure to the circulating blood allows hepatocytes to carry out the aforementioned functions such as secreting serum proteins, hormones and metabolising molecules absorbed from the intestine[3]. The apical surface of the hepatocyte forms a network of bile canaliculi with adjacent hepatocytes. Hepatocytes use transporter proteins to secrete bile salts, drug metabolites and other waste in to the bile canaliculi, which drain in to the bile ducts at the portal tract. The bile ducts are formed from columnar, biliary epithelial cells (BEC), which share a common developmental progenitor with hepatocytes, the hepatoblast[4,5]. The intrahepatic bile ducts connect with the wider biliary system via the common hepatic duct, which supplies bile to the duodenum.

Hepatocytes distributed along the PT to CV axis are heterogeneous and form 3 zones along the axis, according to their function (Figure 1.1c). Changes in liver zonation correspond with changes in the blood oxygen concentration[6] and, importantly, the WNT signalling gradient. Disruption of the WNT pathway by targeting either downstream canonical effectors or administering WNT inhibitors results in loss of liver zonation[7–10]. Arranged around the oxygen rich, WNT low PT, in an acinar formation, are the zone 1 hepatocytes. Zone 1 hepatocytes perform gluconeogenesis, are involved in the early steps of ammonia detoxification that include urea synthesis and have a higher concentration of glutathione, making the cells more resistant to

reactive oxygen species[1]. In contrast, the zone 3 hepatocytes situated in an acinar around the WNT high, oxygen low CV can express high levels of cytochrome P450 giving them a high drug detoxification capacity. Zone 3 hepatocytes also express the WNT target gene glutamine synthetase, which synthesises glutamine from ammonia. Zone 2 hepatocytes are difficult to define, zone 2 often represents the transitional region between the more distinct zone 1 periportal hepatocytes and the perivenular zone 3 hepatocytes, although single cell ribonucleic acid (RNA) sequencing (RNA-Seq) is beginning to reveal unique properties of the zone 2 hepatocytes[11]. All hepatocytes express albumin and can also synthesise serum proteins such as transthyretin and the transferrin transporters[12].

Figure 1.1 – Liver anatomy

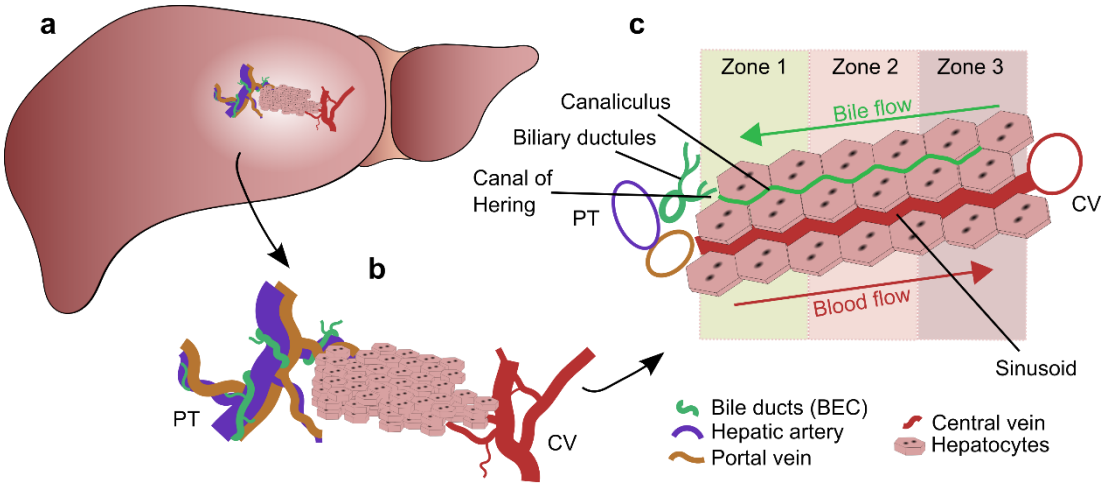

Figure 1.1: Basic illustration of liver structure. **a.** Liver macroanatomy **b**. Liver microanatomy, the liver has multiple lobes, permeated by two vascular networks; the hepatic artery and portal vein accompanied with the bile ducts form a branching network labelled the portal tract (PT); the central vein (CV) forms an opposing vascular network. Situated between the two vascular networks is the hepatocyte epithelium. **c**. Blood flows from the PT to the CV along the liver sinusoids. Bile flows in an opposite direction through the canaliculi to the bile ducts at the PT. There are 3 zones of hepatocytes, Zone 1 begins at the PT progressing to zone 2 and zone 3, around the CV.

Remarkably, the liver can regenerate after acute injury or resection resulting in an organised and regulated expansion of the remaining tissue. This is achieved through cell division to compensate for lost tissue and return to normal liver function. However, severe and repetitive, chronic, injury to the liver causes liver disease, leading to gross alterations in liver architecture and function, eventually more systemic complications develop such as acites, bleeding varices, jaundice and hepatic encephalopathy. Liver disease eventually causes liver cirrhosis, which is fatal and can cause organ failure or develop into hepatocellular carcinoma, for which the only treatment at this stage in the disease is organ transplant.

Liver Disease

Epidemiology and aetiology

Liver disease is a growing burden to healthcare providers worldwide[13,14]. Increased incidence and the prevalence of liver disease are linked to areas with endemic: viral hepatitis infections, excessive alcohol consumption and obesity[15–20].

Hepatitis B virus (HBV) and hepatitis C virus (HCV) infections are the primary cause of chronic liver disease in Asia and Africa, with a lower prevalence in economically developed, western countries. Liver disease arises from HBV and HCV interactions with the host immune system, which over time, results in chronic inflammation and fibrosis[19,20]. HCV combined with human immunodeficiency virus further increase the risk of developing liver disease[21]. Other viral hepatitis infections involve the enterically transmitted HAV and HEV viruses and the unusual, defective RNA virus HDV, which can only infect humans in the presence of HBV or the HBV surface antigen, HBsAg[22]. HAV and HEV infection causes acute liver injury that rarely progresses to chronic disease[23].

Chronic alcohol abuse and subsequent liver disease is a growing problem for economically developed nations in Europe, the United States of America and parts of Asia[17]. The pathological mechanism of alcohol related liver disease can be linked to ethanol metabolism, which contributes to disease through disruption to fatty acid oxidation, promoting steatosis[24]. The loss of gut epithelial integrity caused by excess

alcohol can also induce liver disease as it enables the translocation of lipopolysaccharides (LPS) to the liver, where it stimulates inflammation and excessive TNFα activation, leading to hepatitis[16].

Non-alcoholic fatty liver disease is prevalent in obese people and is more likely in diabetic patients with insulin resistance and individuals that have metabolic syndrome[25]. Accumulation of lipids in hepatocytes cause organelle and cytoskeletal damage, which results in cell ballooning and necrosis, triggering inflammation, fibrosis and eventual cirrhosis[26].

Other causes of liver diseases include autoimmune disorders[27], and iron overload disorders, caused by a genetic defect or a secondary consequence of another pathology[28]. The cholangiopathies are diseases that predominantly affect the BECs in the bile ducts. They include the idiopathic primary biliary cirrhosis, the autoimmune or infection induced sclerosing cholangitis, biliary cysts and the biliary cancer, cholangiocarcinoma[29–31].

Whether liver disease is caused by infection, toxic insult or autoimmunity, the different factors and disorders that induce disease feed in to common processes associated with injury response. Ultimately, they cause necrosis/apoptosis, chronic inflammation, irreversible fibrosis, complete loss of organ function and destruction of the tissue epithelia[32] (Figure 1.2).

Hepatocytes in diseased livers have a defective regenerative capacity

The progression of liver disease and cirrhosis can be determined through histological scoring of liver fibrosis and inflammation along with clinical observations that are combined with the Child-Pugh criteria; which scores the severity of the patient's liver disease according to the severity of their symptoms. Pathological studies have utilised these scoring systems to measure parenchymal cell cycle arrest and senescence in relation to liver disease severity. These studies identified that markers of cell cycle arrest and senescence increase with disease severity[33–36], implying that hepatocyte regeneration becomes impaired as chronic liver disease develops.

Alongside the progression of disease severity and impaired hepatocyte regeneration is the formation of a ductular reaction (DR)[37–39]. It is hypothesised that cells in the DR can act as hepatic progenitor cells (HPC), providing an alternative source for liver regeneration, and therefore compensating for defective hepatocyte regeneration[40–42] (Figure 1.2).

Figure 1.2 – Development of liver disease

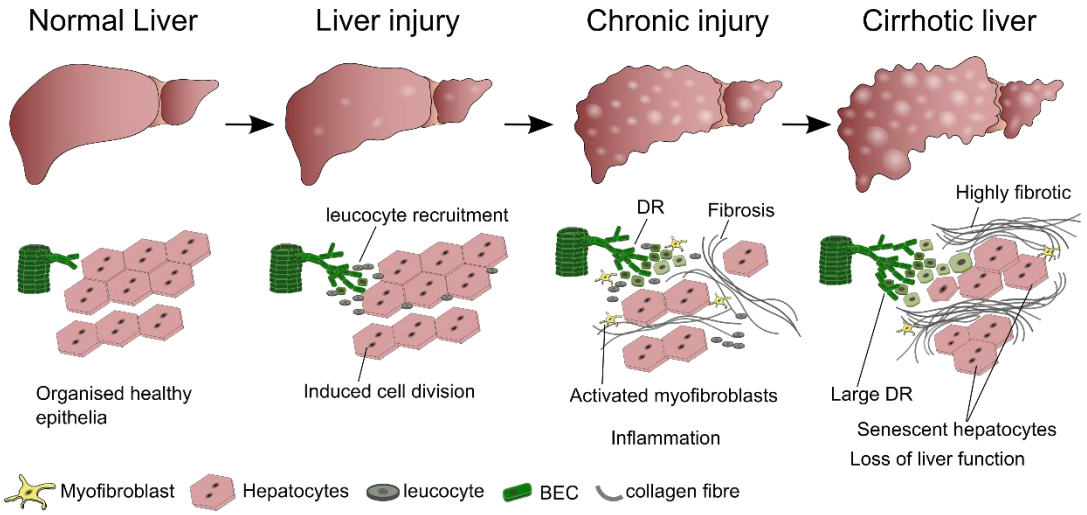

Figure 1.2: Simplified diagram presenting the progression of chronic liver disease from injury to inflammation, fibrosis and eventual liver cirrhosis. Repetitive liver injury caused by toxic insult, high fat diet or viral infection triggers; inflammation and leucocyte recruitment, stellate cell activation to myofibroblasts, fibrosis, disruption of tissue architecture and ductular reaction (DR). The number of senescent hepatocytes also increases.

The ductular reaction

Ductular reactions are thought to originate from the canal of herings, a structure located between the PT and parenchyma (Figure 1.1) where there is contact between BECs and hepatocytes[41,43]. At this interface between the biliary and hepatocyte epithelia, it has been proposed that a bipotent HPC exists[38,44,45], differentiating to either a BEC or hepatocyte cell fate. Although DR are heterogenous[43], they can be broadly

described as an expansion and infiltration of biliary duct like cells in to the parenchyma.

The DR is not solely comprised from epithelial cells; macrophages and activated stellate cells also have an important role in regulating the DR[46,47] via a diverse range of signalling pathways. Infiltrating macrophages regulate DR expansion and cell fate through multiple signalling molecules such as TNFα, TWEAK, IL6, OSM and WNT [48–52]. The stromal, hepatic stellate cell (HSC), has an important role in the formation of the DR[53], and induces DR expansion via FGF7 secretion[54]. Notch mediated cross talk between activated HSCs, myofibroblasts, and BECs promotes BEC proliferation and maintains a biliary phenotype in the DR[52,55–57]. The DR niche also involves a specialised extracellular matrix (ECM)[46,58] that regulates the migration and expansion of the DR through various adhesion molecules such as galectin-3[59], NCAM[60] and integrins αvβ5 and αvβ3[55].

The DR can have pathological consequences in the liver as it is closely linked with fibrosis[42,61–63]. The primary cell responsible for the fibrotic phenotype in the liver is the ECM producing HSC[64]. Hepatocyte damage activates HSCs[65–67], resulting in cytokine secretion and leucocyte recruitment[32]. It has been shown that HSC derived fibrosis may have a limited, pro-survival, benefit after liver injury[68]. However, chronic injury results in overactivation of the HSC population resulting in excessive fibrosis[69] and a poor clinical outcome[36]. It is therefore possible that DRs, containing activated HSCs, can have both beneficial and adverse consequences, dependent upon the duration and type of liver injury. Continuous liver injury, resulting in repetitive stimulation of the DR could imbalance the HSC/myofibroblast population, promoting fibrosis instead of regeneration.

To verify the bipotential regenerative capacity of the DR and clonally link cells from the DR with neighbouring hepatocytes a seminal study by Lin et al used mutations in human mitochondrial deoxyribonucleic acid (DNA) to trace the clonality between the DR and hepatocytes in human tissue[70]. Mutations in the exclusive mitochondrial gene, cytochrome C oxidase (*CCO*), enabled immuno-histochemical tracing of CCO deficient cells. The clonality of the CCO deficient cells was then verified using laser

capture microdissection. Using this technique Lin et al confirmed that hepatocytes and BECs in the DR shared a common cell of origin in the adult human.

Although comprehensive liver pathology studies have clonally linked DR with hepatocytes[45,70–72], they do not definitively prove that a biliary derived ductal HPC regenerates the hepatocyte epithelium. Ductal metaplasia of hepatocytes can also occur in diseased livers[73,74], contributing hepatocyte derived epithelial cells to the DR. Generally, metaplastic hepatocytes do not convert completely to a BEC fate but they do share cell markers and the same cell morphology with the biliary ductules[75]. Therefore, clonal tracing of human cells reveal an ancestral link between the two epithelial populations but do not reveal the direction of cell fate: hepatocyte to BEC or BEC to hepatocyte.

Organ failure and potential treatments

Treatment of liver disease is determined by the severity of organ failure, the degree of fibrosis and the advancement of liver cirrhosis. Primarily, treatment focuses on removing the underlying causes of disease. However, once liver cirrhosis is established, patient treatment also focuses on maintaining liver function through careful modulation of the diet, increasing protein intake and addressing features that cause cirrhotic decompensation[76].

For cirrhotic patients or patients with liver cancer the only curative treatment available is liver transplant. A major limitation with liver organ transplant is the limited number of donors, which does not match the growing demand of recipient patients. Another issue associated with organ transplant is the need for life long immune suppressants to avoid host rejection of the transplanted organ[77].

Cell transplantation therapies have been proposed as an alternative treatment to whole organ transplant[78]. This approach could solve the issue arising from donor liver shortages and immune compatibility, depending on the source of the transplanted cells[78]. Both mouse and human adult hepatocytes can repopulate livers that have the genetic metabolic disorder, hereditary tyrosinaemia type I, caused by mutations in the fumarylacetoacetate hydrolase (*Fah*) gene[79,80]. The $FAH^{-/-}$ mouse can survive when

supplemented with 2-(2-nitro-4-trifluoro-methylbenzyol)-1,3-cyclohexanedione (NTBC) which prevents the accumulation of metabolically derived hepatotoxins in the hepatocytes[81]. Removal of NTBC treatment from the $FAH^{-/-}$ mouse followed by transplantation of $FAH^{+/+}$ hepatocytes creates a competitive environment suitable for hepatocyte engraftment[79,80]. However, the availability of clinical grade primary adult hepatocytes would not be adequate as they cannot be expanded *in vitro* and they would also require the use of immune-suppressants. A solution to this problem would be the use of pluripotent stem cells: either embryonic stem cells (ESC)[82] or induced pluripotent stem cells (iPSC)[83] to acquire an unlimited amount of hepatocytes. iPSC derived hepatocytes could be generated from the patient's fibroblasts allowing for an autograft transplant, avoiding potential complications from host immune rejection. However, one enduring risk with ESC and iPSC based therapies is ensuring that transplanted cells are safe and fully differentiated, to prevent teratoma and aberrant tissue formation[78].

Another, potentially, therapeutic cell would be an expandable HPC. HPCs can be isolated using the HPC markers: CD24, EpCAM, CD133, Sca1 and Lgr5[84–88]. Isolated HPCs from mouse and human have been cultured in organoids or a 2 dimensional monolayer and successfully transplanted into injured mouse livers[86,87,89]. Another source for HPCs has recently been developed, which chemically induces primary adult mouse and rat hepatocytes to convert to a bipotent hepatic progenitor[90]. Using small molecules to inhibit Rho-associated kinase type 1, transforming growth factor-β receptor and glycogen synthase kinase-3 in hepatocytes, Katsuda et al discovered a bipotent progenitor that can be successfully expanded *in vitro* and transplanted in to recipient mouse livers[90]. Technically, the chemically induced HPC method has not been applied to human hepatocytes, it is unknown how effective the chemical cocktail is at converting human hepatocytes to HPCs. Huch et al has shown that tissue culture methods need to be optimised when changing from mouse to human HPCs[89], therefore further characterisation and optimisation is needed to translate this technology to the clinic.

A different, less invasive, approach to cell transplant could be through stimulation of endogenous liver cells to induce liver regeneration. Recently, Rezvani et al showed

that abundant myofibroblasts, generated during liver injury, could be re-programmed *in vivo* to an hepatocyte fate with non-integrating viral vectors that express key transcription factors[91]. Although this experiment revealed an attractive, new, source of regeneration in the liver; there are some significant questions that need to be addressed before it could be applied clinically. Firstly, can the low reprograming efficiency, less than 1%, be improved? Secondly, will the re-programmed hepatocytes maintain a healthy hepatocyte phenotype over a prolonged period? Lastly, can the reprogramming system be controlled sufficiently to ensure there are no off-target effects, or, avoid any abnormal, detrimental, impacts on the resident myofibroblast population?

The resident HPC in the DR is a more obvious endogenous cell population that could be targeted to enhance regeneration in the cirrhotic patient. This approach is dependent on a complete understanding of the regulatory pathways that control the DR and HPC fate. To enable the discovery of these regulatory pathways we would need suitable animal models that recapitulate human disease and allow us to study HPC derived regeneration. A therapeutic approach that focuses on DR modulation to promote HPC derived regeneration, would also need to avoid the harmful fibrosis that occurs in parallel with the DR. This may be possible, as a recent paper by Gieseck III et al showed that supressing HSC fibrosis via specific deletion of part of the IL13 signalling receptor does not influence BEC expansion[92]. Providing evidence that the DR does not require a, fibrotic, HSC to expand the potentially regenerative BEC component of the DR.

To summarise, there is a need for alternative therapies to relieve demand on liver organ donations. Cell therapies are currently the obvious choice if a suitable, clinical grade, and expandable cellular source can be identified. There are also potential risk factors such as: immune-rejection, failure to engraft correctly, and maintenance of a functional liver phenotype that will also need to be addressed. Another, potential therapeutic approach would be to stimulate endogenous regeneration through careful modulation of the DR. This would depend upon a robust understanding of the underlying biology that regulates the DR and what determines HPC fate *in vivo*. One could also foresee a future clinical treatment programme that both transplants pro-regenerative cells and uses small molecules to also enhance endogenous cell regeneration.

Liver regeneration

Adult tissue regeneration

Tissue regeneration is a process of regrowth, to maintain tissue homeostasis and replace lost or damaged tissue after an injurious event. The ability to regenerate varies between species; some organisms, such as the flatworm planaria have an extraordinary capacity to regenerate every part of their body[93]; salamanders can regenerate whole limbs[94]; while mammals, such as the mouse can regenerate a limited number of tissues, for example the intestinal epithelium, which is replaced every 3-5days[95]. Strikingly, there are common features and signals that repeatedly occur in different regenerative scenarios between the various species[93,96]. Developmental morphogens and signals such as WNT[93,97–99], hedgehog (HH)[100,101] and notch[102,103] are commonly detected in sites of regeneration along with stromal[104,105], vascular[106,107] and immune cells[52,108,109], and a specialized basement membrane[110,111], that all have a role in forming the regenerative niche. Although, their function in a particular niche can be different between separate tissues and organs[112]. Broadly, one could describe a general, successful, regenerative response after injury as a sequence of: damage detection, inflammation[113], changes to the tissue microenvironment that stimulate activation of a tissue resident stem cell[114–116] or re-programming of a committed somatic cell into a regenerative cell[117,118], differentiation, replacement of lost tissue, and resolution of inflammation (Figure 1.3).

However, tissue regeneration is not that simple, it is a complex, highly orchestrated, event, which can be disrupted by the duration and severity of the injury[113] along with aging[119]. Indeed, aging has a detrimental effect on regeneration, aged organisms cannot regenerate as effectively as their younger counterparts[120–122]. Interestingly, exposure of an aged tissue to a young systemic environment rejuvenates the aged tissue's regenerative capacity[123]. Another process involving time, the circadian rhythm, can also influence the regenerative response in some tissues, such as the liver[124,125].

Although mammalian regeneration is relatively restricted when compared to other vertebrate and invertebrate species, for example mammals cannot regrow limbs, some tissues can regenerate after injury. One mammalian organ that is capable of regeneration after toxic injury and resection is the liver[126].

Figure 1.3 – Standard epithelial regenerative response

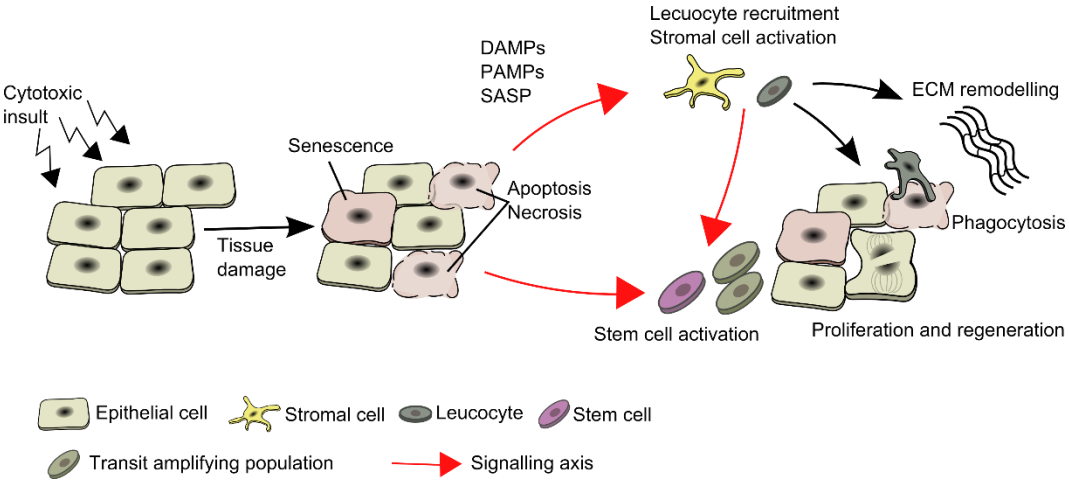

Figure 1.3: Common features observed during epithelial damage and regeneration: cell death/damage (apoptosis/necrosis/senescence), inflammation via DAMPs PAMPs and SASP secretion, leucocyte recruitment, clearance (phagocytosis), ECM remodelling/fibrosis, and signalling to stimulate tissue resident stem cells or induce epithelial division. DAMPs = damage associated molecular patterns, PAMPs = pathogen associated molecular patterns, SASP= senescence associated secretory phenotype.

Hepatocyte mediated regeneration

Under homeostatic conditions, hepatocyte turnover is relatively slow[127] when compared to other epithelia such as the epidermis and intestine[95,128]. However, the liver can undergo rapid growth or re-growth when required. Liver resection or toxic insult stimulates hepatocyte division, this process is regulated by: systemic and local signalling factors, circulating blood flow, ECM changes and cell to cell interactions[126].

Liver resection by partial hepatectomy has been the major model used to study hepatocyte regeneration. Immediately after resection changes to portal blood pressure stimulate hepatocyte growth factor (HGF) secretion from the sinusoidal endothelium and HSCs, which induces hepatocyte division[129]. Additional, secreted cytokines and growth factors that regulate hepatocyte growth include: epidermal growth factor (EGF), transforming growth factor-α (TGFα), interleukin 6 (IL6) and fibroblast growth factors (FGFs)[129]. It has been suggested that many of these signalling axes are

redundant, allowing for alternative pro-proliferation signals to prevent hepatocyte regenerative failure[126]. Hepatocyte hypertrophy also occurs during liver regeneration, proceeding cell division or acting solely to regenerate the liver after mild, 30%, partial hepatectomy[130]. Another hepatocyte feature that increases during regeneration is changes to cell ploidy levels. The number of polyploidy hepatocytes increases, whether this is a cyto-protective mechanism, pro-regenerative mechanism, or a response to changes in metabolism is unclear[131].

Hepatocytes have an important metabolic role in the body; disruption of liver metabolism, influences liver regeneration. After liver resection or toxic injury circulating metabolic products become altered. For example, serum glucose decreases, interestingly, glucose supplements after liver injury have a negative outcome on liver regeneration, and reducing the supply of insulin to the liver impairs growth[129], suggesting that changes to metabolism influence the regenerative response in the liver[132]. Additionally, amino acid and long chain fatty acid supplements enhance hepatocyte DNA synthesis, improving liver regeneration[129].

Liver organ size is dependent on organism size. When a liver is transplanted to a larger host, the organ grows to compensate for this change, increasing in volume[133,134]. Also, rat parabios experiments have shown that liver resection in one organism results in liver growth of both the resected liver and the, connected, neighbouring one[126]. Both these findings highlight the importance of systemic factors on regulating liver size and proliferation.

Other factors that influence the hepatostat (hepatocyte rheostat) include signals that terminate hepatocyte proliferation such as: TGFβ, ILK, glypican3 and the hippo signalling pathway. Peri-cellular TGFβ inhibits hepatocyte proliferation and blocking the TGFβ receptor induces hepatocyte proliferation[135]. Deletion of hepatocyte integrin linked kinase (ILK) results in a failure to terminate liver growth after partial hepatectomy[136,137]. Ablation or knockdown of the ECM protein glypican3 causes hepatomegaly and increased hepatocyte proliferation[138,139]. Finally, overactivation of the hippo pathway, via expression of phosphorylation resistant yes associated protein (YAP) in hepatocytes, results in uncontrolled hepatocyte expansion, hepatomegaly and eventual tumorigenesis[140,141]. Regulation of the Hippo pathway, potentially through

the ECM receptors, the integrins, and ILK, or mechanotransduction[142], adds another dimension to the regulation of liver size that may be controlled by physical properties as well as chemical ones.

In summary, both local and systemic factors regulate liver growth and hepatocyte proliferation. Maintenance of the correct liver size is vital and regulated by multiple processes. The hepatocyte epithelium can regenerate rapidly (with in 48hours) after an injurious event to replace lost tissue and return to pre-injury liver size.

A liver stem cell and hepatic progenitor cell theory: contradictions and uncertainty

Investigations, searching for a liver stem cell have produced contradictory results, generating multiple, inconclusive, theories[143]. Unlike some organs, such as skeletal muscle[144,145] and hair follicles[146], there is not an easily recognisable stem cell compartment in the liver. Cells in the biliary ductules at the canal of herrings are the principal HPC/liver stem cell candidate[43], however, various mouse lineage tracing experiments contradict this theory.

Original HPC lineage tracing experiments used BEC genes such as *Sox9* (SRY (sex determining region Y)-box 9), *Opn* (osteopontin), *Hnf1b* (hepatocyte nuclear factor 1-β) and *K19* (cytokeratin 19) to regulate inducible reporters and trace HPC mediated regeneration *in vivo*[147–150]. A problem with some of these genes is that injured hepatocytes also express them, which causes non-specific labelling[151,152]. A key example is the inducible $Sox9^{CreERT}$ transgene, first used to lineage trace BEC and HPC *in vivo*, resulting in labelled hepatocytes thought to derive from a prelabelled HPC[148]. However, a subsequent study, using a different $Sox9^{CreERT}$ transgene, did not re-produce the same result showing no HPC contribution to the hepatocyte epithelium[153]. The contradictory results could be explained by experiments that revealed hepatocytes express biliary markers such as SOX9 and OPN during injury[151,152]. Other HPC markers, Foxl1[154,155], Lgr5[86], are only expressed during liver injury and can be expressed in both hepatocytes and BEC making it difficult to determine the origin of the HPC. Although, ablation of *Foxl1* positive HPC, via a diphtheria toxin receptor transgene, impairs liver regeneration[155]. As for the HPC lineage tracing models that

are biliary specific, *Hnf1b*^{CreERT} and *K19*^{CreERT}, only a small fraction, less than 2%, of hepatocytes are regenerated by HPCs[150,156] when injured with commonly used mouse liver injury models such as: diethyl-1,4-dihydro-2,4,6-trimethyl-pyridine-3,5-dicarboxylate (DDC) diet and choline-deficient diet with ethionine (CDE) diet.

An alternative approach to detect HPC mediated regeneration of the hepatocyte epithelium used hepatotropic viral Cre or *Alb*$^{CreERT/DreERT}$ transgenes to completely label the hepatocyte epithelium[156–161], over 99% of hepatocytes were labelled with a heritable marker. The experimental hypothesis proposed that a non-hepatocyte source of regeneration, such as the HPC, would cause a reduction in the number of labelled hepatocytes after liver injury. Again, a range of commonly used toxic liver injury models and liver resection failed to reduce the number of labelled hepatocytes, indicating that regeneration occurred through hepatocyte self-duplication and not from a HPC source. Although, in human chronic liver disease hepatocyte regeneration is impaired via cellular senescence and expression of p21, therefore, it is questionable whether the mouse liver injury models that were used, primarily CDE and DDC, are suitable for studying HPC derived regeneration.

Solely focusing on the hepatocyte compartment, two cell populations have been identified as potential hepatocyte progenitors. Under homeostatic conditions, zone3, Axin2 positive hepatocytes around the central vein were shown to clonally expand in to the parenchyma[127]. Axin2 negatively regulates β-Catenin[162], an effector of the canonical Wnt signalling pathway, which induces hepatocyte proliferation[9]. The *Axin2*^{CreERT} transgene, which was inserted in to the endogenous *Axin2* locus[163] and utilised by Wang et al to lineage trace CV hepatocytes was heterozygous. Although heterozygous deletions of *Axin2* has been shown not to disrupt Wnt signalling during a short, 70 hour, *in vitro* experiment using primary osteoprogenitors[164], it is unknown how mutating one *Axin2* gene in hepatocytes influences liver Wnt signalling, and therefore hepatocyte proliferation, over the lifetime of the mouse. The CV progenitor cell theory was also supported by partial hepatectomy experiments in neonatal mice[165], although, the phenotype is lost as the neonates mature into adults.

In contrast, predominant Zone3 hepatocyte damage, caused by the hepatotoxin carbon tetrachloride (CCL_4), results in regeneration from a periportal *Sox9* positive

hepatocyte[166]. Furthermore, label retaining experiments[167] and periportal (zone1) *Mfsd2a* positive hepatocyte lineage tracing[168] also support the theory that hepatocyte regeneration originates periportally. Opposing the idea that there is a spatially defined hepatocyte progenitor, multiple hepatocyte lineage tracing experiments have revealed that there is no zonal bias to hepatocyte regeneration[9,169].

In summary, mouse lineage tracing of HPCs, which express BEC markers, have produced inconsistent results. Further to this, mouse lineage tracing models that label the entire hepatocyte epithelium have revealed that hepatocytes only regenerate via self-duplication, detecting a negligible contribution from a HPC. Uncertainty persists as to whether hepatocyte self-duplication is a stochastic process or spatially restricted to multiple pro-regenerative populations that have been identified in the hepatocyte epithelium. Finally, questions remain; if a HPC expressing BEC markers cannot regenerate hepatocytes, is this representative of the biology seen in humans? Or, is it an experimental artefact produced by mouse liver injury models that do not recapitulate the impaired hepatocyte regeneration seen in human chronic liver disease?

Animal models of liver disease and hepatic progenitor mediated regeneration

Rat models

Rats were the first model organism employed to study HPCs, or oval cells as they are known in the rat due to their unique morphology. To induce a DR, and oval cell regeneration, rats were treated with 2-acetylaminofluorene (AAF), which inhibits hepatocyte proliferation[170], followed by partial hepatectomy (PH), to stimulate liver regeneration[171]. Histological analysis of the regenerating rat livers identified oval cells emerging from biliary ductules[44] and resulted in proliferating periportal hepatocytes[172]. An oval cell response could also be generated by AAF combined with different hepatotoxins, CCL4 and allyl alcohol[173]. The key factor in mediating an oval cell response in the rat was the inclusion of AAF, to inhibit hepatocyte proliferation and impair hepatocyte mediated regeneration.

Mouse models

To utilise the growing availability of mouse transgenic tools and to use a more tractable mammalian model organism researchers began to use mice to study liver regeneration. AAF is not metabolised by mouse hepatocytes[174] and therefore does not induce cell cycle arrest. As an alternative to the AAF-PH injury model, DDC diet and CDE diet were used to study HPCs as they induced a DR and cells that shared some morphological similarities with oval cells[52,143]. However, DDC and CDE toxic injury diets do not inhibit hepatocyte proliferation[155,156]; a potential explanation as to why they do not induce significant HPC mediated regeneration of hepatocytes in the mouse liver[150,156,159].

Recent genetic based models of liver injury have provided evidence that a biliary derived HPC could regenerate hepatocytes in the mouse. Using Cre-*Loxp* to mutate *Mdm2* specifically in mouse hepatocytes, Lu et al showed an accumulation of p53 and subsequent p21 expression in hepatocytes[87]. In this setting of impaired hepatocyte regeneration, a DR emerged along with healthy periportal hepatocytes, reproducing histological features seen in rat and human HPC studies. Lu et al also transplanted biliary derived, labelled, HPC in to the MDM2 KO liver and showed HPC to hepatocyte differentiation; replicating data generated by Huch et al, who also transplanted HPCs in to a liver injury model where hepatocyte survival is impaired[86,89]. Huch et al isolated Wnt responsive Lgr5 positive cells from liver injured by CCL_4 intoxication. These Lgr5 positive HPCs formed organoids when cultured in matrigel and displayed a bipotent phenotype; when transplanted into $FAH^{-/-}$ mice, both human and mouse HPCs engrafted and formed mature, functional, hepatocytes[86,89]. Other genetic injury models that disrupted hepatocyte proliferation via *Dnmt1* or *Birc5* mutations, induced DNA damage and hepatocyte senescence, which resulted in a DR and HPC response, followed by liver recovery[175,176].

Zebrafish models

Experiments in the non-mammalian, vertebrate model organism Danio rerio (the zebrafish) have also produced evidence that cells in the biliary epithelium can regenerate hepatocytes. These experiments utilised the bacterial gene encoding

nitroreductase (Ntr), which metabolically converts the harmless prodrug metronidazole in to a cytotoxic compound[177]. By placing *ntr* expression under the regulation of a hepatocyte specific promoter, *fabp10a* or *ifabp*, the hepatocyte compartment could be ablated by metronidazole administration. Extensive loss of the hepatocyte compartment resulted in a Notch, Wnt and BMP mediated BEC expansion and conversion into hepatocytes[178–180].

To conclude, animal liver injury models that excessively ablate hepatocytes or inhibit hepatocyte proliferation, induce a HPC response in the form of a DR, which is followed by hepatocyte regeneration. Mouse liver injury models, originally used for HPC lineage tracing, induce a DR but do not impair hepatocyte proliferation. To determine if a biliary derived HPC can differentiate in to hepatocytes in the mouse, a liver injury model that impairs the hepatocyte regenerative capacity is required.

Cell fate and differentiation in the liver

The lack of a robust mammalian *in vivo* model to lineage trace HPCs during regeneration has hindered the discovery of cell processes and signalling pathways that regulate HPC fate during adult liver injury and regeneration. However, much is known from developmental studies and hepatocyte lineage tracing experiments.

Development

The two liver epithelia (hepatocytes and BECs) originate from the endoderm lineage during embryonic development. A sequence of cell specification events; involving formation of the definitive endoderm followed by the development of foregut endoderm, results in the generation of the liver diverticulum via mesenchymal bone morphogenetic protein 4 (BMP4) and FGF signalling[181]. The liver diverticulum buds out ventrally from the foregut, it is in this liver bud where the hepatic endoderm differentiates in to the hepatoblast, the hepatocyte and BEC progenitor, and liver organogenesis occurs[5]. In the liver bud, Hex positive hepatoblasts transform from a

columnar to a pseudostratified epithelium followed by delamination and migration in to the septum transversum mesenchyme (STM)[182], where hepatoblast differentiation is induced[183]. Endothelial cells also regulate liver organogenesis, deletion of VEGFR2 causes a loss of endothelial cells during hepatic development, which inhibits liver bud and hepatoblast formation[184].

During hepatic development, there are key regulatory transcription factors that control chromatin organisation and gene expression in the hepatic progenitors, determining cell fate[185]. Transcriptional hierarchy in the developing hepatic endoderm begins with the expression of forkhead box protein-A1/2 (FOXA1/2), GATA binding protein-4/6 (GATA4/6) and hepatocyte nuclear factor-vHNF1 (HNF1β) transcription factors, which are essential for hepatic induction[186–190]. Importantly, FOXA1/2 are pioneer transcription factors[191] that remodel chromatin to expose hepatic genes, enabling progenitor differentiation[186,192]. Further specification of the hepatic endoderm, results in the expression of the Hex homeobox transcription factor (Hhex), which is also essential for liver bud formation[182]. Later, as the hepatic progenitors progress to the hepatoblast stage, hepatocyte nuclear factors 4α, 1β and 6 (HNF4α, HNF1β and HNFF6) are expressed[193,194], regulating hepatoblast expansion and migration in to the STM. Hepatoblast differentiation is partially regulated by the T-box gene repressor TBX3[195] and the CCAAT/ enhancer binding protein-α (C/EBPα)[196], which repress and promote (respectively) biliary transcription factors HNF6 and HNF1β.

Hepatocytic differentiation and maturation requires Oncostatin M (OSM), HGF, WNT and glucorticoids[4]. Two transcription factors HNF4α and PROX1 are essential in hepatocyte specification: HNF4α expression is necessary to develop a mature, organised hepatocyte epithelium[193,197,198], and PROX1 promotes a hepatocyte fate, deletion of *Prox1* results in excessive BEC differentiation, aberrant ECM deposition and liver hypoplasia[199,200].

Development of the biliary network is dependent on mesenchymal jagged-1/notch signalling[201–203], a TGFβ-activin signalling gradient[204,205] and YAP activation[206,207]. These signalling axes regulate biliary specific transcription factors; SOX9, SOX4, HNF6, HHEX and HNF1β , which are essential for biliary development and morphogenesis[196,208–212].

Canonical and non-canonical WNT signalling pathways have distinct functions at various stages in hepatic development. β-Catenin, a target of canonical Wnt signalling is essential for maintaining the endoderm lineage[213]. However, modulated WNT signalling is needed to pattern the anterior and posterior endoderm, secretion of Sfrp5 a negative regulator of WNT ensures foregut development prior to formation of the liver diverticulum, supressing the canonical and non-canonical functions of Wnt11[214]. In the zebrafish, mesodermal derived Wnt2b has been identified as an important signal in liver specification and hepatoblast formation[215] targeting the EpCAM positive hepatic endoderm[216]. At later stages of development, when the hepatoblasts have migrated in to the STM, sinusoidal endothelial cells secrete Wnt9a to induce β-Catenin, which drives hepatoblast proliferation and maturation[217,218]. Another Wnt ligand, Wnt5a, suppresses hepatoblast to biliary differentiation[219], further to this deletion of β-Catenin does not influence biliary development[220], suggesting canonical WNT signalling primarily influences hepatoblast to hepatocyte differentiation at the late stages of liver development.

In conclusion, hepatic development is dependent upon the expression of pioneer transcription factors that modulate chromatin structure and enable hepatic gene expression. Signals from mesenchymal and endothelial cells are essential for cell fate specification and subsequent tissue organisation. Many of the signals present in development are also present in the injured and regenerating adult liver.

In vitro studies

Isolation of hepatic progenitors and differentiation of ESC in vitro have also identified essential factors needed to promote hepatic differentiation. Isolated mouse hepatic progenitors from stage E13.5 embryos when supplemented with HGF and OSM upregulate C/EBPα[221], a factor that promotes hepatocytic differentiation. In the same isolated progenitors[196], ECM components, laminin and type I/IV collagen, suppressed C/EBPβ[221], a pro-biliary differentiation transcription factor[205]. Human ESC differentiation requires WNT3a and activin A to form hepatic endoderm[222]. Further maturation of hepatic endoderm to hepatoblast and hepatocytes requires: retinoic acid,

FGF10, FGF4, HGF, OSM, DMSO, insulin[223,224], and recombinant laminins (LN521 and LN111)[225].

Comparisons between isolated neonatal and adult HPC have revealed an epigenetic mechanism that restricts adult HPC differentiation to hepatocytes. Repression of the micro RNA *Mir122* via the BEC specific transcription factor grainy head-like 2 (GRHL2) prevents adult HPC differentiation. In contrast, expression of *Mir122* in neonatal HPCs enhances hepatocytic differentiation[226,227]. Differentiation of adult HPC organoids is possible when TGFβ and Notch signalling is inhibited, cell growth is reduced, and media is supplemented with BMP7, FGF19 and dexamethasone[86,89].

Although *in vitro* assays do not completely encompass and recapitulate the biology controlling cell fate *in vivo*. They do reveal important candidate ligands and signalling axes that should be investigated *in vivo* to understand how the identified signals integrate with liver regeneration.

In vivo studies

Investigations of factors that affect HPC derived regeneration have been hampered by the lack of an appropriate mouse model. However, work by Boulter et al revealed parallels between signalling in liver development and adult regeneration. Boulter et al, showed, similar to development, WNT signalling induced hepatocytic differentiation and Notch signalling induced BEC differentiation[52]. Although the source of the WNT in adult regeneration was macrophage derived and not endothelial or mesenchymal.

The ECM has also been proposed to influence HPC fate, Español-Suñer et al used a pharmaceutical analogue of prostacyclin, iloprost, to indirectly suppress laminin expression *in vivo*. This resulted in an increase in the amount of OPN^{CreERT} labelled hepatocytes ostensibly derived from a biliary DR origin[149]. Although, it has been previously mentioned that OPN can be expressed by damaged, periportal, hepatocytes[152] and therefore the origin of these hepatocytes is not certain. Also, iloprost does not solely influence laminin expression, it has many off-target effects and can suppress HPC proliferation[172]. Laminin is a key constituent of the BEC and HPC niche[44,46,228], more targeted experiments are needed to evaluate the role of laminin loss on cell fate.

Overactivation of the canonical notch pathway, via activation of a transgene that encodes the Notch intra-cellular domain in hepatocytes, induces transdifferentiation to a BEC fate[74,158]. This phenomenon can be repeated, if a phosphorylation resistant *Yap*, that localises to the nucleus[229], is over-expressed in hepatocytes[230]. However, experiments that induce hepatocyte transdifferentiation through injury and not, artificial, transgenes results in an incomplete transdifferentiation that is reversible[75]. Therefore, Notch and Hippo signalling does influence hepatocyte fate but how these signalling pathways function in the context of liver injury and regeneration is not clear.

Artificial manipulation of BECs and any HPC residing in the biliary epithelium did not produce striking differences in changes to cells fate[56]. Jors et al utilised a conditional *Hnf1b*^{CreERT} transgene to specifically target BECs and activate either an exon 3 deficient β-Catenin that cannot be negatively regulated, resulting in overactivation of the canonical Wnt pathway; or ablate *Rbpj*, a downstream target of the canonical notch signalling pathway, loss of which results in impaired notch signalling. The rational for this experiment was that if loss of notch signalling and activation of Wnt signalling directs HPCs towards a hepatocyte fate, as previously hypothesised by Boulter et al[52], then artificial manipulation of these pathways would promote HPC differentiation. However, Jors et al did not detect HPC differentiation using this model, suggesting other signalling mechanisms may influence HPC to hepatocyte differentiation.

To conclude, detailed developmental studies have identified signalling axes and transcription factors that regulate hepatic cell fate. How these signalling pathways influence cell fate during adult liver regeneration have been partially investigated with respect to the Notch, Wnt and Hippo signalling pathways. However, further characterisation of these pathways, in a reliable HPC model, is needed to fully elucidate factors that regulate HPC differentiation to a hepatocyte fate. Also, little is known about the transcription factors that regulate cell fate during adult liver regeneration and if there are any, pioneer or master, transcription factors involved.

β1-Integrin and liver regeneration

Extracellular matrix and cell adhesion

The ECM is an organised structure, composed from protein and saccharide macromolecules, arranged in a way that provides structural support for cells and facilitates cell migration in all metazoans. For each tissue, the ECM structure and composition is different and can undergo dynamic changes in response to distinct biological processes such as regeneration, development and tissue damage[231]. There are approximately 300 identified mammalian ECM proteins, which can be classified as either collagens, glycoproteins and proteoglycans[232]. Commonly, ECM forms the basement membrane (BM) for all epithelia, key constituents of the BM include: collagen, laminin, nidogen and perlecan[233–235]. The ECM influences cell behaviour by stimulating and modulating cell signalling[233], determining cell polarity[236] and regulating stem cell activity[111,237]. The elasticity of a tissue, determined by the composition of the ECM, can also influence cell fate[238,239] and promote the progression of cancer via integrin activation[240]. Another feature of the ECM is its ability to bind growth factors and other extracellular signalling molecules[233]. The ECM can modulate signals in the cell niche via: activation of latent signalling factors, sequestering factors so they cannot interact with the cell, and correctly presenting signalling ligands to cell surface receptors[233,241].

The integrins, a major ECM receptor family, facilitate adhesion between the cell and the surrounding ECM. Integrin activity is bidirectional, intracellular signals can regulate integrin structure and thereby regulate integrin adhesion, conversely integrin binding to extracellular ligands can induce intracellular signals to influence cell behaviour[242]. Once an integrin mediated adhesion between the cell and the ECM is established an adhesome forms; integrin receptors cluster and recruit components of the cytoskeleton, other plasma membrane receptors and adapter proteins[243]. Integrin adhesomes are heterogenous within cells and between different cell types. The downstream effects of the adhesome are vast and are still being characterised, they have been linked to cytoskeletal rearrangements, facilitating cell migration and changes to cell morphology; and inducing signalling cascades resulting in cell survival, differentiation and proliferation[244].

β1-Integrin: an important mutli-functional protein

The integrin receptor is composed from two subunits, an α-unit and a β-unit that heterodimerise to form the complete receptor. There are 8 β-units that can dimerise with 18 α-units forming a total of 24 possible receptors[242]. One integrin subunit, β1-Integrin, is a major constituent of many integrin receptors. It is also vital to embryogenesis, deletion of β1-Integrin is embryonic lethal, resulting in pre-implantation death[245]. β1-Integrin heterodimerises with 12 different α-subunits[232] and is involved in establishing cell polarity[246,247], regulating stem cells via BM interactions[248,249] regulating cancer metastases[250,251] and activating growth factor signalling axes to promote cell survival and proliferation[252,253]. Conditional loss of β1-Integrin generally results in organ hypoplasia, impaired cell growth and defective regeneration in many tissues[254–257] because it promotes cell survival via ERK-Akt activation[257,258].

ECM and Integrin expression in the liver

In the healthy adult mouse and rat liver; type I, III and IV collagen, fibronectin and heparan sulfate proteoglycans are broadly distributed throughout the liver, lining the sinusoids and forming the ECM at the PT. Laminin and nidogen are also expressed throughout the liver, with a higher concentration around the PT[259,260], particularly the laminin α5 and α1 isoforms[261,262]. β1-Integrin is widely expressed throughout the liver, located in the membrane of both parenchymal (hepatocytes, BEC)[259] and non-parenchymal cells (HSC, Kupffer cells, sinusoid endothelial cells)[263]. Other integrin variants, β6, β4, α6, α3, α2 and αV are expressed in the biliary epithelium; and the α1 and α5 -integrins are expressed in the liver sinusoids[259,264,265]. Hepatocytes express *Itgb1*, *Itgb5*, *Itga1*, *Itga5*, *Itga9* and *Itgav*, forming potentially 5 integrin receptors capable of binding collagen and the RGD domain found in fibronectins[232,266].

The liver ECM and cell adhesion receptors change during injury[260] and as liver disease develops an irreversible fibrosis forms[267]. In human cirrhotic livers, the amount of collagen and laminin increases and their distribution changes, resulting in peri-nodular ECM deposition and fibrous septa[264]. Injury induced alterations to the liver ECM

increase the stiffness of the tissue[268,269], which eventually disrupts liver function and promotes liver cancer[270]

Integrin expression increases in injured livers[271–273] and integrin receptor activity can modulate the injury response. During liver injury, αv-Integrin expressed on stromal myofibroblasts[274] and epithelial cells[265] activate latent, extracellular, TGFβ, which induces a signalling cascade that promotes ECM secretion. Biliary αvβ5/αvβ3-integrin interacts with the matricellular protein CCN1 to induce a biliary derived DR[55]. Hepatocytes require β1-Integrin for growth factor signalling and activation of, pro-survival, protein kinase B (Akt)[263].

Although liver fibrosis, caused by excess ECM deposition, eventually has an adverse impact on liver function and patient survival, aspects of fibrosis can be beneficial, promoting hepatocyte survival[68]. Increased ECM stiffness also induces hepatocellular carcinoma (HCC) proliferation[275]. Together, this demonstrates the benefits of hepatocyte-ECM adhesion for cell survival and growth.

Role of hepatocyte β1-Integrin

Hepatocyte β1-Integrin augments growth factor signalling, enhancing hepatocyte growth and survival. Deletion of β1-Integrin from the hepatocyte epithelium suppresses growth factor signalling and proliferation[263]. Loss of β1-integrin during ESC differentiation *in vitro* resulted in decreased AKT activation and a reduction in differentiation[276], a probable explanation is that β1-Integrin loss disrupts the essential growth factor signals required for hepatic differentiation. Over-expression of *ITGB1A* in immortalised human hepatocytes improved cell survival via activation of MAP kinase and apoptosis resistance[277]. Whether this pro-survival phenotype is caused by β1-integrin mediated adhesion alone or is a consequence of increased growth factor signalling has not been fully defined. β1-Integrin may also have a role in supporting hepatocyte polarity by acting as an intermediate between the ECM and Par1b protein[278]. Furthermore, loss of hepatocyte β1-integrin *in vitro* disrupts cell polarisation and canaliculi formation[266]. A similar mechanism exists in the biliary

epithelium, where β1-Integrin co-ordinates apical-basal polarity during BEC differentiation in development[261].

Loss of β1-Integrin from hepatocytes: lessons from cancer and an acute liver injury model

To determine the role of hepatocyte β1-Integrin in disease two investigations used an inducible, loss of function, *Itgb1* mutation and small interfering RNA (siRNA) to suppress *Itgb1* expression . In an acute liver injury model (2/3 partial hepatectomy), conditional knockout of β1-Integrin mediated by Mx^{Cre} and floxed *Itgb1* resulted in decreased EGFR and c-Met activation[263]. Disruption of hepatocyte growth factor signalling during acute liver injury resulted in impaired regeneration, demonstrated by a decrease in mouse survival, a decrease in hepatocyte proliferation and an increase in parenchymal necrosis. The adverse effect of β1-Integrin loss from hepatocytes was investigated further, by inducing liver cancer with oncogenic c-Met and β-Catenin. RNAi mediated suppression of β1-Integrin in hepatocellular carcinoma reduced tumour burden and improved mouse survival[266]. Again, knock down of β1-Integrin reduced overactivated growth factor signalling axes present in HCC. Together, these investigations demonstrate the role hepatocyte β1-Integrin has in promoting proliferation and cell survival, indispensable for successful liver regeneration.

Summary

As one of the rare visceral organs capable of regeneration, the liver has been the focus of many investigations into mammalian regeneration. This work has established a comprehensive understanding of how the liver regenerates after acute injury and resection, along with the discovery of signalling pathways involved with injury recognition and inducing division of resident hepatocytes and BECs. However, in human chronic liver disease hepatocyte epithelial proliferation is reduced and DR appears. Fate tracing of a biliary derived HPC in the DR, using murine lineage tracing models, have failed to conclusively determine if a biliary derived DR can significantly regenerate the hepatocyte epithelium. Two conclusions can be drawn from this finding: one, that biliary derived DRs cannot regenerate hepatocytes and that human liver pathology studies were describing hepatocyte ductal-metaplasia; or two, that the commonly used mouse liver injury models do not represent human liver disease, because the hepatocyte epithelium is still capable of regeneration. To address this problem and determine if a biliary derived DR can regenerate the liver I propose the following hypothesis.

Hypothesis and aims

Hypothesis: Impairing hepatocyte regeneration, via ablation of β1-Integrin, will induce biliary derived regeneration of the hepatocyte compartment.

I aim to investigate this hypothesis using the following objectives:

- Establish a highly specific model where hepatocyte β1-Integrin can be ablated and concurrent hepatocyte lineage tracing can occur.
- Develop a biliary lineage tracing model where hepatocyte β1-Integrin expression can be targeted independent of a Cre/*Loxp* transgenic.
- If an alternative source of hepatocyte regeneration is detected, I will determine if any non-hepatocyte derived regeneration results in functional restoration of the parenchyma.

Chapter 2

Materials and Methods

Liver injury models

All animal experiments were carried out under procedural guidelines, severity protocols and with ethical permission from the University of Edinburgh Animal Welfare and Ethical Review Body (AWERB) and the UK Home Office, licence number: 70/7847. All animals were housed in a pathogen-free environment and kept under standard conditions with a 14-hour day/10-hour night cycle and access to food and water *ad libitum*.

3,5-Diethoxycarbonyl-1,4-dihydrocollidine (DDC) diet

Supplementation of mouse feed with 3,5-Diethoxycarbonyl-1,4-dihydrocollidine (DDC) generates porphyrin in the liver, which results in blockage of the bile ducts and liver cholestasis[279,280]. Consequences of DDC induced cholestasis include portal fibrosis, necrosis, inflammation and DR[281]. 7-10 week old male and female mice were given 0.1% DDC mixed with Rat & Mouse No1 Maintenance (RM1) diet (Special Diet Services), for 7-10 days.

Methionine and choline deficient (MCD) diet

The methionine and choline deficient (MCD) diet models non-alcoholic steatohepatitis (NASH). The diet's high fructose and fat content in the absence of methionine and choline disrupts mitochondrial β-oxidation and the synthesis of low density lipoprotein resulting in steatosis, inflammation, necrosis and fibrosis[281]. MCD diet (MP Biomedicals) was given for 7-14 days to both male and female mice aged 7-10 week old.

Thioacetamide (TAA)

TAA intoxication models liver fibrosis and chronic TAA application generates liver cancer[282]. Liver damage is induced when TAA is metabolised by zone 1 and zone 3 hepatocytes, generating reactive oxygen species (ROS) that disrupt the cell's macro-molecules, triggering cell death[281]. 7-10 week old male mice were given thioacetamide

(TAA) (Sigma Aldrich). TAA was administered in the drinking water at a concentration of 300mg/L for 21 days.

Choline deficient ethionine supplemented (CDE) diet

The Choline deficient ethionine supplemented (CDE) diet disrupts mitochondrial β-oxidation via choline deficiency and induces liver damage and carcinogenesis via the hepatoxin ethionine; CDE diet causes steatosis, inflammation and DR [283]. 6 week old female mice were first fed a CDE weaning diet for 1 week followed by 4 weeks of CDE diet. The weaning diet was choline sufficient, which was followed by the choline deficient CDE diet; both were custom made by MP Biomedicals (960412). Mice were given normal chow for a 2 week recovery period after CDE diet treatment.

For all hepatotoxic diets, animals that lost more than 20% of their pre-injury body weight were taken off injury diet early as they had reached the allowed severity threshold according to the project licence approved by the UK Home Office.

Transgenic mouse models

The animals in this study had a C57BL6/J background and both equal numbers of male and female mice were used, unless specified in the text (see CDE diet and TAA protocol).

Adeno Associated Virus 8 (AAV8) Cre induction

Mice between 7-10 weeks of age had Cre mediated recombination induced with AAV8.TBG.Pi.Cre.rBG (Penn vector core, CS0644). Control, null, experiments used AAV8.TBG.Pi.null.rBG (Penn vector core, CS0255). The adeno-associated virus 8 serotype has a high tropism for muscle, CNS and the hepatocytes, this, combined with the hepatocyte specific thyroid binding globulin (TBG) promoter restricts Cre expression specifically to hepatocytes[74] (Figure 2.1a, page 32). Viruses were administrated by tail vein injection in a 100µl dose at a concentration of $2.5X10^{11}$

GC/ml. AAV8 viruses were diluted in sterile PBS. Mice were given a 2 week wash out period before being placed on toxic injury diets.

Itgb1$^{fl/fl}$ and *R26R^{LSL}tdTomato* mice

The β1-Integrin$^{fl/fl}$ (*Itgb1$^{fl/fl}$*) mice were purchased from The Jackson Laboratory and crossed with the *R26R^{LSL}tdTomato* mouse (The Jackson Laboratory). The transgene *Itgb1$^{fl/fl}$* contains loxP sites flanking exon 3, which, when exposed to Cre recombinase results in an excision of exon 3 and a frameshift mutation, preventing translation and a loss of the β1-integrin protein[254]. The *ROSA26^{LSL}tdTomato* transgene is activated by Cre mediated excision of the Stop codon, labelling cells with a fluorescent, heritable, genetic marker tdTomato (tdTom). Genotyping was performed using the commercial transnetyx genotyping service. All experiments used mice with either homozygous alleles for *Itgb1$^{fl/fl}$* or *Itgb1^{WT}*, mice were either heterozygous or homozygous for the *R26R^{LSL}tdTomato* allele.

Tamoxifen induction

To lineage trace BECs an estrogen receptor bound Cre transgene (*Cre^{ERT}*) was inserted in to the cytokeratin-19 gene (*K19*) locus, which expresses *Cre^{ERT}* in *K19* expressing cells, such as the biliary epithelium[147]. Administration of tamoxifen triggered the release of the estrogen bound Cre recombinase, allowing for nuclear translocation and genetic recombination, activating *R26R^{LSL}TdTomato* via excision of the STOP codon (Figure 2.1b). Loss of the STOP codon resulted in fluorescent tdTom labelling of the biliary epithelial cells at a 40% recombination efficiency[284]. Recombination in the *K19cre$^{ERT\ LSL}$tdTomato* mice was induced by 3 individual 200µL intraperitoneal (i.p.) injections of Tamoxifen (Sigma UK), on alternative days (Monday, Wednesday and Friday). The tamoxifen was suspended in sunflower seed oil at a concentration of 20mg/ml, equating to a 4mg dose per injection. K19Cre animals received 2-3 weeks of normal diet after the last Tamoxifen injection, before commencing toxic injury diets.

Figure 2.1 – *In vivo* transgene activation targeting either hepatocytes or BECs

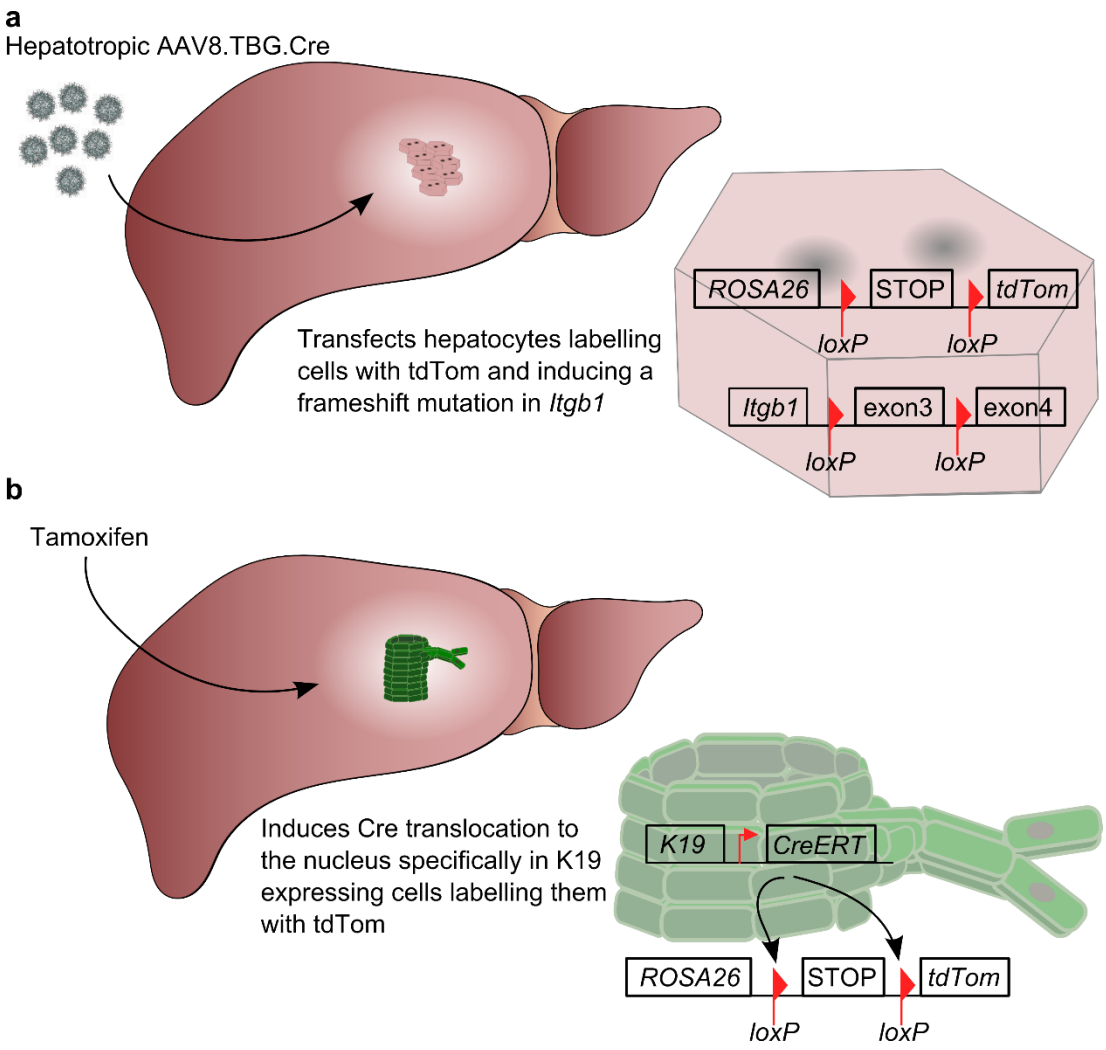

Figure 2.1: Schematic explaining the transgenic models used to lineage trace hepatocytes (**a**) and BECS (**b**).

K19cre$^{ERT\ LSL}$tdTomato Mice

The *K19Cre^{ERT}* mouse was a gift from Dr Guoqiang Gu (Vanderbilt University)[147]. It was crossed with the *R26R^{LSL}tdTomato* mouse (The Jackson Laboratory). Mice homozygous for the *K19Cre^{ERT}* and heterozygous for the *R26R^{LSL}tdTomato* loci were used for lineage tracing experiments.

Tissue harvest

Mice were euthanized according to UK Home Office regulations. Blood was collected by cardiac puncture and centrifuged to collect serum. Organs were harvested and either directly frozen at -80°C, fixed in 10% formalin (in PBS) for 12 hours, or fixed in methacarn for 12 hours. Formalin and methacarn fixed tissue was then stored in paraffin. Animals that exceeded the experimental severity protocol boundaries were excluded from analysis. Otherwise all animals were included in analysis.

siRNA nanoparticles

Small interfering RNA (siRNA) formulated in to lipidoid nanoparticles, kindly gifted by Victor Koteliansky from Skolkovo Institute for Science and Technology, were used to silence *Itgb1* mRNA *in vivo*. These siRNA nanoparticles have been previously shown to specifically suppress hepatocyte β1 integrin expression as the lipid formulated particle has a high affinity for hepatocytes[263,266]. 0.5mg/kg doses, in a volume of 0.1ml were administrated intravenously via the tail vein to each mouse every 5 days according to the schematic on page-107 (Figure 5.1). Depending on the experiment, between 2 and 6 doses of siRNA were administrated to each animal. Alongside the Itgb1 RNAi nanoparticles, control, anti-luciferase RNAi nanoparticles were administrated at the same concentration and frequency.

Histology

Immuno-histochemistry

Formalin fixed tissue was embedded in paraffin and cut in to 4μM sections. Heat mediated antigen retrieval was performed according to the primary antibody used (Table 2.1), heat was generated by a 700Watt microwave. Sections were treated for endogenous peroxidase, avidin and biotin. Bloxall (Vector) was first applied to block peroxidase activity, this was followed by Avidin and Biotin block (Invitrogen), sections were washed between each blocking step. Protein block (Spring Bioscience) was applied for 30 minutes before sections were stained overnight at 4°C using

primary antibodies listed in Table 2.1. Species specific secondary biotinylated antibodies (Vector) targeting the previously applied primary antibody were applied for 30 minutes. A streptavidin conjugated horseradish peroxidase (HRP), Vectastain R.T.U, ABC reageant (Vectar), was then applied for 30 minutes. For the chromogen, 3,3'-Diaminobenzidine (DAB) (Dako) was added to the sections for approximately 3-5 minutes. After each antibody and streptavidin application sections were washed with PBS. A haematoxylin counter stain was used alongside the DAB to label cell nuclei. Isotype controls were used for every immuno-histochemical stain performed (Figure 2.2).

Immuno-fluorescence

Formalin fixed tissue, embedded in paraffin was cut into 4µM sections. Again, heat mediated antigen retrieval was performed according to the primary antibody used (Table 2.1). Sections were blocked with protein block (Spring Bioscience) for 30 minutes and stained overnight at 4°C using primary antibodies listed in Table 2.1. Primary antibodies were detected using fluorescent conjugated secondary antibodies (alexa 488/alexa555 and alexa657; invitrogen). Fluorescent secondary antibodies were raised in donkey and selected to target the species of the primary antibody. Sections were stained with Dapi and mounted with fluromount (SouthernBiotech).

When two antibodies from the same species were used, SOX9/RFP/HNF4α immunofluorescent stain, primary antibodies were applied sequentially. The first antibody to be applied, anti-RFP, was detected using a species specific secondary antibody (Dako) conjugated to HRP and a Perkin Elmer TSA Plus Cyanine 3, signalling amplification, kit (NEL744B001KT). This was followed by a second antigen retrieval to denature any antibodies in the tissue and prevent cross-reaction with the second primary antibody application.

Histochemistry

Haematoxylin and Eosin (H&E) stains were automatically produced using a Shandon Varistain Automated Slide Stainer. PicroSirius Red (PSR) stains used reagents from

Sigma Aldrich; picric acid Cat No:P6744-1GA, fast green Cat No:F7258-25G, direct red Cat No: 365548-25G. Staining was performed by the histology department in the University of Edinburgh's Shared University Research Facilities (SURF).

Table 2.1 – Primary Antibodies used for immuno-histochemistry and immunofluorescence

Antibody	Supplier	Fixation	Antigen retrieval	Antibody concentration
HNF4α (C-19) (Goat)	SC-6556 Santa Cruz	Formalin	Heat mediated, Tris EDTA (pH9)	1/50
SOX9 (Rabbit)	ab5535 Millipore	Formalin	Heat mediated, Tris EDTA (pH9)	1/200
CK19 (TromaIII) (rat)	DSHB	Formalin	Heat mediated, sodium citrate (pH6)	1/200
Smooth Muscle Actin α (mouse)	A2547 Sigma Aldrich	Formalin	Heat mediated, sodium citrate (pH6)	1/2000
RFP (Rabbit)	ab62341 Abcam	Formalin	Heat mediated, Tris EDTA (pH9)	1/200
HNF1β (Rabbit)	Novus Biologicals NBP1-89680	Formalin	Heat mediated, Tris EDTA (pH9)	1/200
CYP 2D (Sheep)	Gift from R. Wolf, University of Dundee	Formalin	Heat mediated, Tris EDTA (pH9)	1/200
mCherry (Goat)	AB0081-500 SICGEN	Formalin	Heat mediated, sodium citrate (pH6)	1/200
Glutamine Synthatase (Rabbit)	ab73593 Abcam	Formalin	Heat mediated, sodium citrate (pH6)	1/100
Ki67 (Rabbit)	ab16667 Abcam	Formalin	Heat mediated, sodium citrate (pH6)	1/200
P21 (Rabbit)	SC-471 Santa Cruz	Formalin	Heat mediated, sodium citrate (pH6)	1/50
PCNA (Mouse)	ab29 Abcam	Formalin	Heat mediated, sodium citrate (pH6)	1/10000
HMGB1 (Rabbit)	ab18256 Abcam	Formalin	Heat mediated, sodium citrate (pH6)	1/100
HNF4α (Rabbit)	ab181604 Abcam	Formalin	Heat mediated, Tris EDTA (pH9)	1/200
B-Catenin (Rabbit)	ab2365 Abcam	Frozen, methanol	NA	1/200
Integrin-β1 (Rat)	MAB1997 Millipore	Frozen, methanol	NA	1/200

Figure 2.2 – Control images of isotype treated tissue

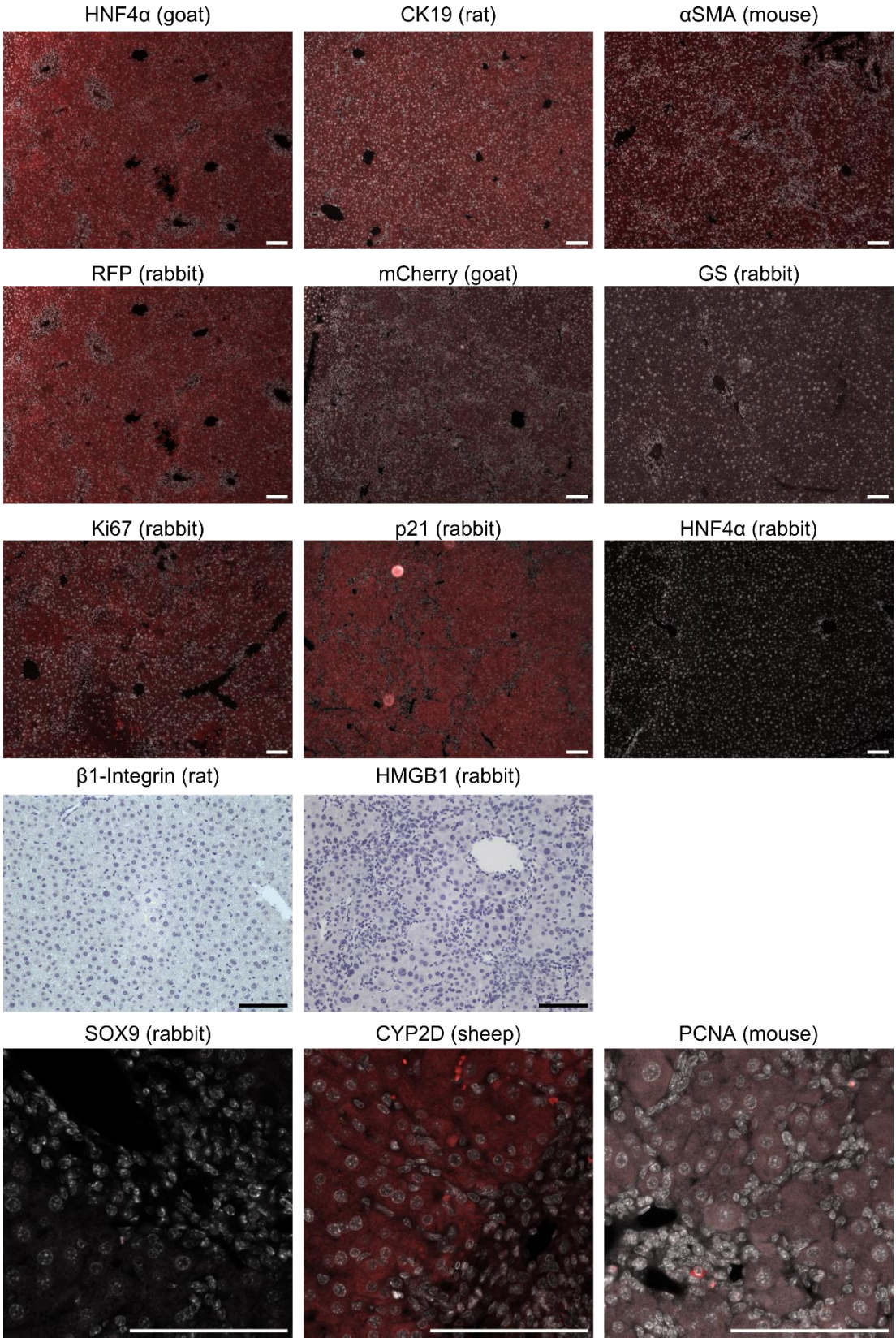

Figure 2.2: Isotype control images. Label above image refers to immuno-stain used in conjunction with the isotype control. DNA is stained with either dapi or haematoxylin; for fluorescent images, dapi is in grayscale. Generally, secondary antibodies were detected with a black and white camera, in these images the fluorescent signal has been coloured red. Scale bar: 100µM.

Histological analysis

Microscopy

For confocal microscopy either a Leica SPE inverted microscope or a Zeiss LSM 780 was used and images were deconvoluted using Fiji ImageJ. Brightfield images were taken using a Nikon Eclipse e600 microscope and Retiga 2000R camera (Q-Imaging) and acquired with image pro premier software. The PSR analysis used an AxioScan Z.1 (Zeiss) to acquire tiled images at a 20X magnification. De-tiled images were then analysed using a standard colour threshold in Fiji Image-J, to measure PSR positive fibrosis. Necrotic areas were quantified using H&E histochemistry and the trainable WEKA segmentation tool in Fiji Image J, to distinguish between parenchymal and necrotic areas. Fluorescent tiled images were generated on a Perkin Elmer Operetta high content imaging system, subsequent image stitching was done on Fiji ImageJ using the pairwise stitching plugin [285]. DAPI, Alexafluore 488, and 555 were detected using band paths of 415-480, 495-540 and 561-682nm for 405, 488 543 nm lasers respectively.

Fluorescent cell quantification and analysis

Images were acquired in up to four fluorescent channels at 10X magnification on a Perkin Elmer Operetta high content imaging system and subsequently analysed using the Columbus software. An average of 25 images were taken per liver section. One field of view corresponds to 1.37mm^2.

For cell quantification, Dapi stained nuclei were identified based on pixel intensity using method 'B' with approximately 7000 nuclei identified per field. Nuclear size and morphology was then determined (figure 2.3a). Illumination correction and background normalization was performed using the sliding parabola module. Depending on the experiment, nuclei were then assigned as positive or negative based on the mean pixel intensity in the corresponding channel in either the nucleus (HNF4α, tdTomato, Ki67, P21 and PCNA) (figure 2.3b) or a 7μM thick region surrounding the nucleus (CK19 and αSMA). For each experiment identical thresholds were used in all images for assigning nuclei to a specific population.

To quantify the distribution of $tdTom^{neg}$ (tdTomato) and $tdTom^{pos}$ hepatocytes either cytokeratin 19 positive ($CK19^{pos}$) bile ducts or glutamine synthetase positive (GS^{pos}) hepatocytes where identified. Non-overlapping zones at various distances form the identified cells were established and the number of labelled hepatocytes in each zone were quantified (Figure 2.4)

Figure 2.3 – Single cell tissue analysis strategy

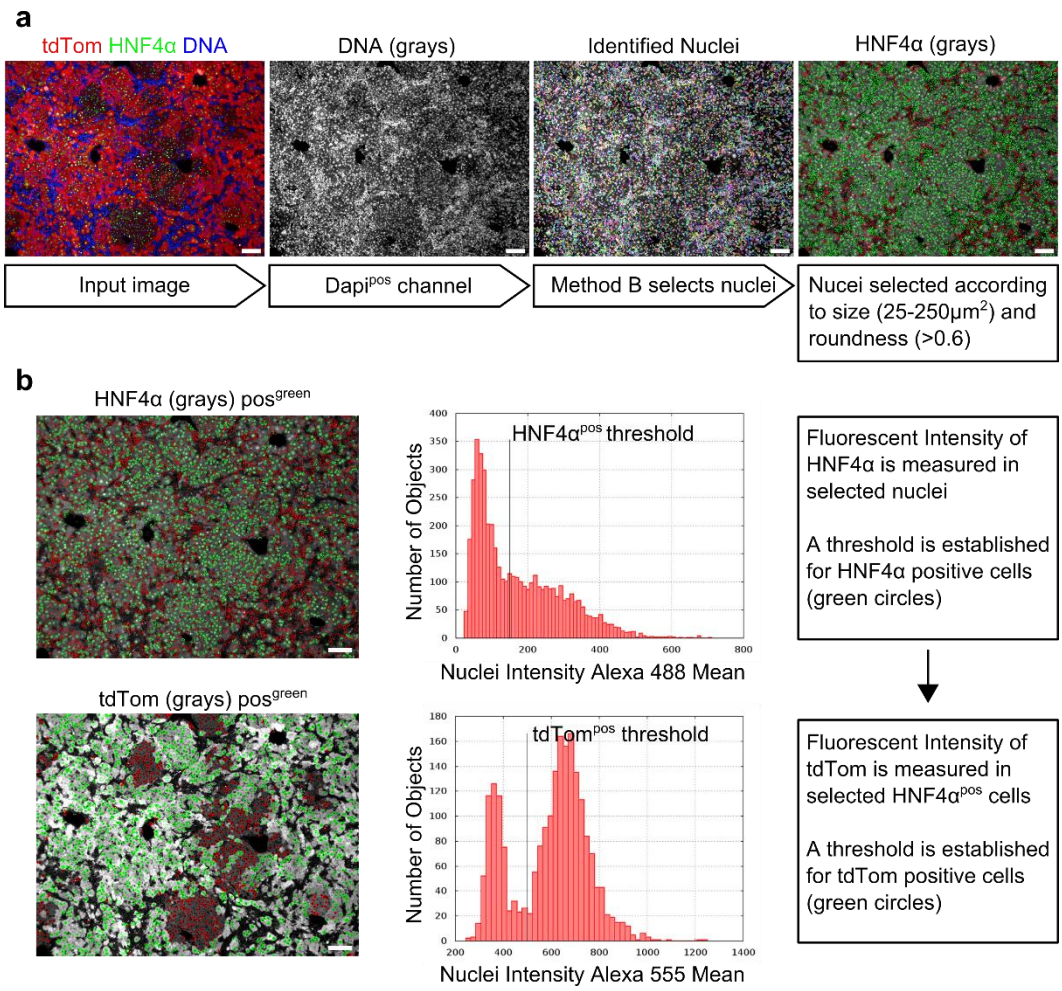

Figure 2.3: A Perkin Elmer Operetta microscope and the analysis software Colombus were used for histological measurements of cell populations. **a**. Example pipeline used to identify cell nuclei in immunofluorescent tissue sections, Method B refers to a pre-existing algorithm created by Perkin Elmer that identifies nucleus like objects. **b**. Example images from DDC/recovery treated β1-Integrin$^{fl/fl}$ liver and their corresponding histograms used to measure nuclei fluorescent intensity and detect HNF4α positive and tdTom positive or negative cell populations. Scale bar: 100μM.

Figure 2.4 – Strategy to measure distribution of labelled hepatocytes in relation to CK19 positive biliary ducts

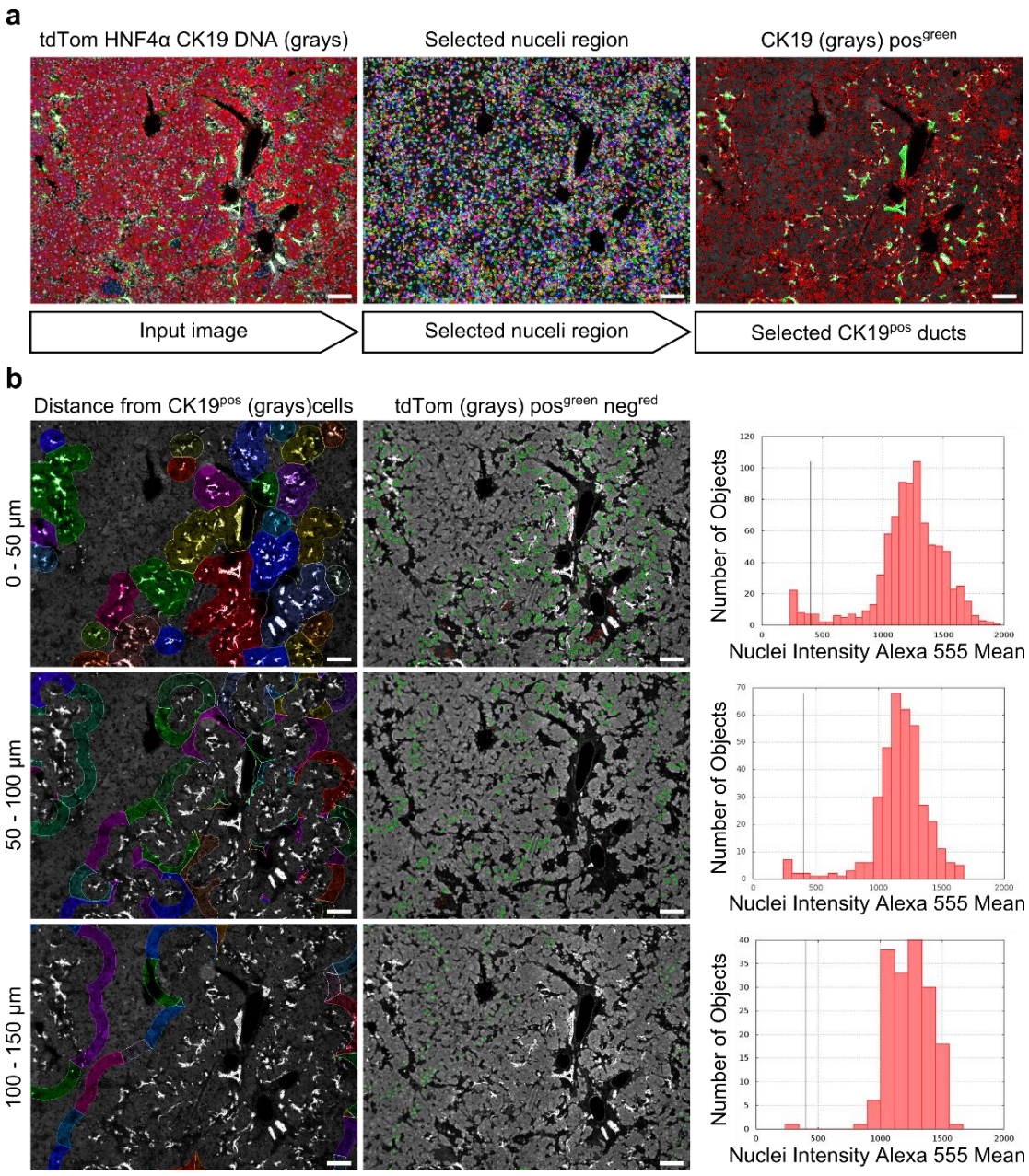

Figure 2.4: A Perkin Elmer Operetta microscope and the analysis software Colombus were used for histological measurements tdTom^{pos} hepatocyte distribution in relation to CK19^{pos} ducts. **a**. Example pipeline used to identify CK19^{pos} cell nuclei in immunofluorescent tissue sections. **b**. Example image segmented in to 50µM zones from the CK19^{pos} ducts, in each zone nuclei fluorescent intensity is measured to detect HNF4α^{pos} hepatocytes which are either tdTom positive (green circles) or negative (red circles). Scale bar: 100µM.

Quantative PCR analysis

Liver tissue was homogenised in Trizol (Life Technologies). Homogenates were mixed with chloroform (1:5 ratio Chloroform:Trizol) and centrifuged at 4°C, 1'200g, for 15 minutes. The aqueous supernatant was removed and mixed 1:1 with 70% ethanol. RNA was extracted using a Qiagen RNeasy mini kit and the manufacturer's instructions. Reverse Transcription and Real Time-qPCR was performed using Qiagen Quantitect and Quantifast reagents on a LightCycler 480 II (Roche). Commercial primers from Qiagen's Quantitect range were used; *Itgb1* (β1-Integrin (Qiagen, QT00155855)); *Wnt7b* (Qiagen, QT00168812); *Wnt9b* (Qiagen, QT00144256); *Wnt11* (Qiagen, QT00103663); *Wnt7a* (QT00131719); *Wnt10* (QT00110089); and peptidylprolyl isomerase A (*PPIA*) (Qiagen QT00247709). Gene expression was normalised to the house keeping gene, *PPIA.* Samples were run in triplicate. The RT2 Profiler PCR Array, Drug Metabolism: Phase I Enzymes was purchased from Qiagen (330231 PAMM- 068Z), and complementary DNA (cDNA) was synthesized from extracted RNA using the RT2 First Stand Kit (Qiagen; 330401) according to the manufacturer's instructions. The RT2 Profiler PCR Array was run on a Roche LightCycler 480 II with RT2 SYBR Green qPCR Mastermix (Qiagen; 330500), an optimal PCR programme was provided by the manufacturer. Analysis were performed using the manufacturer's templates and guidelines.

Protein homogenates and western blots

Protein was isolated from whole liver. Small, 1-2mm^3 pieces of liver were homogenised using a tissue tearor (Biospec Products) and lysis buffer (lysis buffer: 150mM NaCl, 20mM Tris pH7.5, 1mM EGTA, 1mM EDTA, 1% Triton X-100, 2X Protease inhibitor Cocktail(Sigma Aldrich)). Samples were mixed at 4°C for 30 minutes and then centrifuged for 10 minutes at 20'000g. The aqueous supernatant was removed and the protein concentration was determined using a Pierce BCA Protein Assay Kit (Thermo Scientific). Proteins were separated using SDS-page and transferred to nitro cellulose membranes, anti-β1-Integrin (Millipore, MAB1997) 1/1000 and anti-β-actin (Cambridge Biosciences) 1/2000 were used to detect proteins.

Serum analysis

Serum analysis used commercial kits according to the manufacturer's instructions; alanine transaminase, albumin, bilirubin (Alpha Laboratories); aspartate aminotransferase and alkaline phosphatase (Randox laboratories). All kits were adapted for use on a Cobas Fara centrifugal analyser (Roche). Serum analysis was performed by Dr Forbes Howie in the The Queen's Medical Research Institute, University of Edinburgh

Isolation of biliary ducts and hepatocytes and FACS.

Hepatocytes and biliary ducts were isolated using the classical perfusion protocol. Briefly, animals received an overdose of anaesthetic followed by laparotomy: the portal vein was cannulated and injected with Liver Perfusion Medium (Gibco) and Liver Digest Medium (Gibco). For duct isolation, ducts were digested and isolated as previously described[86]. For hepatocyte isolation, the liver was removed and mechanically disaggregated. The resulting disassociated cells were filtered through a 70 μ m filter (BD Biosciences). Hepatocytes were purified with a density gradient centrifugation[286], which isolated cells with hepatocyte morphology and expression of CYP2D6 (a mature hepatocyte marker) at a purity greater than 99%[87]. Briefly, cells were layered above various Percoll solutions: 1.06, 1.08, and 1.12 mg ml−1 Percoll (Sigma) in PBS. Cells were spun at 750g for 20 min. The hepatocyte layer, between the 1.08 and 1.12 mg ml−1 Percoll layers, was collected for Fluorescence Activated Cell Sorting (FACS). Purified hepatocytes were sorted on a BD Biosciences Fusion Flow Cytometer. Sorted cells where lysed and the RNA was extracted

RNA sequencing analysis

Whole liver RNA was extracted (see RNA isolation section), RNA integrity was analysed and RNA integrity number (RIN) scores determined using a Agilent 2100 Bioanalyzer and RNA Nano chip. RNA with a RIN >8 was used for RNA sequencing. mRNA enrichment (by poly-A capture), library construction and sequencing was

performed by GATC-Biotech, Germany. Analysis was done on count data by Dr Jonathan Manning. Counts were normalised with the Trimmed Mean of M values method[287] as implemented in the EdgeR method of Bioconductor (version 3.12)[288]. Differential analyses were carried out with edgeR, adjusting for the effect of gender, and for ease of interpretation a final matrix was generated using limma's removeBatchEffects method[289], with the effect of gender removed. The Gene set library was downloaded from version 5.0 of the molecular signatures database[290,291]. Identifiers for the gene set was mapped to mouse via homology relationships downloaded from the MGI database (HOM_MouseHumanSequence.rpt, downloaded 28th August 2015)[292]. Differences in gene set expression between experimental groups were examined via the statistically robust ROAST method[293], as implemented in the limma package of Bioconductor (version 3.27.4)[289].

For whole genome RNA sequencing (RNA-Seq) of hepatocytes. Samples were treated with DNase (Ambion), and sample integrity verified on an Agilent Bioanalyser with the RNA Nano chip. Illumina Tru-Seq paired end strand specific sequencing (Illumina, USA) was performed on a NextSeq-550 sequencer by the Edinburgh Clinical Research Facility, Western General Hospital, Edinburgh, UK. Total RNA (500 ng) underwent ribosomal RNA depletion before purification, fragmentation, random hexamer cDNA generation, and purification with AMPure XP beads (Beckman-Coulter, USA). Multiple indexing adapters were ligated to double-stranded cDNA with subsequent hybridization onto flow cells, and DNA fragment enrichment by 15-cycle PCR for sequencing. Completed libraries were quantified by qPCR using a KAPA Illumina Library Quantification Kit (Illumina, USA) before multiplexing in two equimolar pools and running on two flow cells on an Illumina NextSeq 550. Bioinformatics of RNA-Seq data was performed by Dr John Thomson. The resulting FastQ files were mapped to the reference genome (mm9) using the Tophat alignment tool (version 2) on Illumina Basespace software and reads per kilobase per million (RPKM) scores calculated for each gene. Differential gene expression was done using DEseq with cutoffs of log2(fold change) > 2 and adjusted $P < 0.05$ within replicates applied. Global analysis of total RPKM data sets to assess overall transcriptional states was done by calculating and plotting Pearson's correlation scores visualized as a heatmap with Euclidian and Ward clustering applied. Principal component analysis plots were also

performed with the use of Illumina Basespace software. Plots for Pearson's correlation scores with hierarchical clustering were also performed on all genes displaying significant gene expression changes relative to the control set. Visual examples of the transcriptional data were generated by calculating the average expression per group (control, β1-integrein$^{fl/fl}$, AAV8-p21, and biliary duct) and loading onto the Broad Institute's Integrative Genomics Browser (https://software.broadinstitute.org/software/igv/download). RPKM values for select gene sets (hepatocyte, biliary, Notch signalling, and Wnt signalling) were also clustered by Euclidian and Ward methods and expression

Statistical Analysis

The use of the letter 'N' refers to number of biological (mice) replicates used for each experimental condition.

Prism software (GraphPad Software, Inc) was used for all statistical analysis. Data is presented as mean ± s.e.m. n refers to biological replicates. Normal distribution of data was determined using D'Agostino and Pearson omnibus normality test. For parametric data, data significance was analysed using a two-tailed unpaired Students t-test. In cases where more than two groups were being compared, then a one-way ANOVA was used. In cases where two groups were split between two independent variables a two-way ANOVA was used. In instances where the N was too small to determine normal distribution or the data was non-parametric then a two-tailed Mann Whitney U-test was used. F tests were used to compare variances between groups. In cases, which randomisation was used (including animal studies), samples were randomized by a 'blinded' third party before being assessed separate 'blinded' assessor. Un-blinding was performed immediately prior to final data analysis.

Chapter 3

Loss of hepatocyte β1-Integrin induces liver injury and ductular reaction

Introduction

HPCs in the ducts can, hypothetically, differentiate to hepatocytes. However, murine lineage tracing studies have produced contradictory results; either reporting a small HPC contribution to the hepatocyte epithelium[149,150] or none at all[56,153,156,159,166]. These previous investigations used different lineage tracing methods with, established, hepatotoxic diet models, CDE and DDC, to stimulate liver injury and provoke HPC derived regeneration. Although these models induced DR, it is questionable whether the toxic diet models recapitulated the impaired hepatocyte regeneration seen in human chronic liver disease[33,42] as hepatocyte division and regeneration still occured[87,156]. In an environment where hepatocyte regeneration is compromised, as shown in the AhCre MDM2$^{fl/fl}$ model where loss of MDM2 leads to an accumulation of p53 in hepatocytes and subsequent senescence, transplanted, biliary derived, HPCs can regenerate the hepatocyte epithelium[87]. To determine if there is an endogenous non-hepatocyte source of regeneration, when the regenerative ability of the hepatocyte epithelium is compromised, I established a model that impairs hepatocyte regeneration and simultaneously labels the hepatocyte epithelium.

Ablation of β1-Integrin in an acute liver injury model reduced hepatocyte growth factor signalling and impaired hepatocyte regeneration[263]. I decided to utilise this phenotype with a transgene and viral Cre system that conditionally deletes β1-Integrin from hepatocytes to impair their regenerative capabilities. The transgene *Itgb1*$^{fl/fl}$ contains loxP sites flanking exon 3, which, when exposed to Cre recombinase results in an excision of exon 3 and a frameshift mutation, preventing translation and a loss of the β1-integrin protein[254]. Throughout this thesis, mice homozygous for the *Itgb1*$^{fl/fl}$ alleles will be referred to as β1-Integrin$^{fl/fl}$ and control mice without the *Itgb1*$^{fl/fl}$ alleles will be designated β1-Integrin^{WT}. To lineage trace recombined cells a *ROSA26*^{LSL}*tdTomato* transgene was also included; activation of this transgene via Cre mediated excision of the Stop codon labels cells with a fluorescent, heritable, genetic marker, tdTomato (tdTom). The *Itgb1* KO alleles and the *ROSA26*^{LSL}*tdTomato* reporter only become activated in the presence of Cre. To Specifically target Cre expression to hepatocytes I employed a hepatotropic virus, AAV8.TBG.Cre[74,156], to ablate β1-Integrin and concurrently label hepatocytes with tdTom. The adeno-

associated virus 8 serotype has a high tropism for hepatocytes, this, combined with the hepatocyte specific thyroid binding globulin (TBG) promoter restricts Cre expression only to hepatocytes[74] (Figure 2.1a, page 32).

This chapter aims to describe the *Itgb1*$^{fl/fl}$ and *ROSA26*^{LSL}*tdTomato* transgenic model I used to study liver regeneration. I will describe the recombination efficiency and specificity of the AAV8.TBG.Cre system and the impact of hepatocyte β1-integrin deletion on liver homeostasis.

Results

AAV8.TBG.Cre labelled 99.5% of the hepatocytes in the liver

To lineage trace hepatocytes the AAV8.TBG.Cre (AAV8^{Cre}) virus was administered to both β1-Integrin$^{fl/fl}$ and β1-Integrin^{WT} mice aged between 6-8 weeks, liver tissue was then analysed 14 days later. The hepatotropic virus targeted the *ROSA26*^{LSL}*tdTomato* locus labelling HNF4α^{pos} hepatocytes tdTom positive (Figure 3.1a, top left image). In contrast, *ROSA26*^{lsl}*tdTomato* mice treated with an AAV8.TBG.null (AAV8^{null}) virus did not express tdTom in HNF4α^{pos} hepatocytes (Figure 3.1a, bottom left image). To quantify the recombination efficiency of the AAV8^{Cre} a Perkin Elmer Operetta imaging system was used to measure tdTom fluorescent intensity in HNF4α^{pos} hepatocytes, figure 2.3 presents an example of the analysis pipeline. Using this method, AAV8^{Cre} was shown to have a recombination efficiency of 99.5% in the hepatocyte population (Figure 3.1b). AAV8^{Cre} did not label any other cells in the liver, particularly the CK19^{pos} biliary ductal cells (Figure 3.1a).

To ensure a similar recombination efficiency was occurring in the β1-Integrin$^{fl/fl}$ mice the analysis was repeated. No difference in AAV8^{Cre} recombination efficiency was detected between β1-Integrin^{WT} mice and β1-Integrin$^{fl/fl}$ mice (Figure 3.1a and b).

Figure 3.1 – AAV8.TBG.Cre labels 99.5% hepatocytes

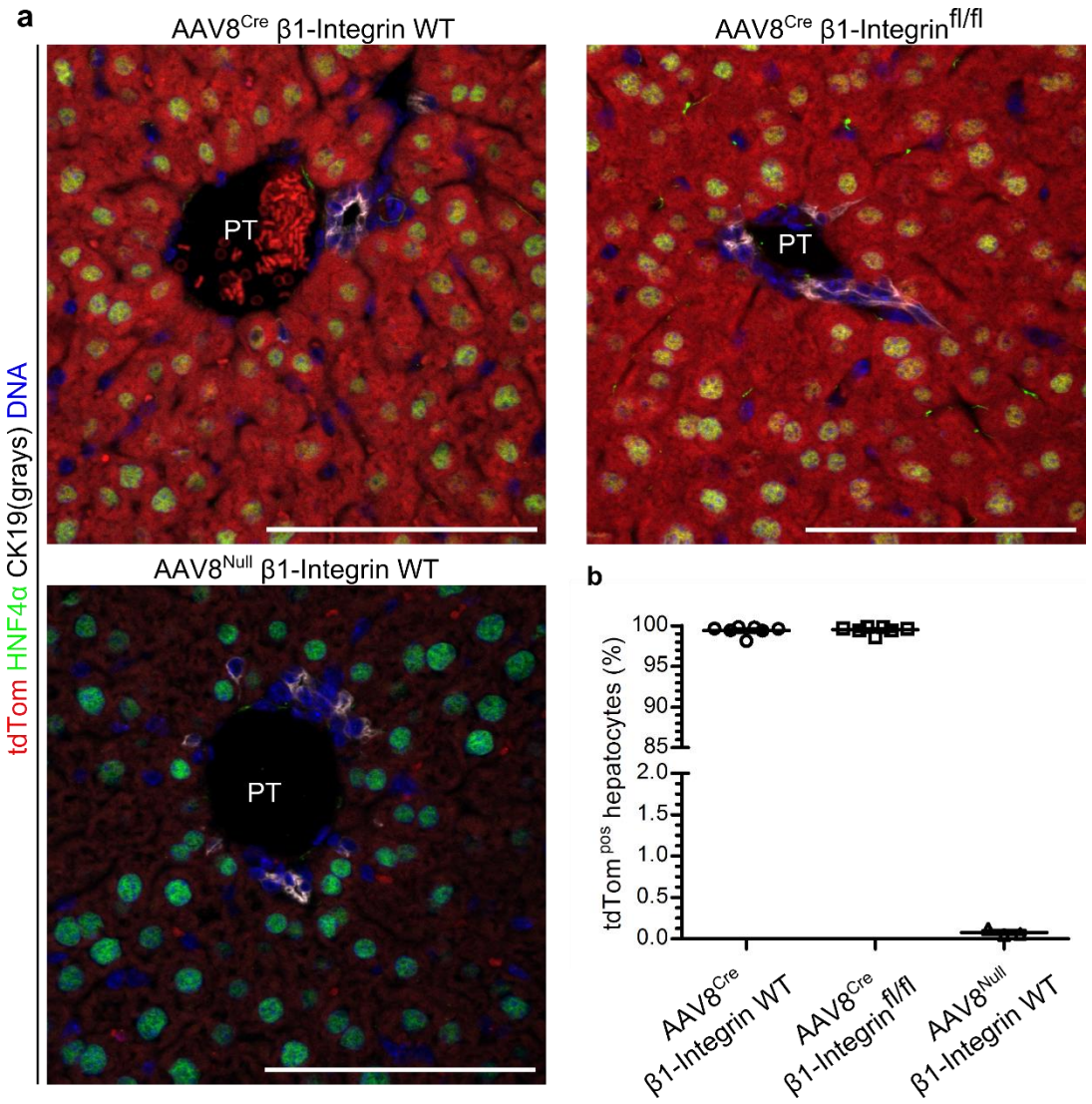

Figure 3.1: **a**. 14 days post AAV8.TBG.Cre ($AAV8^{Cre}$) intravenous administration, tdTom/HNF4α/CK19 immunofluorescent confocal images, $AAV8^{Cre}$ labels $HNF4\alpha^{pos}$ hepatocytes. **b**. Tissue quantification measuring $tdTom^{pos}$ $HNF4\alpha^{pos}$ hepatocytes after either $AAV8^{Cre/null}$ administration, 99.5% hepatocytes are tdTom positive in $AAV8^{Cre}$ treated livers. N=7 for $AAV8^{Cre}$ mice per condition, N=3 for $AAV8^{null}$ mice. The experiment was performed twice. PT = Portal tract. Scale bars: 100µM.

AAV8.TBG.Cre ablated β1-Integrin from hepatocytes

The AAV8^{Cre} recombined *loxP* sites at the *ROSA26*^{lsl}*tdTomato* locus 14 days after administration. To verify that AAV8^{Cre} was also targeting the *loxP* sites in the *Itgb1* gene, liver sections were stained with an anti-β1-Integrin antibody and whole liver *Itgb1* expression was assessed using qPCR. At the protein level hepatocyte β1-Integrin could be detected in β1-Integrin^{WT} livers, demonstrated by membrane positive fluorescent staining, which co-localised with the membrane marker β-Catenin (Figure 3.2a, white arrows). Compared to β1-Integrin$^{fl/fl}$ livers where hepatocyte membrane β1-Integrin expression could not be detected, except on small non-parenchymal cells (Figure 3.2a, white arrowheads). Western blots of whole liver homogenates for β1-Integrin supported the immunofluorescence data, with a reduction in β1-Integrin protein in the β1-Integrin$^{fl/fl}$ samples (Figure 3.2b and c). Consolidating the protein analysis, assessment of whole liver *Itgb1* expression with qPCR revealed a significant reduction in the β1-Integrin$^{fl/fl}$ liver (Figure 3.2d).

Figure 3.2 – AAV8^{Cre} ablated β1-Integrin from β1-Integrin$^{fl/fl}$ hepatocytes

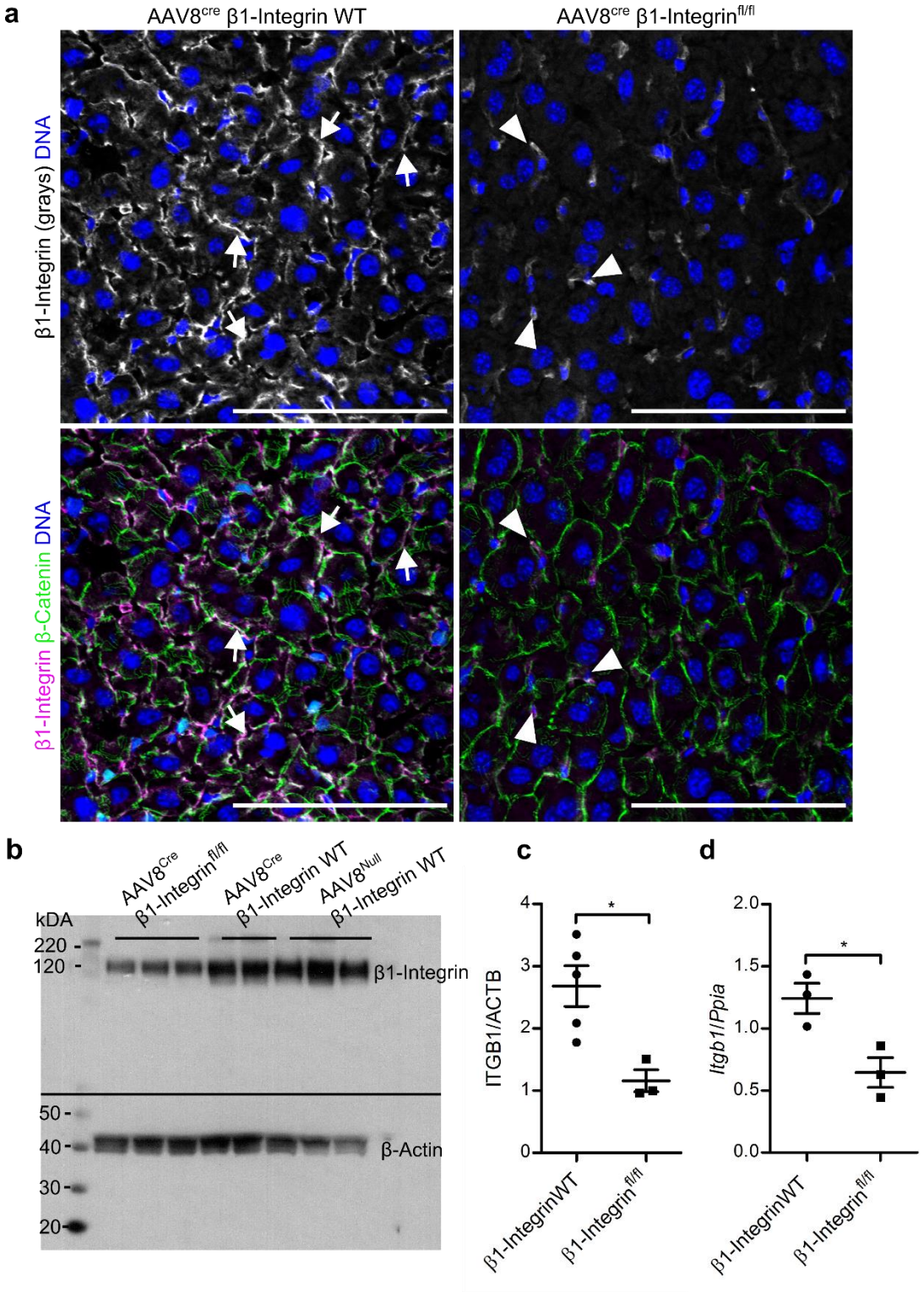

Figure 3.2: **a**. 14 days post AAV8.TBG.Cre ($AAV8^{Cre}$) intravenous administration, β1-Integrin/β-Catenin immunofluorescent confocal images, $AAV8^{Cre}$ ablates β1-Integrin from $\beta\text{-Catenin}^{pos}$ hepatocyte membranes in $\beta1\text{-Integrin}^{fl/fl}$ mice in contrast to $\beta1\text{-Integrin}^{WT}$ mice (white arrows). **b-d**. $AAV8^{Cre}$ reduces whole liver β1-Integrin protein and gene expression in $\beta1\text{-Integrin}^{fl/fl}$ mice. **c**. Image densitometry of western blot gel, measuring relative ITGB1 in relation to ACTB. **d**. QPCR measuring relative *Itgb1* expression in relation of the house keeping gene *Ppia*. Data are means ± s.e.m.; two-tailed unpaired student t-test; * P=0.05. N=3 mice. The experiment was performed once. Scale bars: 100μM.

Hepatocyte β1-Integrin ablation caused liver injury

To evaluate the impact AAV8.TBG.Cre/null infection had on liver function serum markers associated with liver function (LFTs) were assessed 14 days post viral administration. Although there was variation between biological replicates, the mean LFT values for each group; $AAV8^{Cre}$β1-$Integrin^{WT}$, $AAV8^{Cre}$β1-$Integrin^{fl/fl}$ and $AAV8^{null}$β1-$Integrin^{WT}$ were similar to published healthy LFT values (Figure 3.3a-e).

Ablation of β1-Integrin did not cause abnormal LFTs two weeks after $AAV8^{Cre}$ treatment, to test if β1-Integrin ablation effected liver homeostasis over a longer period liver tissue and serum was analysed 9 weeks post $AAV8^{Cre}$ injection (Figure 3.4a). Serum ALT was raised in the β1-$Integrin^{fl/fl}$ mice; other serum markers of liver function were not significantly different but there was greater variation in the LFTs from the β1-$Integrin^{fl/fl}$ mice compared to the controls (Figure 3.4b).

To assess other markers of liver damage, the acknowledged 'Danger Associated Molecular Pattern' (DAMP) protein HMGB1 was stained for using immuno-histochemistry. HMGB1 was restricted to the nucleus of hepatocytes in β1-$Integrin^{WT}$ mice, this differed from the β1-$Integrin^{fl/fl}$ mice where a mixture of hepatocytes had either nuclear or cytoplasmic HMGB1 expression (Figure 3.4c, white arrowheads and arrows). A proportion of the hepatocytes that had cytoplasmic HMGB1 expression no longer expressed nuclear HMGB1.

Long term loss (9weeks) of hepatocyte β1-Integrin caused liver injury, to assess hepatocyte regeneration cell markers of proliferation, Ki67, and cell cycle arrest, p21, were stained for using immuno-fluorescence. 7.4% of the hepatocytes in the injured, β1-Integrin ablated, livers were positive for the proliferation marker Ki67 (Figure 3.5a, c). This was 10 times higher when compared to the healthy β1-$Integrin^{WT}$ samples where infrequent $Ki67^{pos}$ hepatocytes were detectable (Figure 3.5a, white arrows). 2% of hepatocytes were $p21^{pos}$ in the β1-$integrin^{fl/fl}$ samples, 20 times higher when compared to β1-$Integrin^{WT}$ livers which expressed rare, 0.2%, $p21^{pos}$ hepatocytes.

Figure 3.3 – Serum biochemistry 2weeks after viral AAV8$^{Cre/null}$ treatment

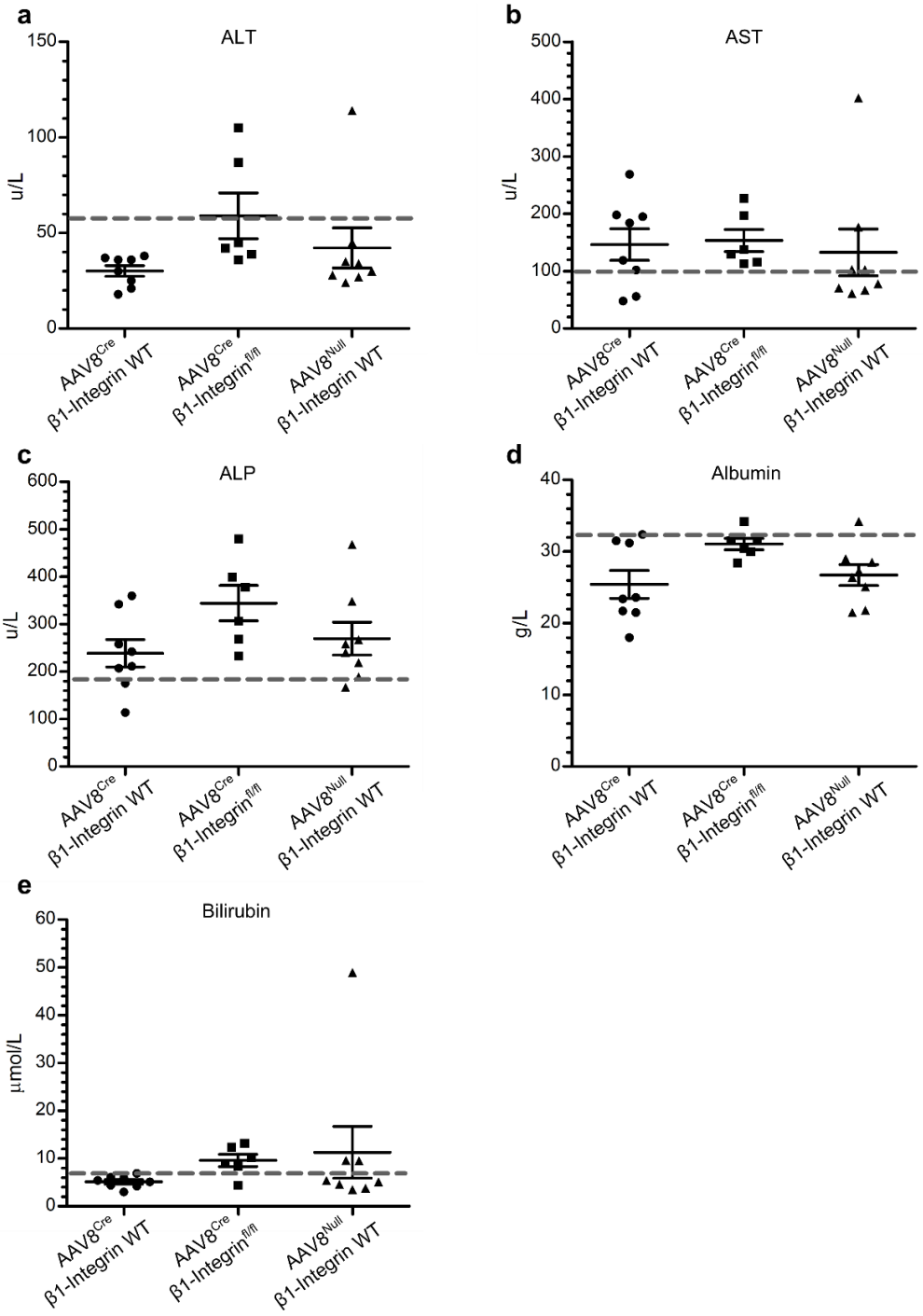

Figure 3.3: Serum biochemical markers of liver function 2 weeks post AAV8 intravenous administration, **a**. Alanine transaminase (ALT) **b**. Aspartate transaminase (AST) **c**. Alkaline phosphatase (ALP) **d**. Albumin and **e**. Bilirubin. Grey dashed lines represent mean values for published, healthy, age matched, C57 bl6 mice[294,295]. Data are means ± s.e.m.; N=6-8 mice. The experiment was performed twice.

Figure 3.4 – β1-Integrin$^{fl/fl}$ mice developed makers of liver injury 9 weeks after AAV8^{Cre} administration

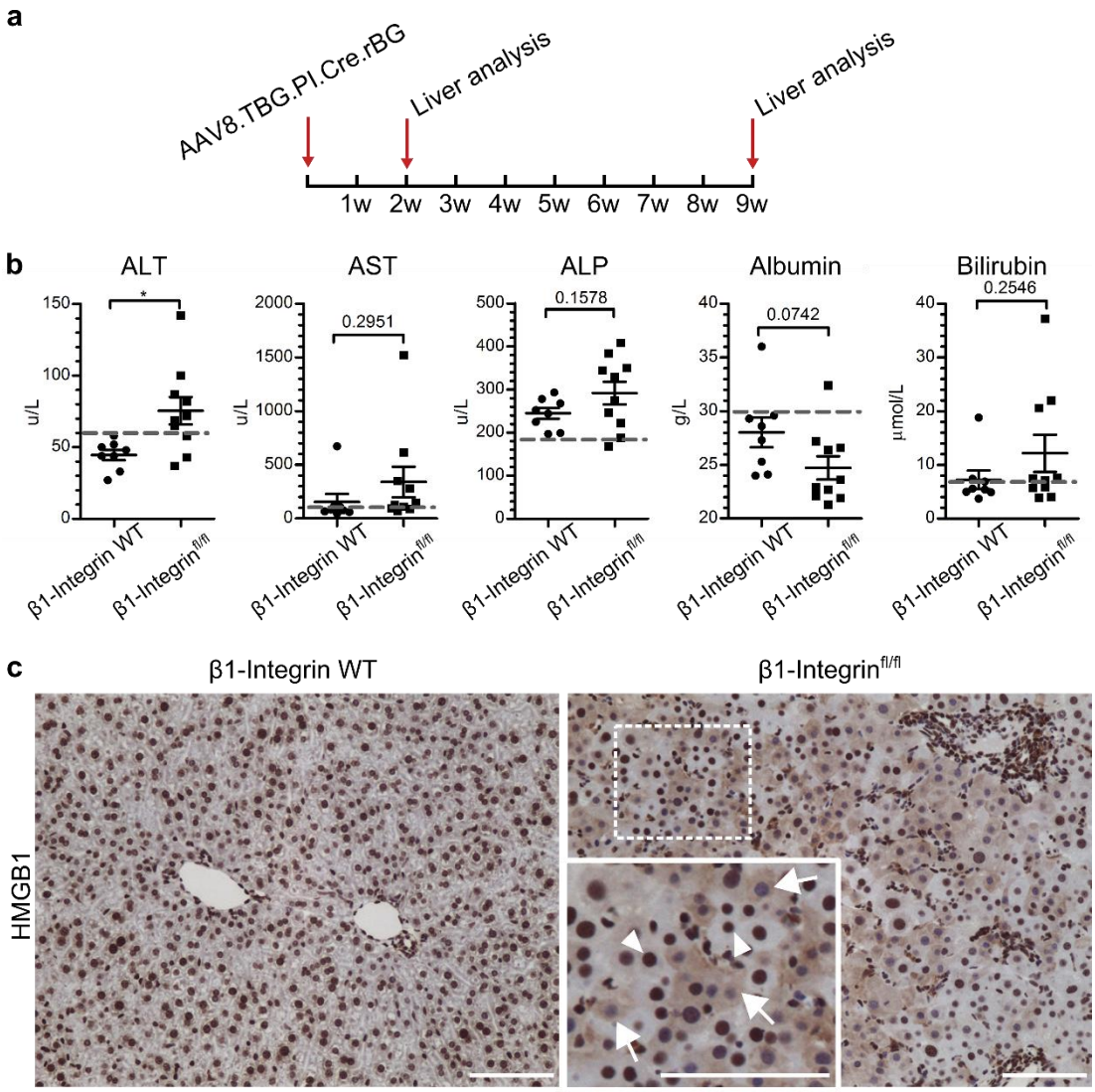

Figure 3.4: **a**. Experimental timeline **b**. Serum biochemical markers of liver function 63 days post AAV8^{Cre} intravenous administration, Alanine transaminase (ALT), Aspartate transaminase (AST), Alkaline phosphatase (ALP), Albumin and Bilirubin. Grey dashed lines represent mean values for published, healthy, age matched, C57 bl6 mice[294,295]. **c**. HMGB1 immuno-histochemistry 9 weeks post AAV8^{Cre} administration, β1-Integrin$^{fl/fl}$ samples had hepatocytes where HMGB1 had translocated from the nucleus to the cytoplasm (white arrows). Data are means ± s.e.m.; two-tailed unpaired t-test; * P=0.05, ** P=0.01. N=9 mice. The experiment was performed twice Scale bars: 100µM.

Figure 3.5 - β1-Integrin$^{fl/fl}$ livers had abnormal Ki67 and p21 expression 9 weeks after AAV8^{Cre} treatment

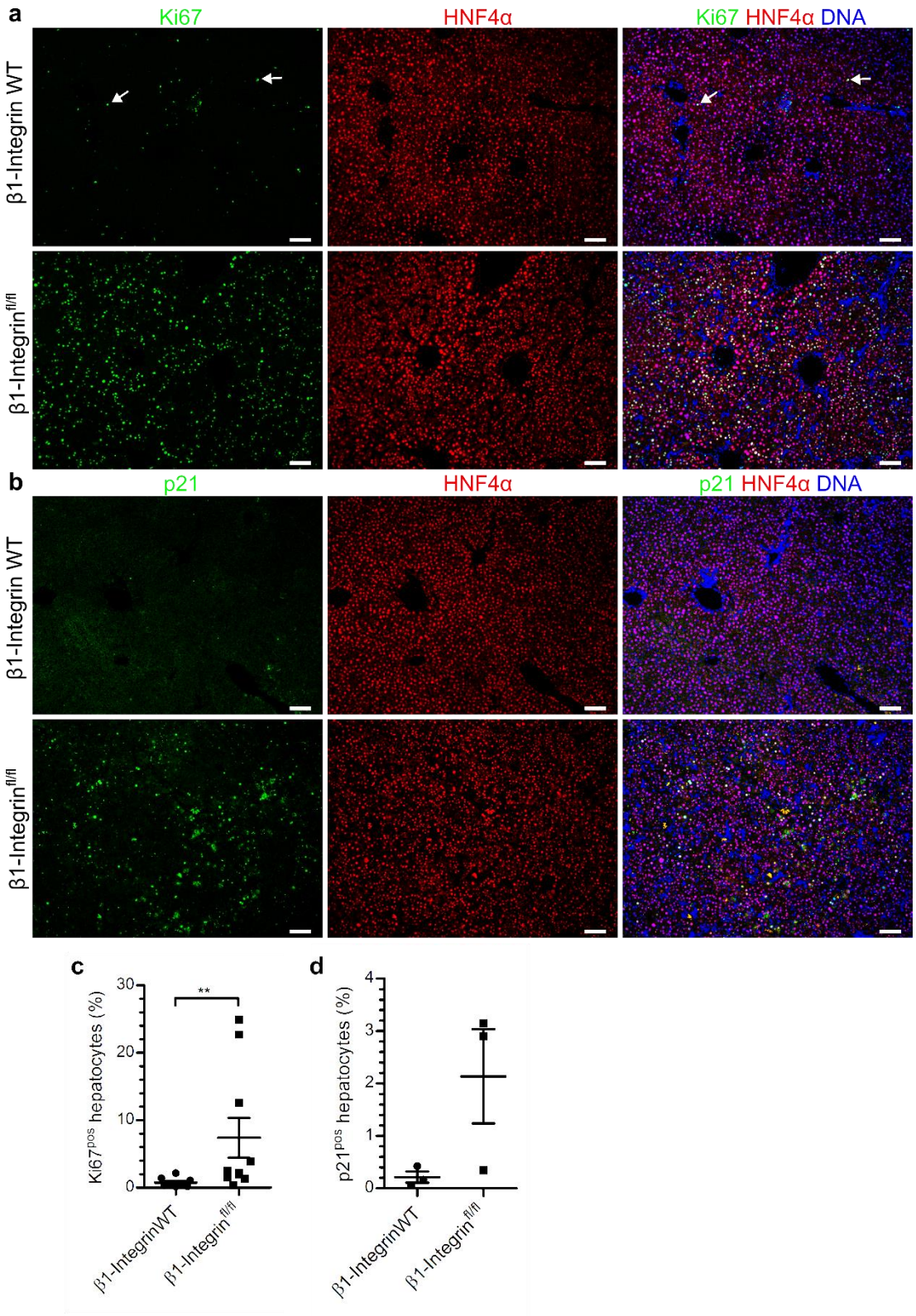

Figure 3.5: **a,b.** 9weeks post AAV8^{Cre} administration, Ki67/HNF4α and p21/HNF4α immunofluorescence. **c**, **d**. Single cell quantification measuring Ki67 and p21 in HNF4α^{pos} hepatocytes, Ki67 and p21 expression are raised in β1-Integrin$^{fl/fl}$ livers. N=3 for p21 measurements and N=8 for Ki67 measurements. Data are means ± s.e.m.; Mann-Whitney U test; ** P=0.01. The experiment was performed twice. Scale bars: 100μM.

Aberrant bile canaliculi structure in β1-Integrin ablated livers

Loss of β1-Integrin from hepatocytes caused liver injury stimulating both parenchymal proliferation and cell cycle arrest. To determine if there were any further abnormalities, specifically to tissue architecture, Haematoxylin and Eosin (H&E) histochemical stains were performed. H&E staining of β1-Integrin$^{fl/fl}$ samples revealed the presence of infiltrating cords of cells, disseminated throughout the parenchyma (Figure 3.6a, yellow arrowheads).

To study the bile canaliculi in the β1-Integrin$^{fl/fl}$ livers immunohistochemistry for the Multi-Dug Resistance protein (MDR1) was performed. MDR1 staining showed changes to the bile canaliculi structure in β1-Integrin$^{fl/fl}$ livers. In normal homeostatic conditions, as seen in the β1-Integrin^{WT} livers, MDR1 is expressed at the apical domain of the hepatocyte surface, labelling the canaliculi between adjacent hepatocytes (Figure 3.6b; black arrows). Loss of β1-Integrin disrupted the canaliculi structure; MDR1 staining revealed aberrant, multi-branched canaliculi (Figure 3.6b; black arrowheads). Further immunofluorescent staining of E-Cadherin and MDR1 also highlighted changes to the hepatocyte epithelium morphology and structure, caused by β1-Integrin loss.

Figure 3.6 – β1-Integrin ablated livers had abnormal bile canaliculi

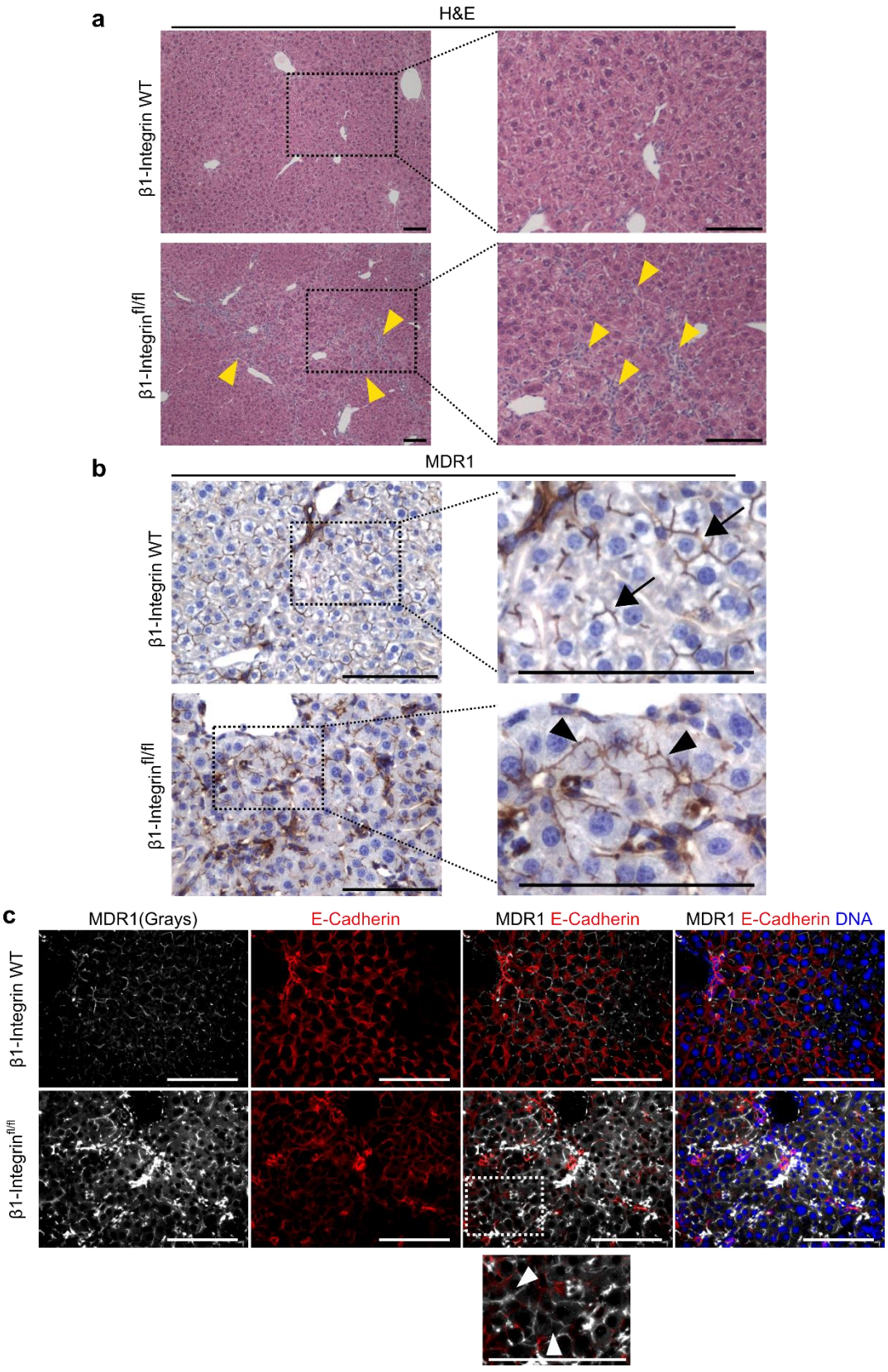

Figure 3.6: **a**. Haematoxylin and Eosin (H&E) histochemistry 9 weeks post AAV8^{Cre}; β1-Integrin$^{fl/fl}$ livers had abnormal liver tissue architecture and small infiltrating cells were present (yellow arrowheads). **b**. Anti-MDR1 immunohistochemistry 9 weeks post AAV8^{Cre}; β1-Integrin$^{fl/fl}$ livers had aberrant bile canaliculi (black arrowheads) compared to β1-Integrin^{WT} livers (black arrows). **c**. E-Cadherin/MDR1 Immuno-fluorescence; white arrowheads highlight bile canaliculi 9 weeks post AAV8^{Cre} administration. Images are representative from stains performed on N=3 mouse samples per experimental group. Scale bars: 100μM.

β1-Integrin ablated livers had prominent ductular reactions

An anti-CK19 antibody was used to assess the distribution and amount of biliary ductal cells in β1-Integrin$^{fl/fl}$ and β1-Integrin^{WT} livers that had received AAV8^{Cre} and a 9-week incubation period. β1-Integrin$^{fl/fl}$ livers had a remarkably different biliary ductal arrangement compared to the β1-Integrin^{WT} livers, where the ductal cells had a typical morphology, were arranged in to ducts and were located to the portal tract (Figure 3.7a, upper panels, arrowheads). In the β1-Integrin$^{fl/fl}$ livers a prominent, invasive, DR could be identified (Figure 3.7a, lower panels, arrows and 3.7b), there were significantly more, approximately 3-fold increase, CK19^{pos} biliary ductal cells, which had an atypical morphology appearing elongated. The CK19^{pos} cells in the β1-Integrin$^{fl/fl}$ liver were no longer restricted to the portal tract, disseminating out in to the parenchyma (Figure 3.7d).

Ductular reactions are associated with an activated stromal cell, the myofibroblasts, which are α-smooth muscle actin (αSMA) positive. Dual immuno-fluorescence revealed the presence of αSMA^{pos} myofibroblasts with the invasive CK19^{pos} biliary ductal cells (Figure 3.7a). Quantification of αSMA^{pos} cells showed a significant, 3-fold, increase in the β1-Integrin$^{fl/fl}$ liver (Figure 3.7c).

Figure 3.7 – Hepatocyte β1-Integrin loss induced ductular reaction

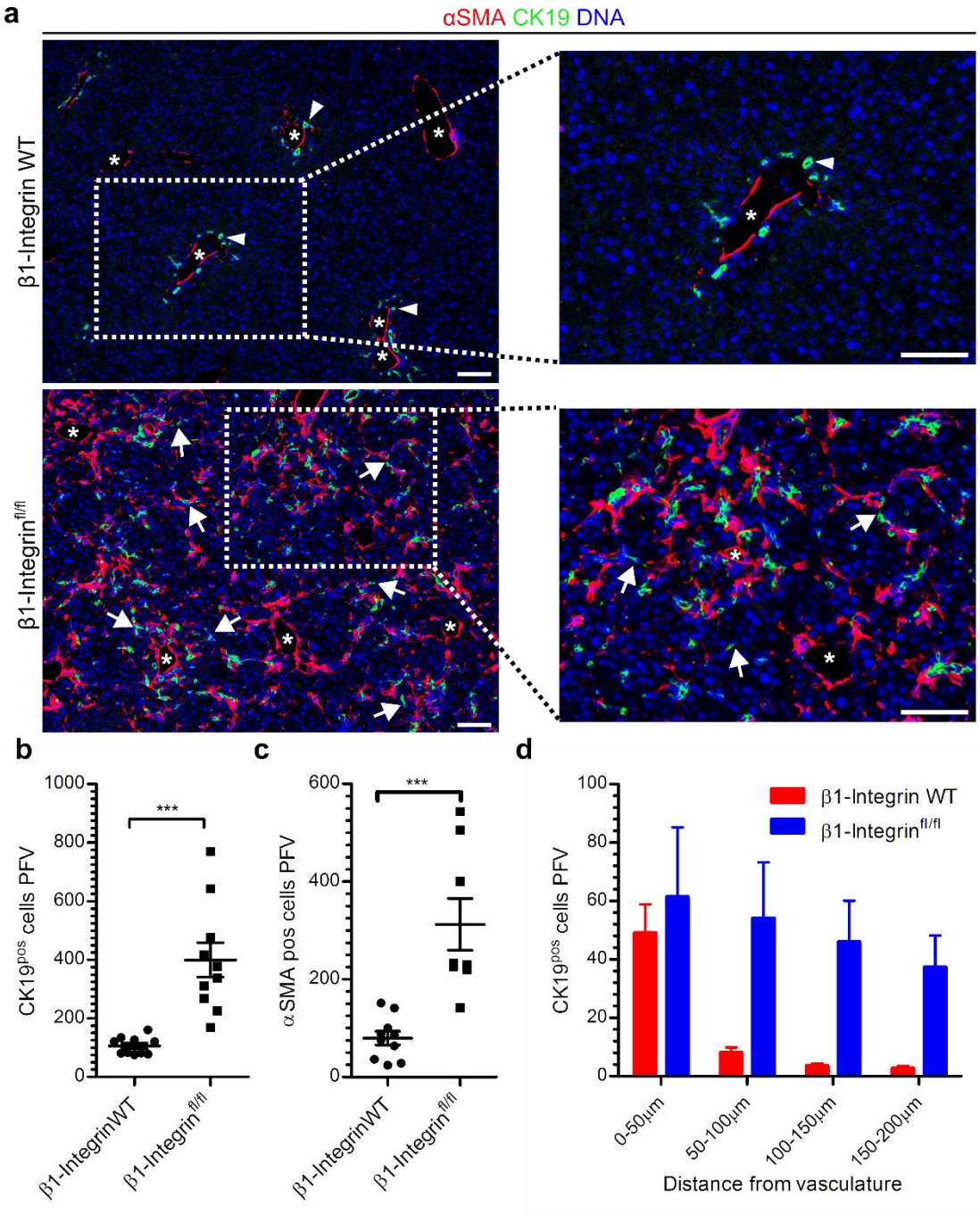

Figure 3.7: **a**. 9 weeks post AAV8^{Cre} administration αSMA/CK19 Immuno-fluorescence, white arrowheads highlight normal CK19^{pos} biliary cell arrangement in the β1-Integrin^{WT} liver, white arrows highlight atypical CK19^{pos} biliary ductal cells undergoing ductular reaction. **b**. and **c**. Single cell quantification measuring CK19^{pos} and αSMA^{pos} cells. PFV=per field of view. **d**. Single cell quantification measuring CK19^{pos} cells distribution in relation to large vessels (white asterisks in panel **a**.) Data are means ± s.e.m.; Man-Whitney U test; *** P=0.0001, N=≥6 biological replicates. Experiment was repeated twice. Scale bars: 100μM.

Hepatocyte β1-Integrin ablation reduced tdTom labelling in hepatocytes, leading to periportal patches of tdTom^{neg} hepatocytes

Long-term hepatocyte β1-Integrin loss disrupted homeostasis and caused liver injury, to determine if this phenotype had also altered the cellular source of regeneration I assessed hepatocyte tdTom expression in the liver.

Analysis of tdTomato expression in hepatocytes 2 weeks after AAV8^{Cre} revealed a 99.5% recombination efficiency (Figure 3.1b). Prolonged loss of hepatocyte β1-Integrin caused a decrease in the number of labelled hepatocytes, with 84% of hepatocytes tdTom^{pos} after 9 weeks (Figure 3.8a and b). In contrast, the control, β1-Integrin^{WT} livers, maintained a 99.5% tdTom labelling efficiency of the hepatocyte epithelium. The degree of tdTom^{neg} hepatocytes in β1-Integrin$^{fl/fl}$ livers varied greatly from 1% to 46% of the total hepatocyte population.

Further histological inspection of the tdTomato negative (tdTom^{neg}) hepatocytes revealed that they were in small patches adjacent to the portal tract (PT) (Figure 3.8a) and not the glutamine synthetase (GS) positive hepatocytes that are adjacent to the central vein (CV).

Figure 3.8 – Long-term β1-Integrin loss caused a reduction in hepatocyte labelling

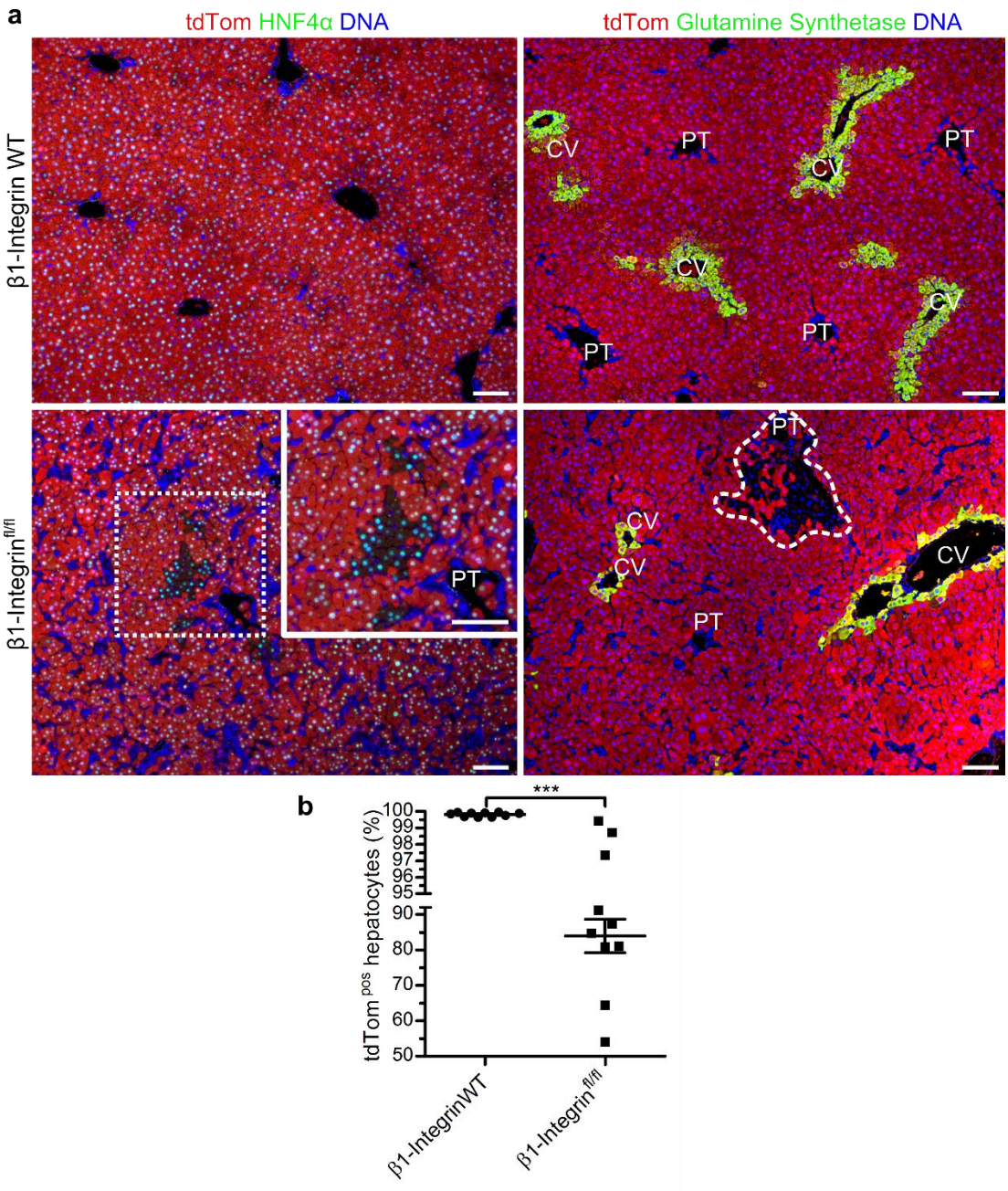

Figure 3.8: **a**. 9 weeks post AAV8^{Cre} administration tdTom/HNF4α and tdTom/Glutamine Synthetase immuno-fluorescence, β1-Integrin$^{fl/fl}$ livers had small, periportal, patches of tdTom^{neg} HNF4α^{pos} hepatocytes; PT = portal tract, CV = central vein. **b**. Single cell quantification measuring tdTom^{pos} HNF4α^{pos} hepatocytes. Data are means ± s.e.m.; Man-Whitney U test; *** P=0.0001. N=≥6 biological replicates. Experiment was repeated twice.; Scale bars: 100μM.

Discussion

Loss of hepatocyte β1-Integrin impairs hepatocyte regeneration in acute liver injury[263], however the long-term effect of β1-Integrin loss in the liver has not been previously described. Initial loss of β1-Integrin from the hepatocyte epithelium, 2 weeks post AAV8^{Cre} treatment, did not appear to effect liver homeostasis. This is to be expected as β1-Integrin is a highly stable protein *in vivo*, remaining at the cell membrane for approximately 10 days[266] and therefore any phenotype resulting from β1-Integrin loss would not be obvious at day 14. However, at the later time point 9 weeks' post AAV8^{Cre}, β1-Integrin ablation had disrupted liver homeostasis. There were elevated makers of hepatocyte damage and gross changes to the tissue architecture noticeable by the aberrant bile canaliculi and prominent DRs infiltrating the parenchyma. AAV8^{Cre} administration and the subsequent expression of tdTom in β1-Integrin^{WT} hepatocytes did not appear to cause any gross abnormalities to the tissue architecture. MDR1 staining of the bile canaliculi was normal and biliary epithelial cells were restricted to the portal tract in typical duct formation. Confirming the phenotype observed in the β1-Integrin$^{fl/fl}$ liver was exclusively caused by loss of β1-Integrin and not by the AAV8 virus or expression of tdTom.

The nature of the liver injury caused by β1-Integrin ablation was different to commonly used mouse hepatotoxic models as it did not produce significantly different serum LFT results when compared to the control β1-Integrin^{WT} mice. A plausible reason for this lack of difference would be the timescale of the experiment relative to the magnitude of the injury. The half-life of the serum transaminases (ALT and AST) is between 17-48 hours[296] and therefore any large changes to these serum markers would be undetectable over the prolonged injury caused by β1-Integrin loss, similar to what is seen in the clinic with human cirrhotic patients[296]. Serum ALP, albumin and bilirubin have a longer half-life ranging from 7-20 days, although some β1-Integrin$^{fl/fl}$ mice did have noticeable changes to the levels of these markers, with a trend to increase for ALP and bilirubin and decrease for albumin, there was no significant differences. To investigate other markers of liver injury I assessed the spatial distribution of a recognised liver DAMP, HMGB1[297,298]. Release of HMGB1 from its common, healthy position in the nucleus to the cytoplasm of hepatocytes in the β1-

Integrin$^{fl/fl}$ mouse suggests that it is acting as a DAMP for injured β1-Integrin deficient hepatocytes.

The pathophysiology caused by β1-Integrin loss could involve multiple mechanisms, the disruption of growth factor signalling has been previously mentioned[263]. Additional features recognised in this chapter such as the loss in hepatocyte epithelial integrity and activation of inflammatory pathways through DAMPs could also be contributing to liver injury. The integrin adhesome has multiple cellular functions[244] and it is therefore difficult to ascertain how perturbations to the integrin adhesome by deletion of β1-Integrin specifically damages hepatocytes.

AAV8.TBG.Cre mediated β1-Integrin ablation did not completely remove β1-Integrin expression from the liver as it is widely expressed on non-parenchymal cells such as stellate cells/myofibroblasts, endothelial cells and Kupffer cells[263]. However; AAV8^{Cre} did specifically ablate β1-Integrin expression from hepatocytes. This specificity was advantageous as loss of β1-Integrin from other cell types would have added complexity to an already complex phenotype and may have confounded the results.

The labelling efficiency of the AAV8^{Cre}-tdTom system was strikingly robust; 99.5% of the hepatocyte epithelium was tdTom positive, rare non-recombined hepatocytes were occasionally detected. This recombination efficiency makes the AAV8^{Cre}-tdTom system a powerful tool to detect non-hepatocyte derived regeneration as any non-hepatocyte source of regeneration would dilute the 99.5% epithelial labelling. In the healthy β1-Integrin^{WT} liver the hepatocyte epithelium retained a 99.5% labelling efficiency 9 weeks after AAV8^{Cre} treatment, confirming that under homeostatic conditions hepatocytes are the sole source of regeneration[127,156,157]. In contrast, the defective β1-Integrin$^{fl/fl}$ liver showed a marked decrease in the number of labelled hepatocytes. Patches of tdTom^{neg} hepatocytes were found in the hepatocyte epithelium of all β1-Integrin$^{fl/fl}$ mice. These patches appeared periportally which suggested they were not randomly distributed through the parenchyma. There was also great variation in the degree of tdTomato labelled hepatocytes between livers from the β1-Integrin$^{fl/fl}$ mice. This variation could be caused by the extended duration (9weeks) of the experiment, allowing for large differences between samples to form. A better

understanding of the β1-Integrin$^{fl/fl}$ disease mechanism may also explain the large variation.

Additionally, the β1-Integrin$^{fl/fl}$ liver had prominent ductular reactions, recognisable by the invasive, atypical CK19^{pos} cells and neighbouring activated αSMA^{pos} myofibroblasts. The ductular reaction also had a peri-portal origin, coinciding with the appearance of the tdTom^{neg} hepatocytes. This observation supports a hypothesis that a biliary derived HPC in the ductular reaction can regenerate the hepatocyte epithelium by differentiating in to tdTom^{neg} hepatocytes.

These data together demonstrate that AAV8.TBG.Cre mediated β1 Integrin ablation causes parenchymal damage, triggering both hepatocyte regeneration and a ductular reaction with 16% of parenchymal regeneration emanating from a non-parenchymal origin. To investigate whether this non-parenchymal contribution is enhanced during toxic liver injury I will injure both β1-Integrin^{WT} and β1-Integrin$^{fl/fl}$ livers and evaluate the emergence of tdTom^{neg} hepatocytes.

Chapter 4

Liver injury diets combined with hepatocyte β1-Integrin deletion results in a delayed regenerative response from cells of non-hepatocyte origin

Introduction

The deletion of hepatocyte β1-Integrin disrupted liver homeostasis and resulted in the appearance of small un-labelled periportal hepatocyte patches, implying hepatocyte regeneration can derive from a non-hepatocyte origin. To further stimulate non-hepatocyte derived regeneration, I decided to induce liver injury and regeneration using injury diets that contain hepatotoxic agents. I damaged β1-integrin^{WT} and β1-integrin$^{fl/fl}$ livers with three independent regimes: DDC (3,5-diethoxycarbonyl-1,4-dihydrocollidine) diet, methionine and choline deficient (MCD) diet, and thioacetamide (TAA) in the drinking water. DDC imitates human cholestatic liver disease, causing ductular reaction and portal fibrosis[280,299], in severe incidents bile infarcts arise causing parenchymal necrosis. MCD, a model of NASH, has a high fructose and fat content, the absence of methionine and choline disrupts mitochondrial β-oxidation and the synthesis of low density lipoprotein resulting in steatosis, inflammation, necrosis and liver fibrosis[281]. TAA is a model of liver fibrosis, which, when applied chronically can generate liver cancer. The pathophysiology of TAA arises when TAA is metabolised in the zone 1 and zone 3 hepatocytes, generating reactive oxygen species that disrupt the cell's macro-molecules, resulting in necrosis and eventually fibrosis[281].

Utilising these distinct liver injury models, I designed an experiment that involved the initial ablation of hepatocyte β1-Integrin followed by exposure to injury diet and subsequent tissue analysis at various time points in recovery (Figure 4.1). A two week wash out period after AAV8^{Cre} administration was used to ensure no residual AAV8^{Cre} would interfere with hepatocyte labelling during injury and regeneration[156]. Using this experimental approach, I could study the regenerative dynamics in livers with a functioning hepatocyte epithelium (β1-Integrin^{WT}) and a defective one (β1-Integrin$^{fl/fl}$).

Figure 4.1 – Experimental time line to study the regenerative dynamics in β1-Integrin^{WT} and β1-Integrin$^{fl/fl}$ livers after administration of a liver injury diet

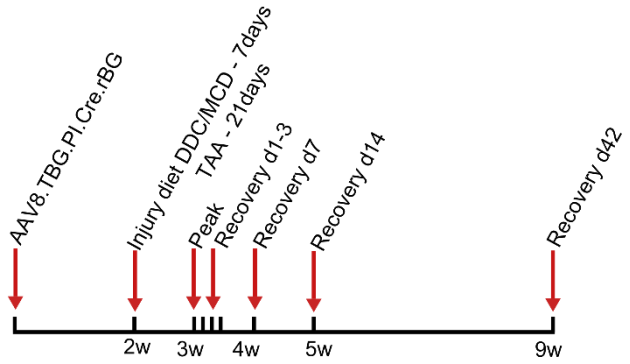

Results

Hepatocyte β1-integrin loss delayed recovery after DDC induced liver injury

To stimulate liver injury and regeneration mice were maintained on a hepatotoxic diet, DDC, for a 7-10-day period. During initial experiments a small proportion of mice from both experimental groups, β1-Integrin^{WT} and β1-Integrin$^{fl/fl}$, exceeded the permitted maximum weight loss limit. These animals were taken off DDC diet before the planned 10-day schedule, therefore a 7-day injury regime became the standard. To assess liver function and the degree of injury caused by DDC, LFTs of blood serum were performed at peak injury and subsequent time points after DDC diet was removed.

LFT measurements in both the β1-Integrin^{WT} and β1-Integrin$^{fl/fl}$ mice were elevated at peak injury indicating that DDC diet had reduced liver function and caused liver injury (Figure 4.2a-d). Mice from the β1-Integrin^{WT} group had higher serum ALT, AST and bilirubin at peak injury compared to the β1-Integrin$^{fl/fl}$ group. However, the high amounts of serum ALT, AST, ALP and bilirubin in the β1-Integrin^{WT} group rapidly decreased during recovery; serum bilirubin returned to normal after 2-days of recovery followed by ALT, AST, ALP at day-7 of recovery. In stark contrast, the β1-Integrin$^{fl/fl}$ group retained elevated serum ALT, AST, ALP and bilirubin, which did not return to normal until day-14 of recovery, with serum ALP and bilirubin increasing further

during the first 3-days of recovery. The LFTs affirmed that DDC diet induces liver injury and indicated that hepatocyte β1-Integrin ablation was delaying the regenerative response.

Changes to body weight can be associated with liver damage, mice were weighed daily to monitor the impact of DDC diet during the experiment. All animals from both the β1-Integrin^{WT} and β1-Integrin$^{fl/fl}$ groups had a transient decrease in body weight when given DDC diet (Figure 4.2e). The β1-Integrin^{WT} group returned to pre-injury body weight 2-days after re-introduction to normal diet. Similar to the trend seen with the serum LFTs, the duration of the β1-Integrin$^{fl/fl}$ groups return to pre-injury body weight was delayed, re-gaining their pre-injury weight 12-days after removal from DDC diet.

To further assess DDC induced liver damage, HMGB1 expression was investigated using immuno-histochemistry. Early in the recovery phase, day-3, cytoplasmic and corresponding nuclear loss of HMGB1 could be detected in a subset of hepatocytes from the β1-Integrin^{WT} and β1-Integrin$^{fl/fl}$ groups, indicating the release of HMGB1 due to injury. Cytoplasmic HMGB1 positive hepatocytes were common around areas of necrosis and more frequent in β1-Integrin$^{fl/fl}$ livers (Figure 4.2f, white arrows).

Figure 4.2 – Hepatocyte β1-integrin ablation resulted in a delayed recovery after DDC induced liver injury

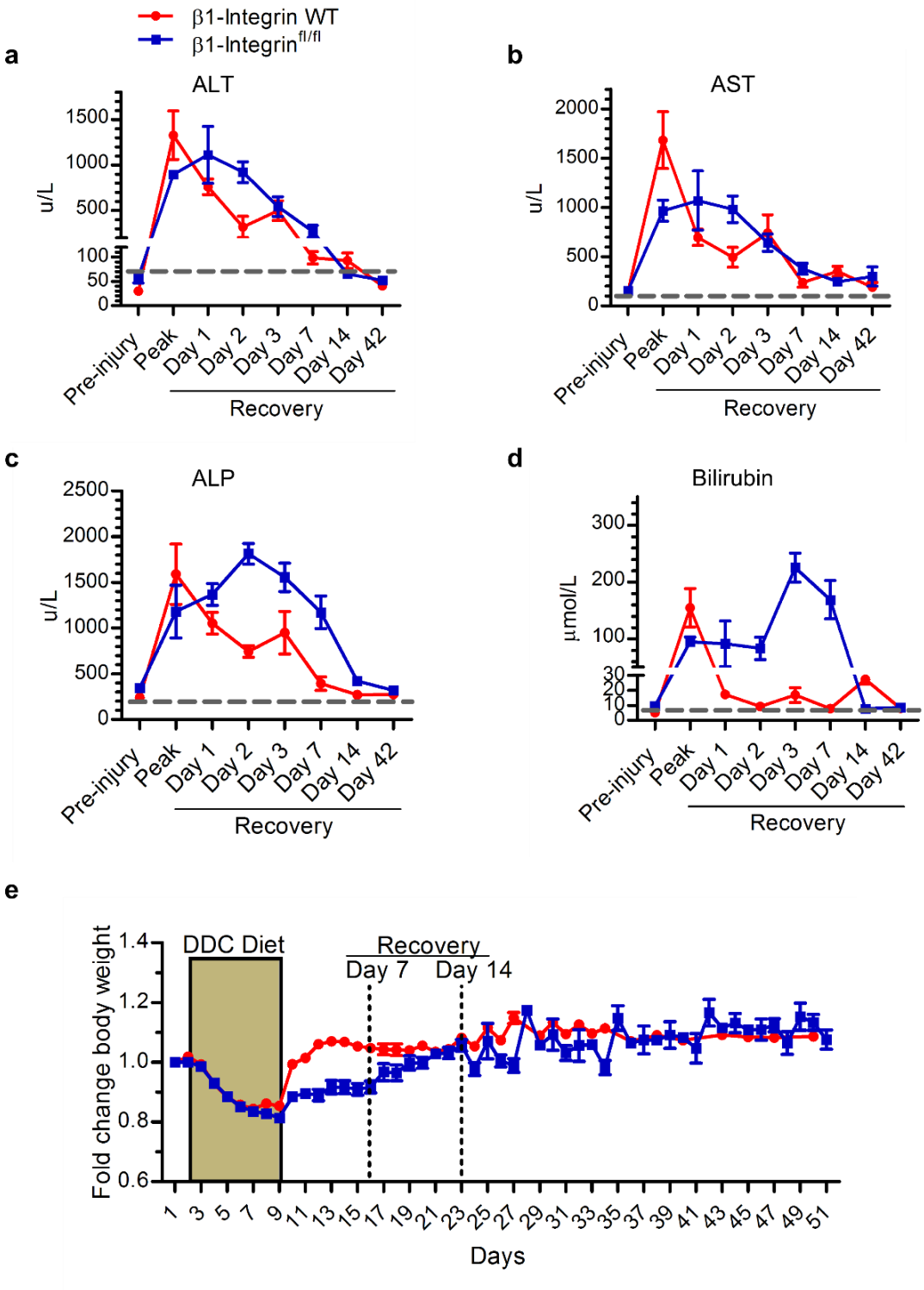

Figure 4.2 – continued

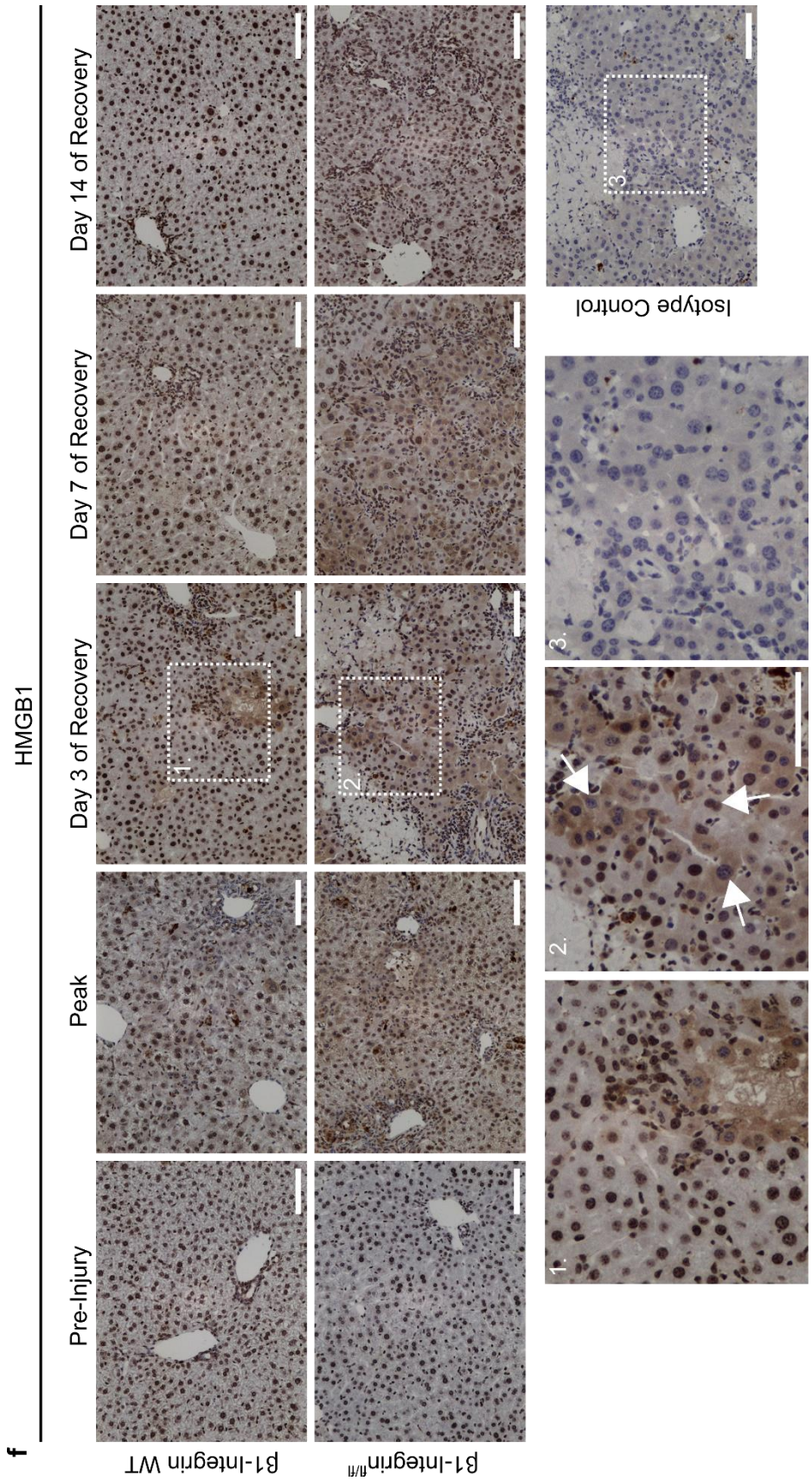

Figure 4.2: **a** – **d**. Serum markers associated with liver function from either β1-Integrin^{WT} or β1-Integrin$^{fl/fl}$ mice before, during and after DDC diet induced liver injury; grey dashed lines represent mean values for published, healthy, age matched, C57 bl6 mice[294,295]. **e**. Mouse body weight measurements during DDC diet and the subsequent recovery. **f**. Immuno-histochemistry for the DAMP HMGB1; High power images correspond to numbered inserts (1-3). Data are means ± s.e.m. N=5 biological replicates; Scale bars: 100μM.

Ki67 and p21 expression was altered after DDC injury in livers with hepatocyte β1-integrin ablation

DDC diet induced liver injury in both the β1-Integrin^{WT} and β1-Integrin$^{fl/fl}$ groups, triggering a delayed recovery phenotype in β1-Integrin$^{fl/fl}$ livers. To determine if the delay was caused by either alterations to proliferation or cell cycle arrest hepatocyte Ki67 and p21 expression were examined.

During the early phase of recovery, between day1-3, both β1-Integrin^{WT} and β1-Integrin$^{fl/fl}$ hepatocytes upregulated Ki67 expression, with a higher proportion of hepatocytes expressing Ki67 in the β1-Integrin^{WT} group (Figure4.3a). Ki67 expression in β1-Integrin^{WT} hepatocytes declined after day-3 of recovery, returning to a constant 4% of all hepatocytes expressing Ki67 by day 7 of recovery (Figure4.3c). In the β1-Integrin$^{fl/fl}$ group 10-12% of all hepatocytes continued to express elevated levels of Ki67, returning to β1-Integrin^{WT} level at Day-14 of recovery.

The β1-Integrin^{WT} and β1-Integrin$^{fl/fl}$ groups had a similar hepatocyte p21 expression profile during the first three days of recovery (Figure4.3b and c). 10-20% of hepatocytes were p21 positive at the end of DDC treatment, increasing to over 20% at day-1 of recovery followed by a decline at day-2 and 3. After day-3 of recovery the expression profiles of the β1-Integrin^{WT} and β1-Integrin$^{fl/fl}$ groups diverged, β1-Integrin^{WT} livers had near undetectable amounts of hepatocyte p21 expression. In contrast, the β1-Integrin$^{fl/fl}$ livers maintained elevated hepatocyte p21 expression, with 10% of hepatocytes p21^{pos} at day 7 of recovery and returning to β1-Integrin^{WT} levels at Day-14 of recovery. Generally, Ki67 and p21 expression was mutually exclusive with rare dual positives occasionally detectable (Figure 4.3d).

The differences in Ki67 and p21 expression between the β1-Integrin^{WT} and β1-Integrin$^{fl/fl}$ groups in recovery followed a developing theme: in the β1-Integrin^{WT} group p21/Ki67 expression declined after Day-3 of recovery, expression was prolonged in the β1-Integrin$^{fl/fl}$ group not declining until after day-7 of recovery. In both groups the decline of p21 and Ki67 expression coincided with the loss of injury markers (Figure 4.2).

Figure 4.3 – DDC diet induced prolonged expression of Ki67 and p21 in hepatocytes after liver injury

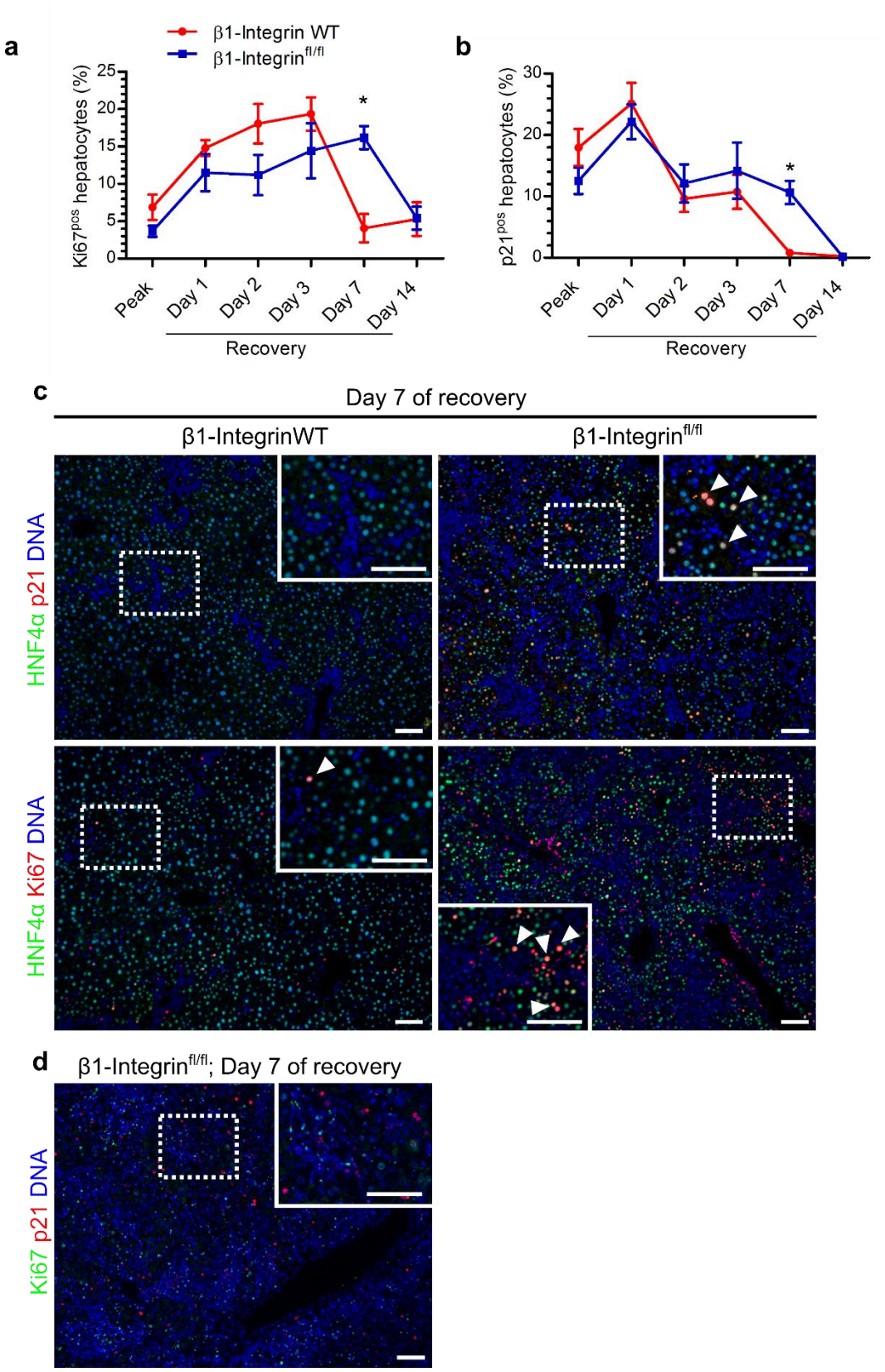

Figure 4.3: **a** and **b**. Quantification of Ki67 and p21 expression in hepatocytes during DDC induce liver injury and subsequent recovery. **c**. Panel of representative images displaying HNF4α/p21 and HNF4α/Ki67 immuno-fluorescence from livers at day 7 of recovery, after DDC induced liver injury. **d**. Ki67/p21 immuno-fluorescent image of β1-Integrin$^{fl/fl}$ liver at day 7 of recovery post DDC induced liver injury. White arrowheads highlight dual positive cells. Data are means ± s.e.m.; 2-way ANOVA with Bonferroni post-test; * P=0.05; N=5 biological replicates. Scale bars: 100μM.

Hepatocyte β1-integrin ablation and DDC injury resulted in a highly necrotic event early in recovery

A hepatocyte proliferation defect did not appear to be causing the β1-Integrin$^{fl/fl}$ associated delay in liver recovery. To ascertain if there was a greater turnover of tissue in the recovering β1-Integrin$^{fl/fl}$ liver a tissue necrosis analysis was performed.

Histological analysis of β1-Integrin^{WT} and β1-Integrin$^{fl/fl}$ livers revealed a higher propensity for necrosis in the β1-Integrin$^{fl/fl}$ group. 12.5% of the parenchyma was necrotic in the β1-Integrin$^{fl/fl}$ livers at peak injury compared to 1.3% in the β1-Integrin^{WT} liver. Between day 1-3 of recovery the β1-Integrin^{WT} liver displayed a transient 3.5-fold increase, 5% of the parenchyma, in necrosis. In contrast, there was a 2-fold decline in necrosis during the first day of recovery in β1-Integrin$^{fl/fl}$ livers, down to 4.4% parenchymal necrotic area, followed by a major necrotic event between day-2 and 3 resulting in 23.5% of the parenchyma becoming necrotic (Figure 4.4a, black asterisks, and b).

The H&E histochemistry used to study liver necrosis also revealed another significant phenotype in the β1-Integrin$^{fl/fl}$ liver. Cords of small cells were observed infiltrating the parenchyma at day-7 and 14 of recovery (Figure 4.4a, black arrows).

Figure 4.4 – β1-Integrin$^{fl/fl}$ livers were highly necrotic early in recovery after DDC induced liver injury

a

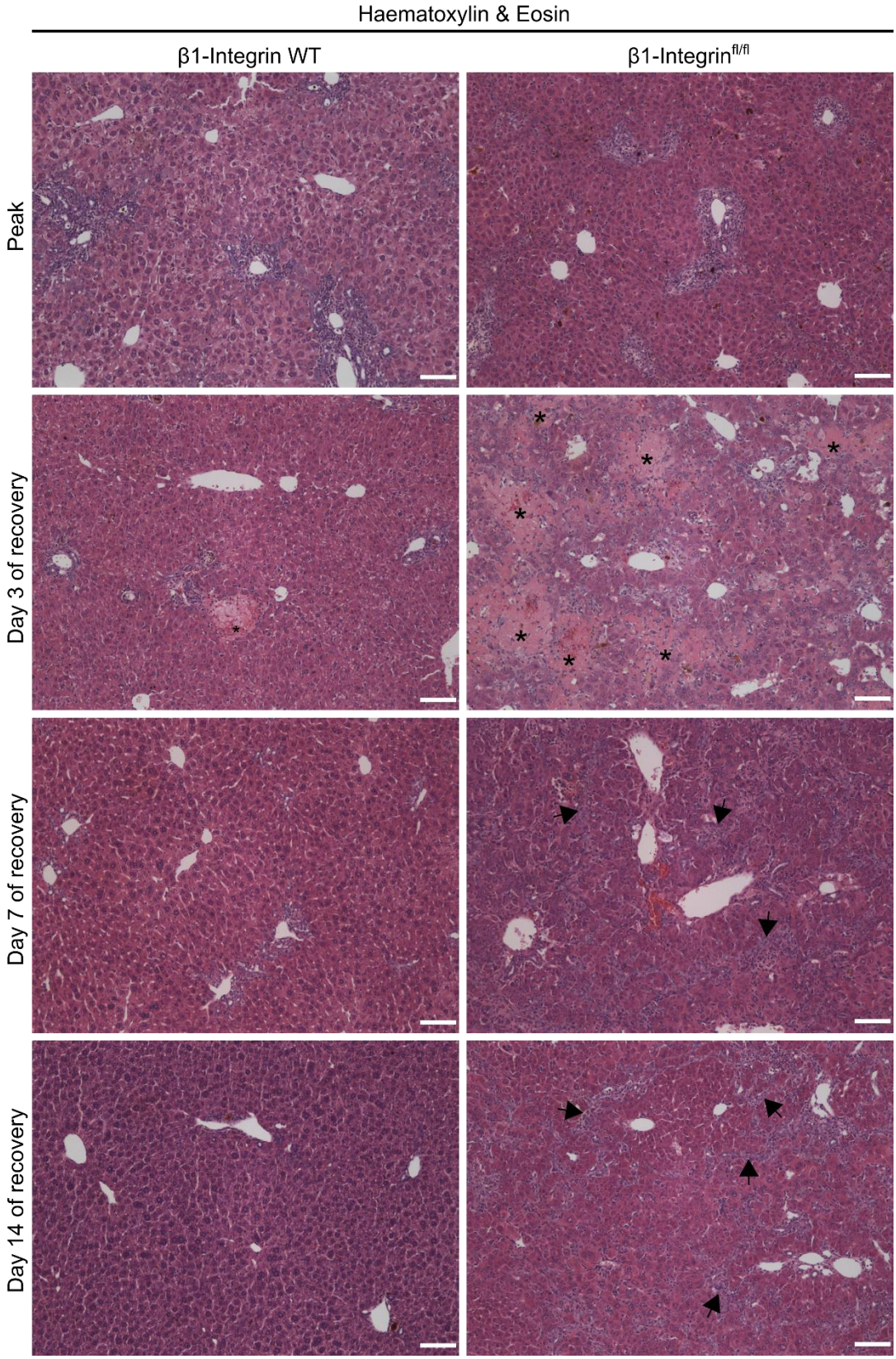

Figure 4.4 – continued

b

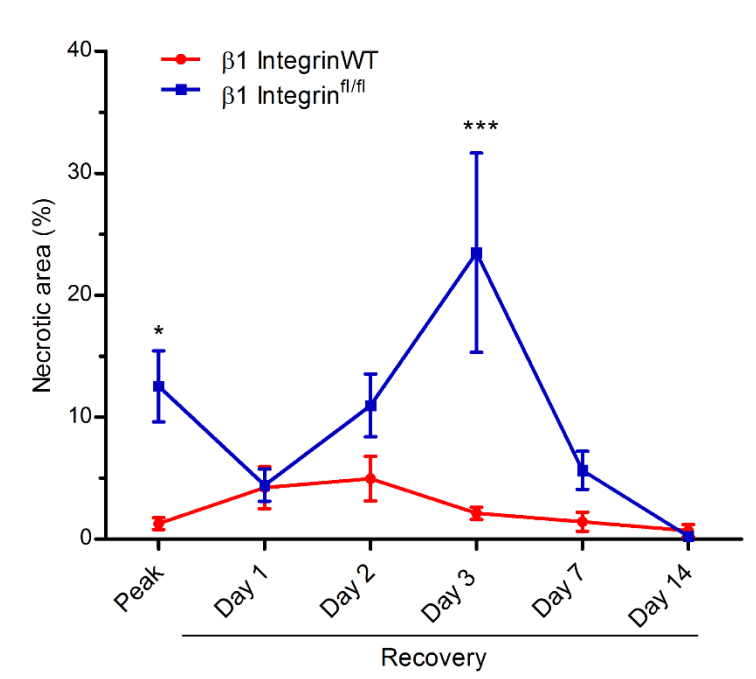

Figure 4.4: **a**. H&E histochemistry from β1-Integrin^{WT} and β1-Integrin$^{fl/fl}$ livers during DDC diet and subsequent recovery; black asterisks = necrotic areas, black arrows = small infiltrating cells. **b**. Necrosis analysis using pixel based image segmentation to measure necrotic areas in H&E sections from β1-Integrin^{WT} and β1-Integrin$^{fl/fl}$ livers. Data are means ± s.e.m.; 2-way ANOVA with Bonferroni post-test; * P=0.05, *** P=0.005; N=5 biological replicates. Scale bars: 100μM.

DDC induced ductular reaction

To further investigate the infiltrating cells detected at day-7 and 14 of recovery in the β1-Integrin$^{fl/fl}$ liver (Figure 4.4a), samples were stained for the biliary epithelial marker CK19. Atypical CK19^{pos} biliary epithelial ductal cells were identified in β1-Integrin$^{fl/fl}$ livers from day 3 of recovery. The atypical ductal cells appeared elongated and invasive (Figure 4.5a white arrowheads) when compared to CK19^{pos} ductal cells in the β1-Integrin^{WT} livers, which were arranged into biliary ducts with lumens (Figure 4.5a white arrows). From day 7 of recovery the atypical biliary epithelial cells in the β1-Integrin$^{fl/fl}$ liver were no longer restricted to the portal tract, disseminating in to the parenchyma (Figure 4.5a and 4.7a). Both the β1-Integrin$^{fl/fl}$ and β1-Integrin^{WT} liver had an approximate 3-fold increase in CK19^{pos} cells during DDC diet induced liver injury, proceeded by a transient decline in CK19^{pos} cells at day 1 and 2 of recovery (Figure 4.5b). The β1-Integrin^{WT} liver had a subsequent CK19^{pos} cell expansion phase between day 3 and 7 of recovery where the number of CK19^{pos} cells increased 4-fold, at day 14 of recovery the number of CK19^{pos} cells had decreased back to pre-injury levels. At day 7 of recovery in the β1-Integrin$^{fl/fl}$ group, quantification of the CK19^{pos} cell population revealed a significant, 8-fold, increase in CK19^{pos} cells (Figure 4.5b). Large amounts of CK19^{pos} cells, remained in the liver during the recovery phase, with elevated CK19^{pos} cell numbers still detectable 42days after removal of DDC diet.

To determine if the β1-Integrin$^{fl/fl}$ DDC diet induced ductular reactions were associated with activated myofibroblasts, sections were stained for the activated myofibroblast marker, αSMA. Large amounts of activated myofibroblasts surrounded the atypical CK19^{pos} ductal cells in the β1-Integrin$^{fl/fl}$ group (Figure 4.5a). There was a 3-fold increase in αSMA^{pos} cells preceding the increase in CK19^{pos} cells, beginning at day-3 of recovery and decreasing after day-7. Quantification of αSMA^{pos} cells in the control, β1-Integrin^{WT} group, revealed a similar profile to the CK19^{pos} cell quantification with an increase at peak injury and day 3-7 of recovery, approximately 300-400 αSMA^{pos} cells PFV, followed by a return to normal, pre-injury, amounts at day 14 of recovery.

Figure 4.5 – Hepatocyte β1-Integrin deletion combined with DDC induced liver injury enhanced ductular reaction during recovery

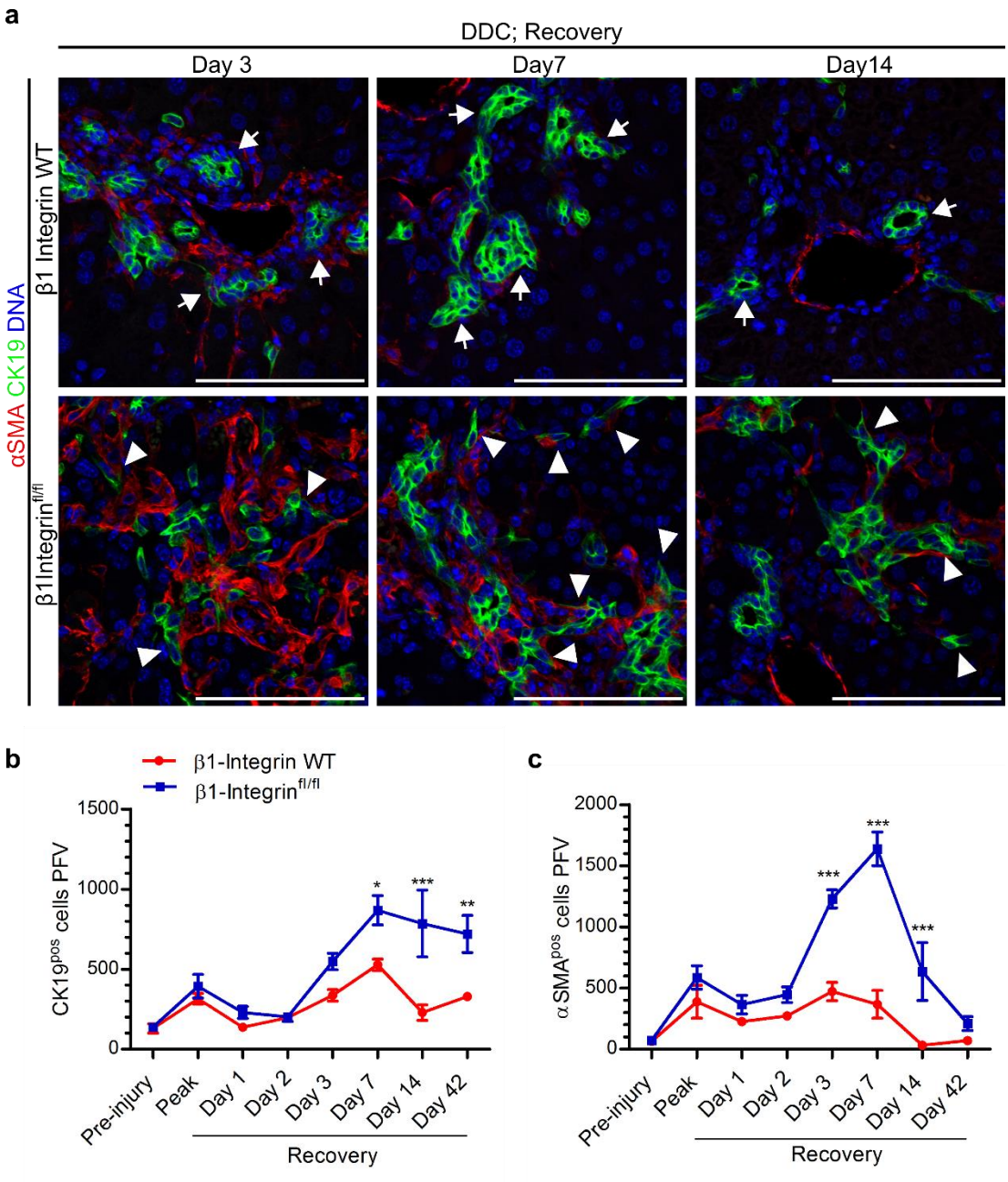

Figure 4.5: **a**. Confocal images of ductular reaction, αSMA/CK19 immuno-fluorescence on β1-Integrin^{WT} and β1-Integrin$^{fl/fl}$ livers at various time points after DDC induced liver injury; white arrows = typical biliary ductal cells, white arrowheads = atypical biliary ductal cells. **b** and **c**. Single cell quantification measuring CK19^{pos} cells and αSMA^{pos} cells in β1-Integrin^{WT} and β1-Integrin$^{fl/fl}$ livers before, during and after DDC induce liver injury. PFV=per field of view. Data are means ± s.e.m.; 2-way ANOVA with Bonferroni post-test; * P=0.05, ** P=0.01, *** P=0.005; N=5 biological replicates. Scale bars: 100μM.

β1-integrin ablation and DDC injury resulted in liver fibrosis

Ductular reactions are associated with liver fibrosis, to determine if the β1-Integrin$^{fl/fl}$ DDC diet induced ductular reaction had accompanying fibrosis, livers were stained for collagen with PicroSirius Red (PSR). DDC induced periportal liver fibrosis in both the β1-Integrin^{WT} and β1-Integrin$^{fl/fl}$ groups (Figure4.6a and b). In the β1-Integrin$^{fl/fl}$ group fibrosis continued to increase, but was no longer confined to the portal tract, forming bridging, fibrous septa.

Figure 4.6 – β1-Integrin$^{fl/fl}$ livers developed substantial fibrosis after DDC induced liver injury

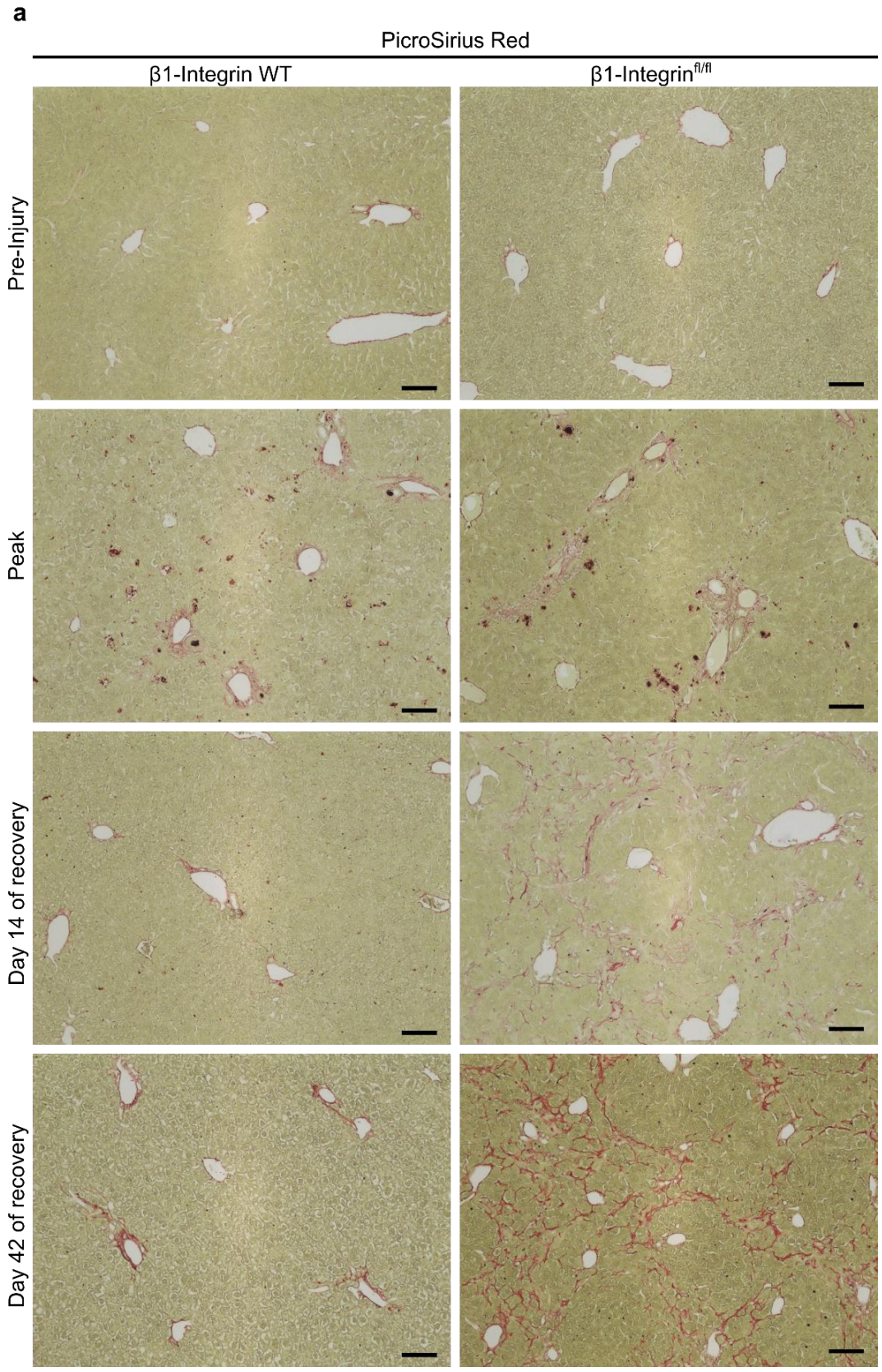

Figure 4.6 – continued

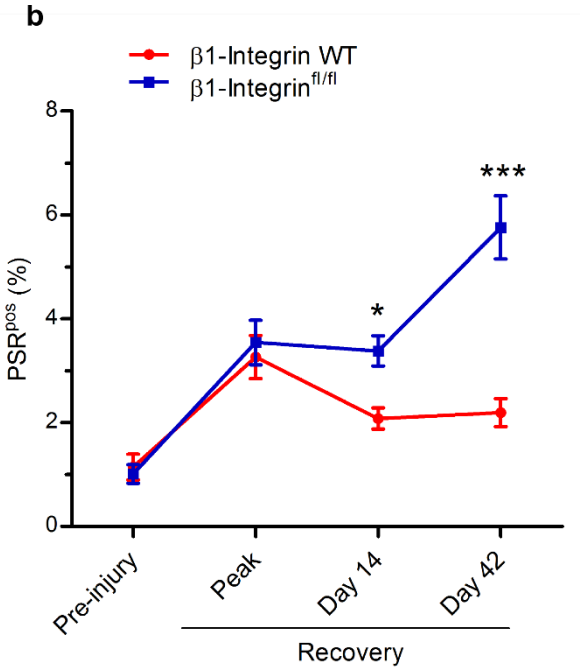

Figure 4.6: **a**. PicroSirius Red (PSR) histochemistry from β1-Integrin^{WT} and β1-Integrin$^{fl/fl}$ livers during DDC diet and subsequent recovery. **b**. Fibrosis analysis, percentage of pixels PSR positive, before, during and after DDC injury. Data are means ± s.e.m.; 2-way ANOVA with Bonferroni post-test; * P=0.05, *** P=0.005; N=5 biological replicates. Scale bars: 100µM.

DDC injury and subsequent regeneration reduced hepatocyte labelling in the β1-Integrin$^{fl/fl}$ liver

There was greater cell death and a prolonged regenerative period in the β1-Integrin$^{fl/fl}$ group; to determine if the hepatocyte epithelium was the only source of cell regeneration tdTomato labelling in the liver was investigated. In β1-Integrin deficient livers large areas of the parenchyma were tdTom^{neg} (Figure 4.7a, insert 2) at day-14 of recovery. CK19^{pos} ductal cells were predominantly distributed between the remaining tdTom^{pos} cells (Figure 4.71, insert 1 white arrows). In contrast, livers from the β1-Integrin^{WT} group had no tdTom^{neg} patches, the parenchyma was completely tdTom^{pos} and CK19^{pos} ductal cells were in the bile ducts at the portal tract (Figure 4.7a, insert 3 and 4, white arrowheads).

The tdTom^{neg} cells identified in the β1-Integrin$^{fl/fl}$ liver expressed the mature hepatocyte markers CYP2D and HNF4α (Figure 4.8b and 4.9a). Interestingly, at peak injury tdTom^{pos} cells lost their CYP2D expression (Figure 4.8a), however these cells were not observed at day-14 of recovery. The tdTom^{neg} hepatocytes appeared between day-3-7 of recovery and eventually reconstituted 25% of the hepatocyte epithelium in the β1-Integrin$^{fl/fl}$ group (Figure 4.9b).

Figure 4.7 – 14 days after DDC induced liver injury parenchymal tdTom^{neg} areas were detected in β1-Integrin$^{fl/fl}$ livers

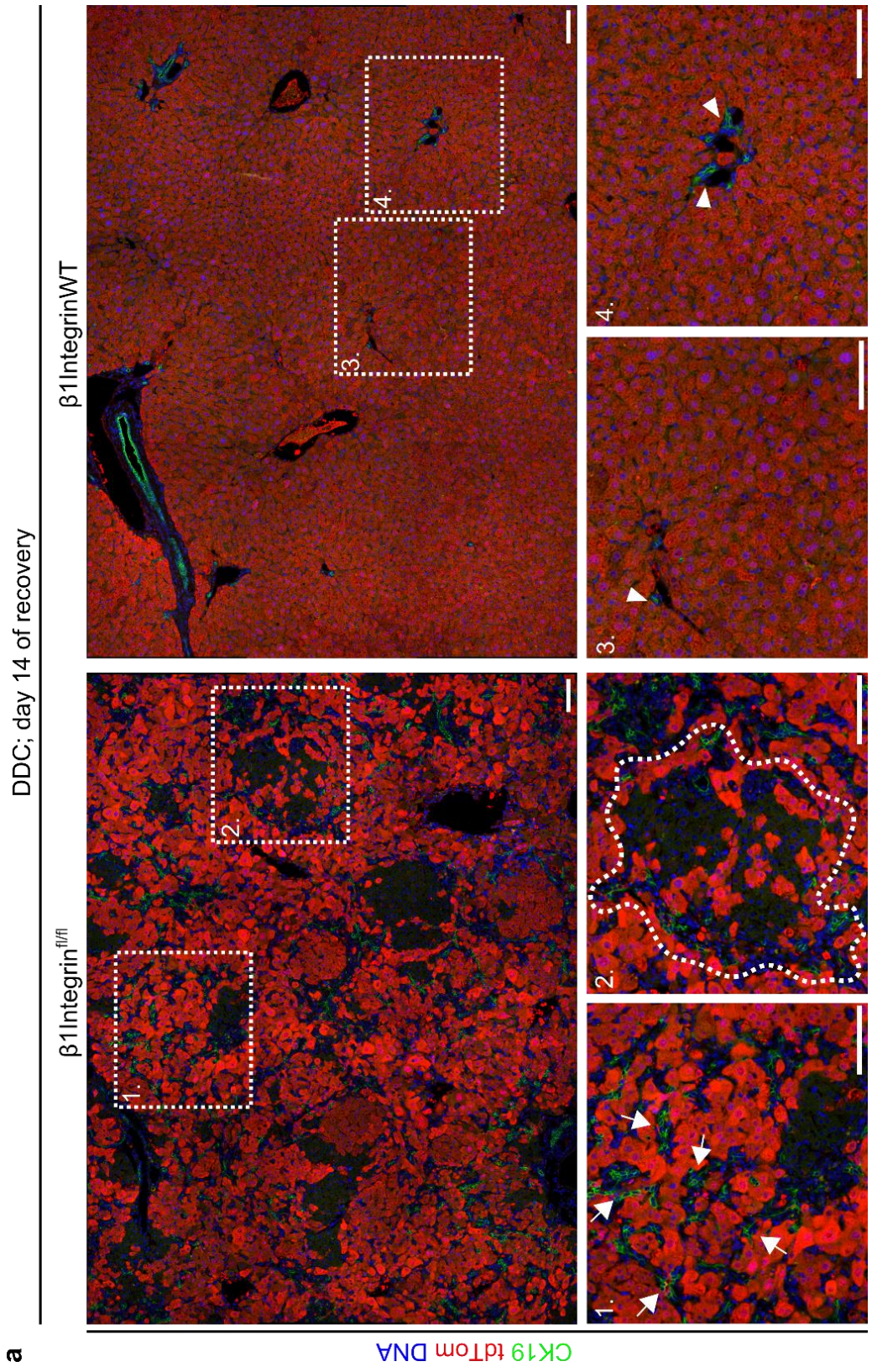

Figure 4.7: **a**. Tiled image, tdTom/CK19 immuno-fluorescence on β1-Integrin^{WT} and β1-Integrin$^{fl/fl}$ livers 14 days after DDC induced liver injury; white arrows = infiltrating CK19^{pos} biliary ductal cells, white arrowheads = CK19^{pos} biliary ductal cells at the portal tract. Scale bars: 100µM.

Figure 4.8 – Parenchymal tdTom^{neg} areas were positive for the mature hepatocyte maker CYP2D

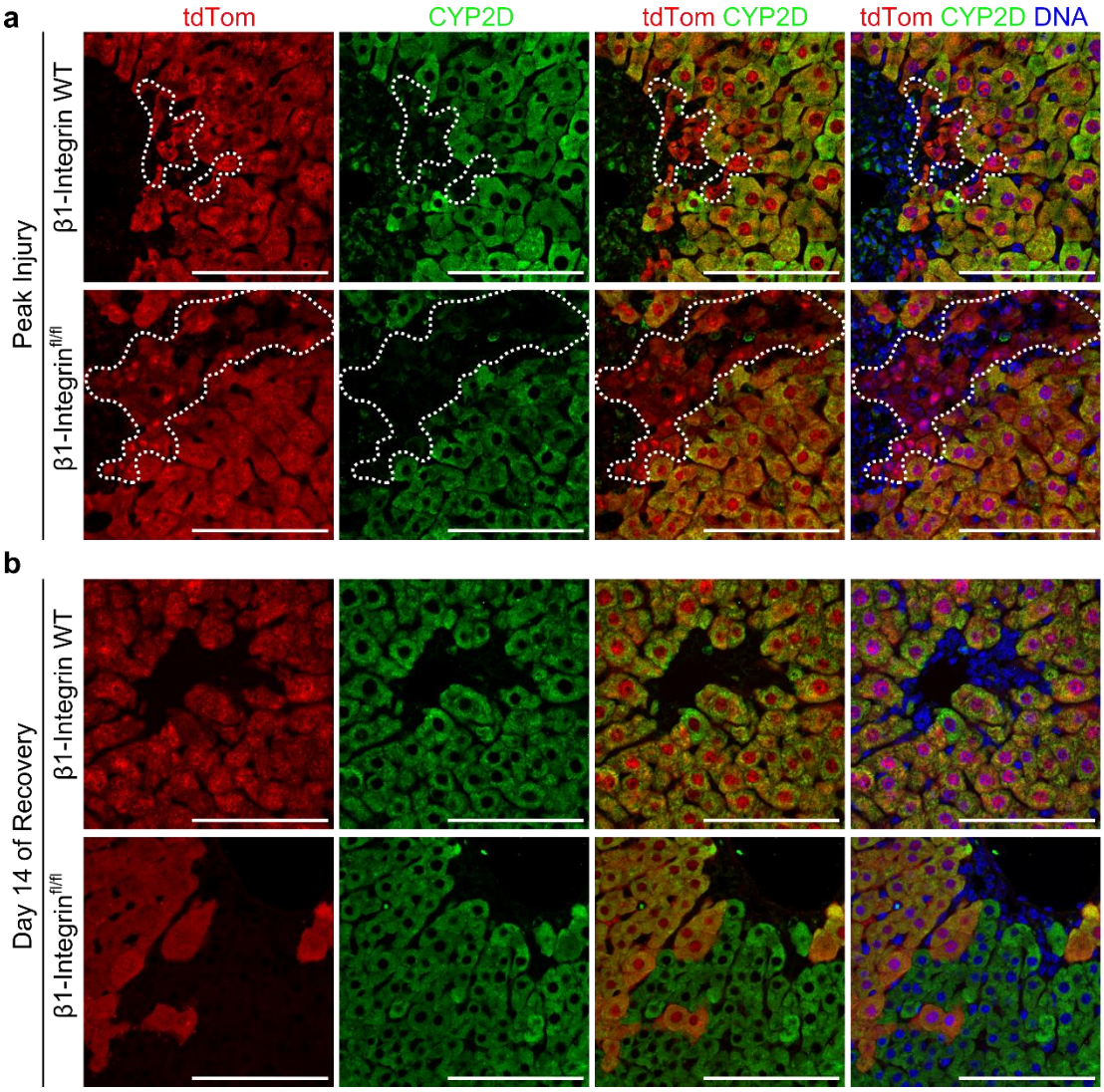

Figure 4.8: Confocal images. **a**. CYP2D/tdTom immuno-fluorescence of β1-Integrin^{WT} and β1-Integrin$^{fl/fl}$ livers after 7 days of DDC diet, a subset of periportal tdTom^{pos} cells were CYP2D^{neg}. **b**. CYP2D/tdTom immuno-fluorescence of β1-Integrin^{WT} and β1-Integrin$^{fl/fl}$ livers 14 days after DDC induced liver injury. Scale bars: 100µM.

Figure 4.9 – Hepatocyte tdTom labelling was reduced by 25% after DDC induced liver injury in β1-Integrin$^{fl/fl}$ livers

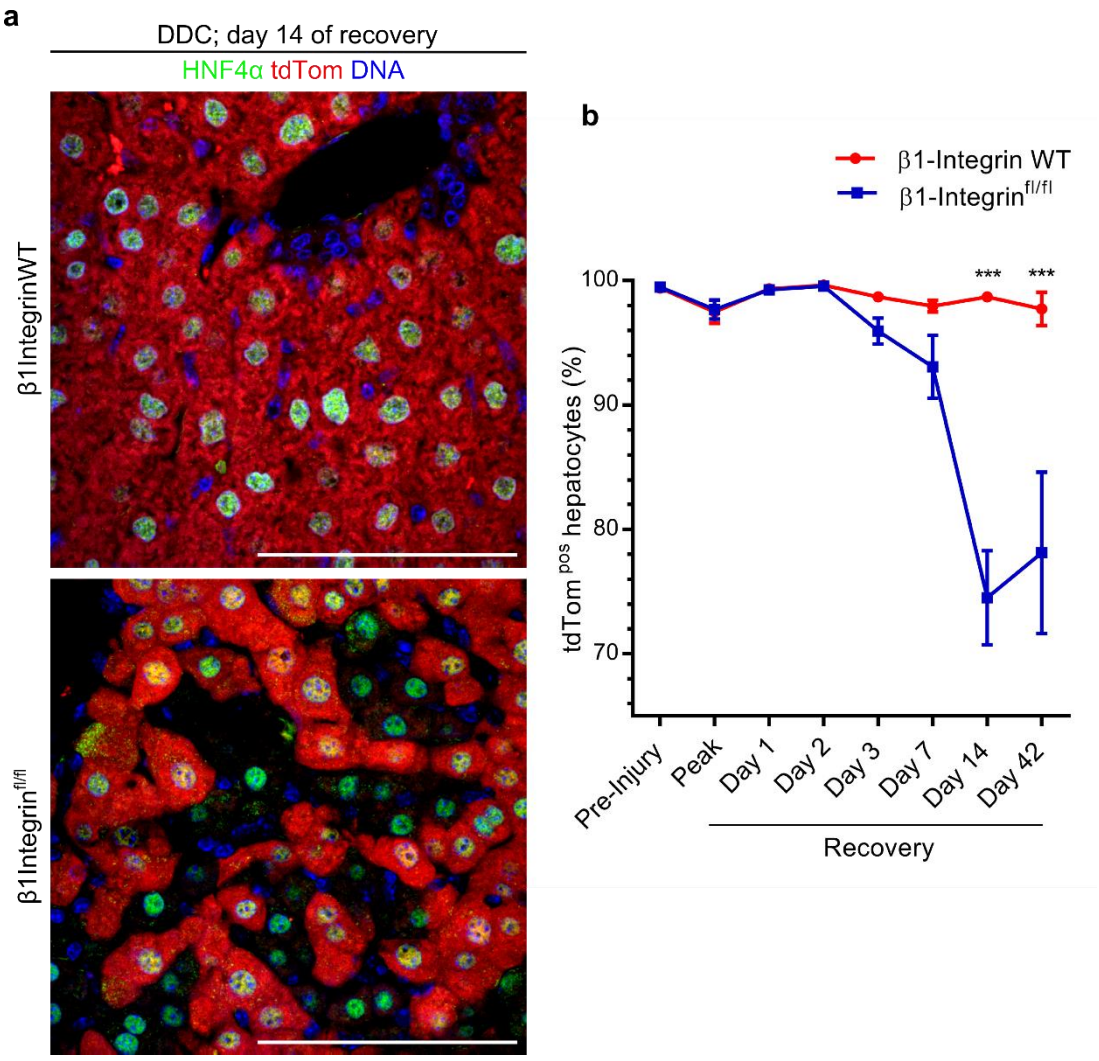

Figure 4.9: **a**. Confocal images of tdTom labelling, tdTom/HNF4α immuno-fluorescence on β1-Integrin^{WT} and β1-Integrin$^{fl/fl}$ livers 14 days after DDC induced liver injury. **b**. Single cell quantification measuring tdTom positive and negative HNF4α^{pos} hepatocytes in β1-Integrin^{WT} and β1-Integrin$^{fl/fl}$ livers before, during and after DDC induce liver injury. Data are means ± s.e.m.; 2-way ANOVA with Bonferroni post-test; *** P=0.005; N=5 biological replicates. Scale bars: 100µM.

DR and loss of labelled hepatocytes also occurred with other liver injury models

To verify the altered hepatocyte regeneration phenotype observed in the DDC injured β1-Integrin$^{fl/fl}$ livers was not an artefact of the DDC model the experiment was repeated using the TAA and MCD liver injury models (Figure 4.1). The MCD and TAA liver injury models recapitulated the phenotype seen in the β1-Integrin$^{fl/fl}$ group. There was a reduction in the proportion of tdTom^{pos} HNF4α^{pos} hepatocytes from 99.5% to 75-80% 14 days after removal of the hepatotoxic agent (Figure 4.10a and c). A small percentage of hepatocytes, 6.5%, were tdTom^{neg} after 21 days of the TAA model (Figure 4.10a).

Another common feature observed in β1-Integrin$^{fl/fl}$ livers treated with TAA and MCD were elevated amounts of CK19^{pos} biliary ductal cells at day-14 of recovery. Although, the MCD and DDC treated livers had approximately 3 times more CK19^{pos} cells PFV than the TAA treated group (Figure 4.10b).

The hepatocyte epithelium in the control, β1-Integrin^{WT}, livers subjected to the MCD injury model continued to remain tdTom^{pos}. A small decrease in labelled hepatocytes, 4%, was detected in the, β1-Integrin^{WT} TAA treated livers at day-14 of recovery. MCD and TAA induced liver injury did not stimulate an increase in the number of CK19^{pos} biliary ductal cells in the β1-Integrin^{WT} group (Figure 4.10a-c).

Figure 4.10 – β1-Integrin$^{fl/fl}$ livers had reduced hepatocyte labelling and ductular reactions when injured with alternative liver injury models

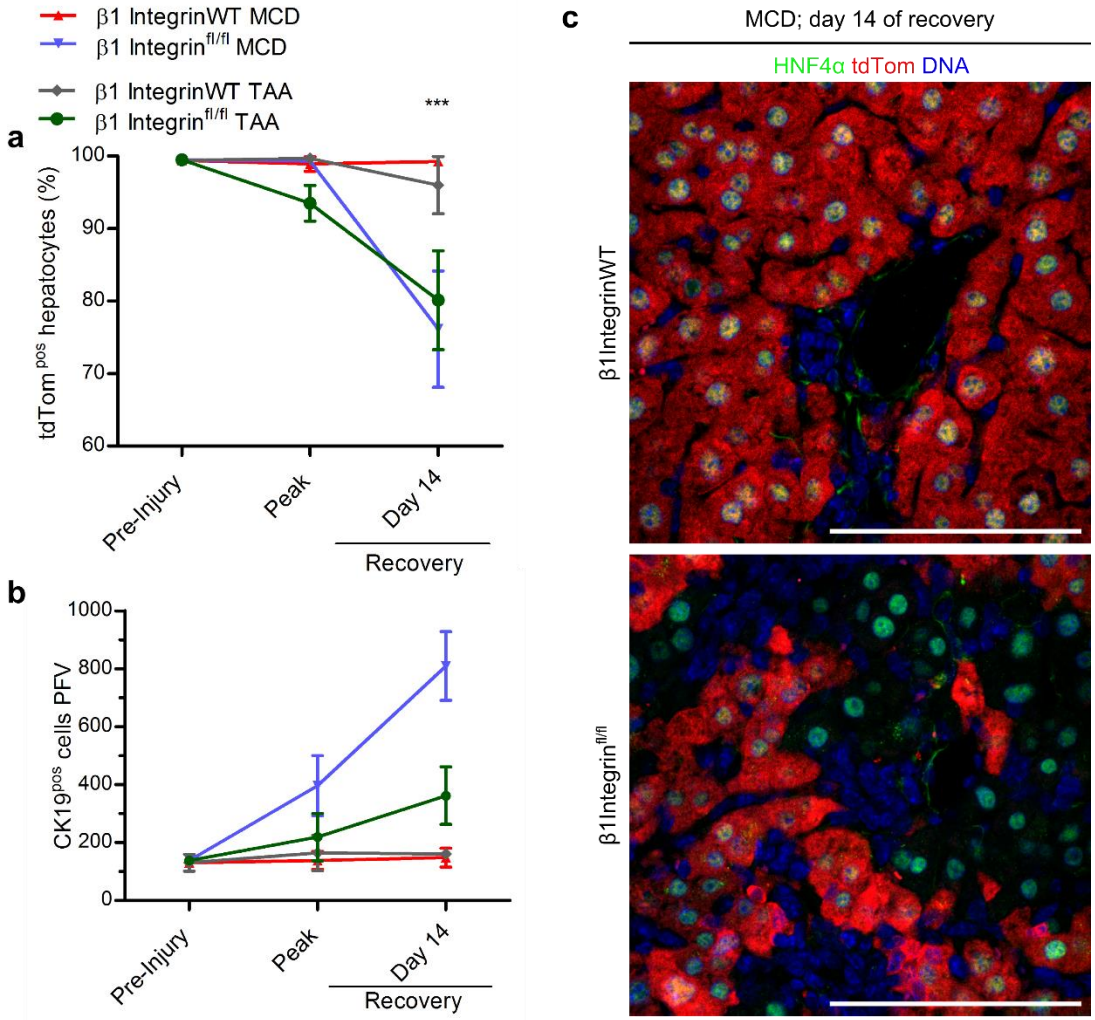

Figure 4.10: **a**, **b**. Quantification measuring tdTom positive and negative HNF4α^{pos} hepatocytes and CK19^{pos} cells in β1-Integrin^{WT} and β1-Integrin$^{fl/fl}$ livers before, during and after either TAA or MCD induced liver injury. **c**. Confocal images of tdTom labelling, tdTom/HNF4α immuno-fluorescence on β1-Integrin^{WT} and β1-Integrin$^{fl/fl}$ livers 14 days after MCD induced liver injury. Data are means ± s.e.m.; 2-way ANOVA with Bonferroni post-test; *** P=0.005; N=3 for MCD and N=2 TAA, biological replicates. Scale bars: 100μM.

tdTomato negative hepatocytes were adjacent to the DR

The loss of β1-Integrin from hepatocytes altered the regenerative response, with $tdTom^{neg}$ hepatocytes appearing in the parenchyma between day-3-7 of recovery. To investigate the spatial location of the emerging $tdTom^{neg}$ hepatocytes I analysed histology of $\beta1\text{-}Integrin^{fl/fl}$ livers from day 7 of recovery.

$tdTom^{neg}$ hepatocytes were adjacent to the $CK19^{pos}/SOX9^{pos}$ ductular reaction (Figure 4.11a). The distribution of $tdTom^{neg}$ hepatocytes could be quantified using the PerkinElmer 'Columbus' software to segment regions of tissue at various distances from the $CK19^{pos}$ ductular reaction (Figure 2.4, page 39). The location of $tdTom^{neg}$ hepatocytes was inversely correlated to the distance from $CK19^{pos}$ cells (Figure 4.11b,c). Another feature identified at day 7 of recovery was the presence of $tdTom^{neg}/SOX9^{pos}/HNF4\alpha^{pos}$ cells at the border between the new hepatocytes and the ductular reaction (Figure 4.11a, yellow arrows). This rare cell type may represent a putative intermediate cell state between $SOX9^{pos}$ biliary cells and $HNF4\alpha^{pos}$ hepatocytes.

Hepatocyte ductal-metaplasia was also detectable at day-7 of recovery, previously labelled, $tdTom^{pos}$ hepatocytes had downregulated HNF4α and were expressing SOX9 (Figure 4.11a, cyan arrowheads). Along with the change in cell markers the $tdTom^{pos}$ cells had an altered morphology, appearing small and duct like.

Figure 4.11 – At day 7 of recovery tdTom^{neg} hepatocytes emerged adjacent to the ductular reaction

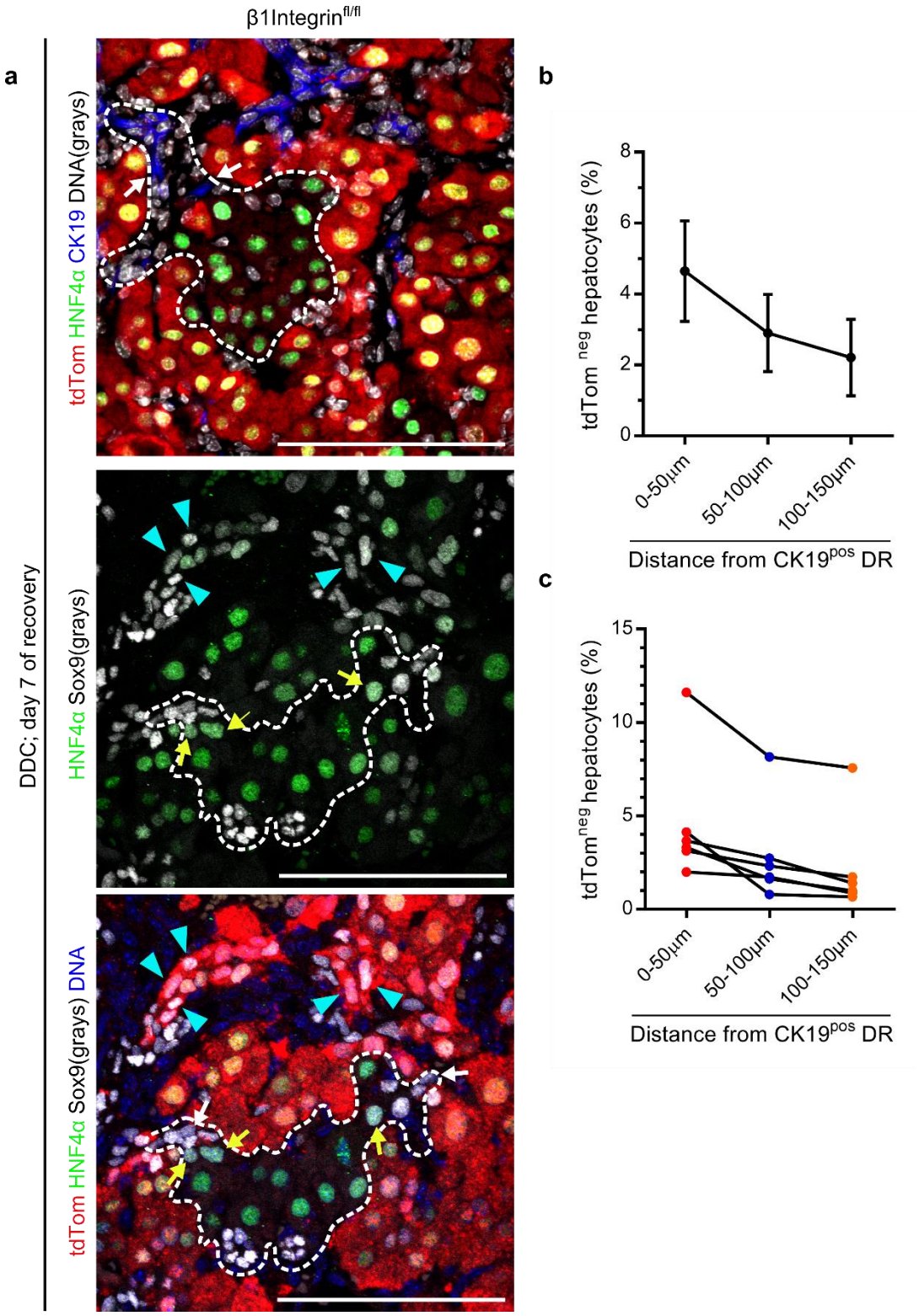

Figure 4.11: **a**. Confocal images of tdTom/HNF4α/CK19 and tdTom/HNF4α/SOX9 immuno-fluorescence on β1-Integrin$^{fl/fl}$ livers 7 days after DDC induced liver injury; white arrows = biliary ductal cells, either CK19^{pos} or SOX9^{pos}; yellow arrows = putative, intermediatory, cells expressing the hepatocyte marker HNF4α and the biliary epithelial marker SOX9; Cyan arrowheads = hepatocyte-ductal metaplasia, tdTom^{pos}/SOX9^{pos}/HNF4α^{neg} cells. **b** and **c**. Quantification of distribution of tdTom^{neg} hepatocytes in relation to CK19^{pos} biliary ductal cells; **b**. Data are mean ± s.e.m. **c**. Presents paired data for each β1-Integrin$^{fl/fl}$ liver analysed. N=5 biological replicates Scale bars: 100μM.

At Day 14 of recovery tdTomato positive hepatocytes were mainly distributed around the central vein

There was a bias to the distribution of emerging tdTom^{neg} hepatocytes at day-7 of recovery with the tdTom^{neg} hepatocytes adjacent to the ductular reaction, which originates from the portal tract. To investigate if there was a bias in the distribution of remaining tdTom^{pos} hepatocytes towards a central venous location, distal to the portal tract, tdTom positive hepatocytes were quantified in relation to their position with the central venous (CV), glutamine synthetase (GS) positive, hepatocytes (Figure 4.12a). At day-14 of recovery, post DDC induced liver injury, remaining tdTom^{pos} hepatocytes were arranged around GS^{pos} CV, decreasing in density as the distance from the GS^{pos} CV increased (Figure 4.12b,c).

Figure 4.12 – At day 14 of recovery remaining tdTom^{pos} hepatocytes were concentrated in zone 3 around the central veins

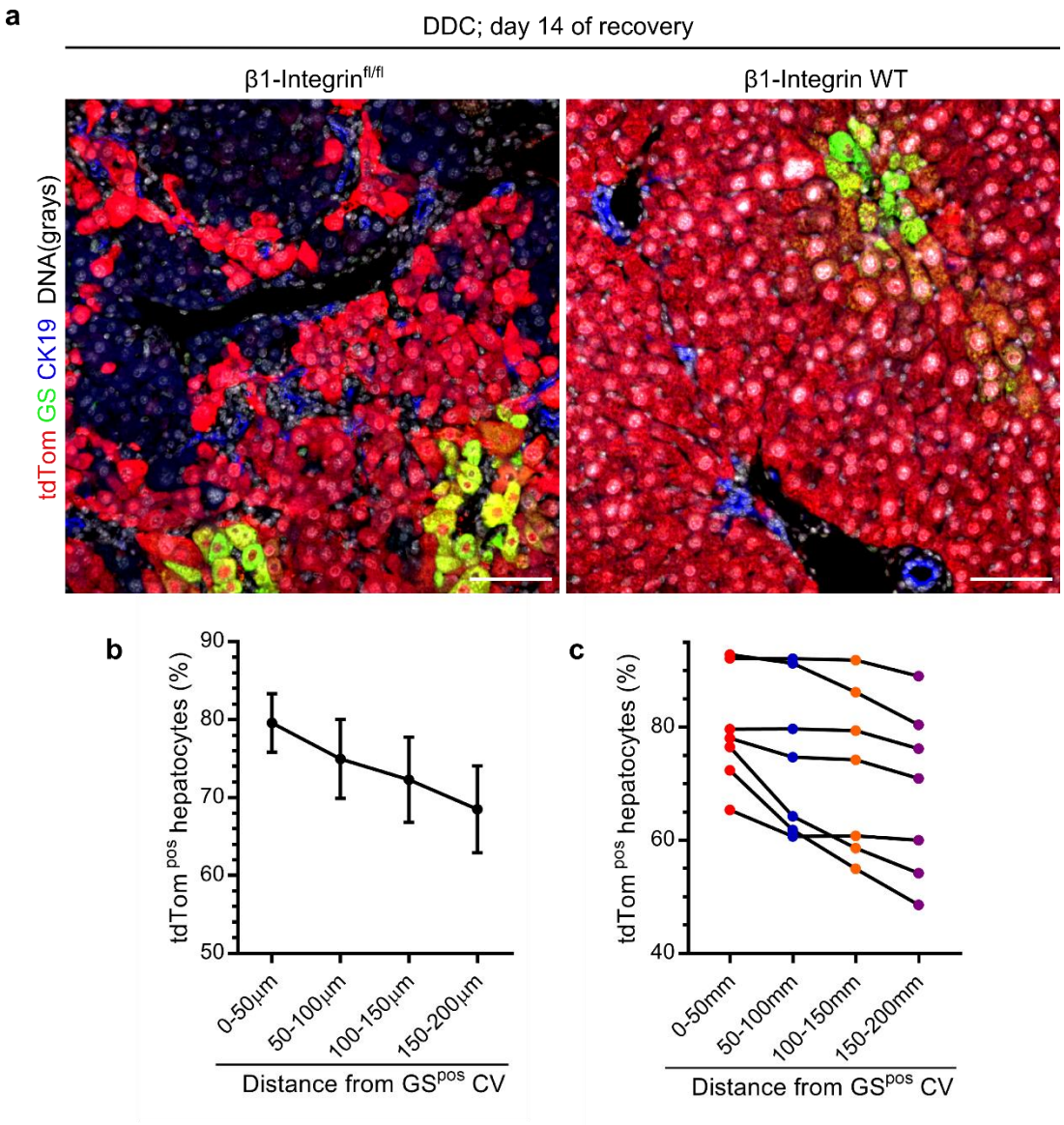

Figure 4.12: **a**. tdTom/GS/CK19 immuno-fluorescence on β1-Integrin$^{fl/fl}$ livers 14 days after DDC induced liver injury. **b** and **c**. Quantification of tdTom^{pos} hepatocytes distribution in relation to GS^{pos} central veins; **b**. Data are mean ± s.e.m.. **c**. Presents paired data for each β1-Integrin$^{fl/fl}$ liver analysed. N=6 biological replicates Scale bars: 100μM.

tdTomato negative hepatocytes were more proliferative and had smaller nuclei when compared to neighbouring tdTomato positive hepatocytes

To further characterise biological differences between the $tdTom^{pos}$ and $tdTom^{neg}$ hepatocytes I compared cell proliferation, nuclear size and β1-Integrin expression between the two groups.

Loss of β1-Integrin disrupts growth factor signalling, and impairs hepatocyte proliferation[263]. To detect this phenotypic difference 'Proliferating Cell Nuclear Antigen' (PCNA) expression was examined between the $tdTom^{neg}$ hepatocytes and their neighbouring $tdTom^{pos}$ hepatocytes. Histological analysis revealed that $tdTom^{neg}$ hepatocytes were more proliferative than neighbouring $tdTom^{pos}$ hepatocytes, and the average nuclear size was smaller in the $tdTom^{neg}$ hepatocyte population (Figure 4.13a,b). At the later recovery time point, 42 days after DDC induced liver injury, $tdTom^{neg}$ hepatocytes were no longer highly proliferative when compared to the $tdTom^{pos}$ hepatocytes, but continued to display a smaller nuclear size.

$AAV8^{Cre}$ induced gene recombination labelled 99.5% of hepatocytes $tdTom^{pos}$ and ablated β1-Integrin; to verify that the new $tdTom^{neg}$ hepatocytes were either β1-Integrin positive or negative anti β1-Integrin immunohistochemistry was performed on tissue from day 14 of recovery. Analysis of serial tissue sections confirmed that $tdTom^{neg}$ hepatocytes were positive for β1-Integrin (white dashed line and white arrowheads, Figure 4.13d) and remaining $tdTom^{pos}$ hepatocytes were β1-Integrin negative.

Figure 4.13 – Proliferation was more frequent and nuclear size was smaller in the β1-Integin^{pos} tdTom^{neg} hepatocytes

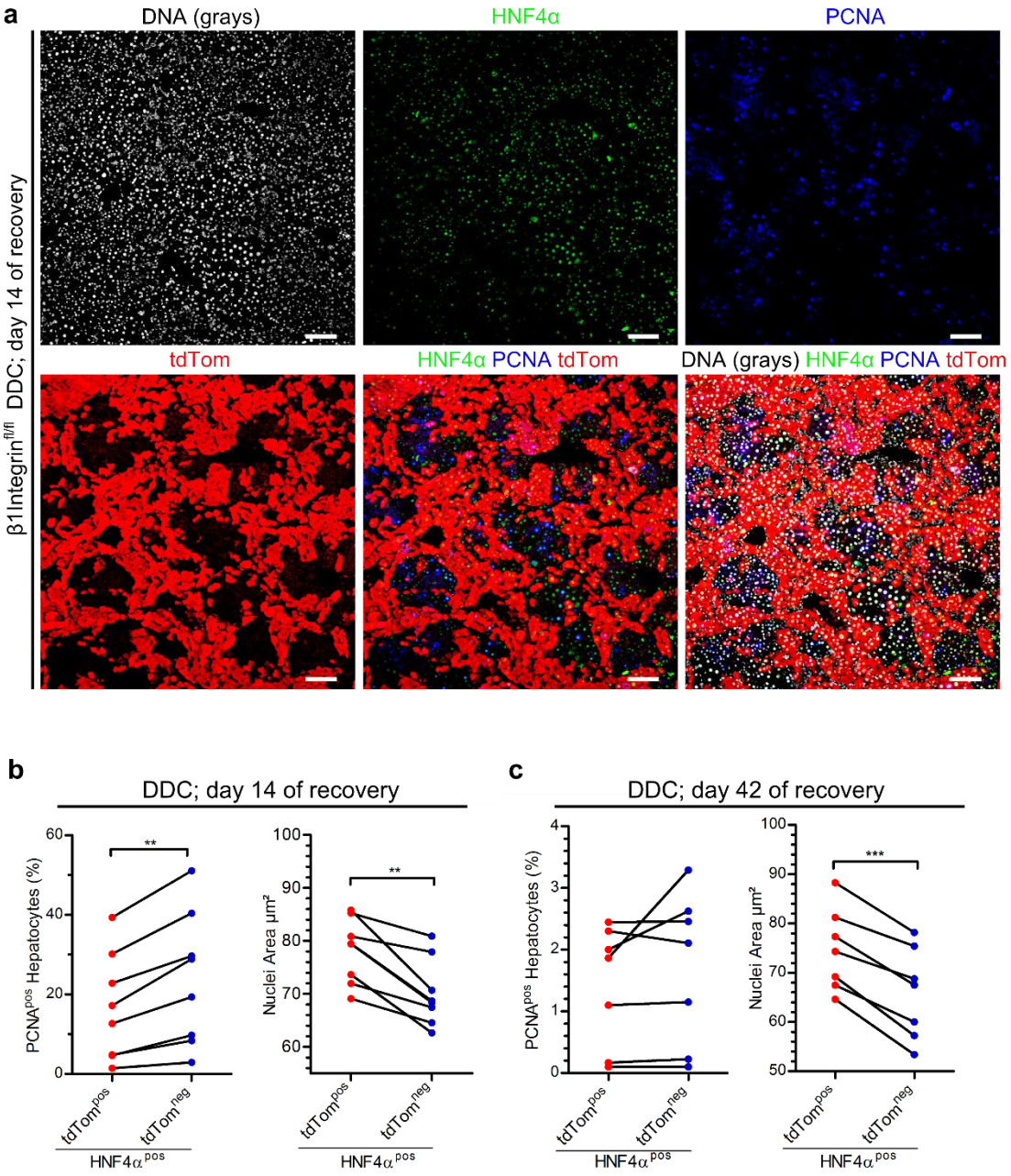

Figure 4.13 – continued

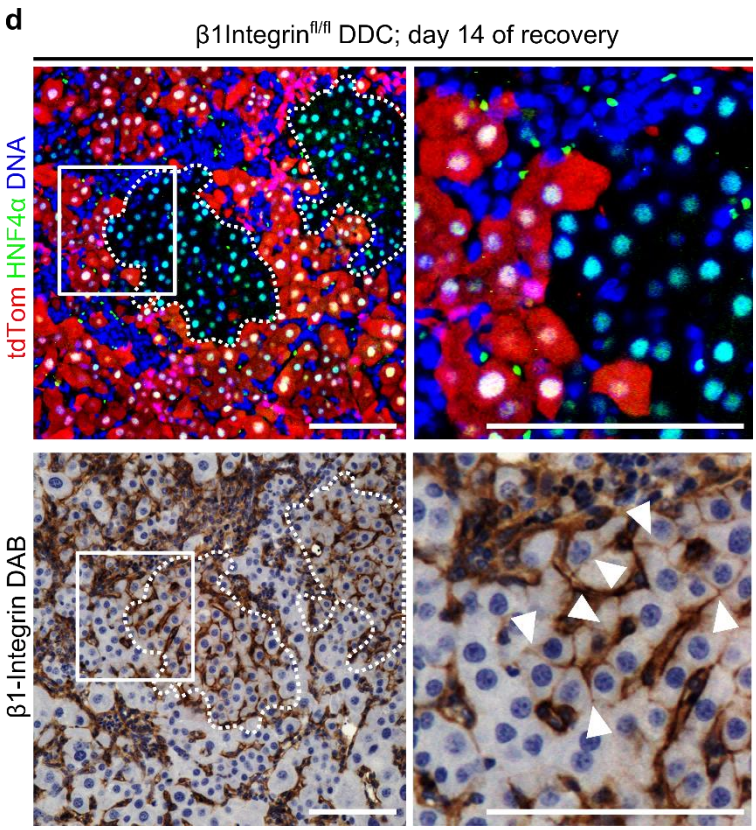

Figure 4.13: **a**. Representative PCNA/HNF4α/tdTom immunofluorescent image comparing PCNA expression and nuclear size between tdTom^{pos} and tdTom^{neg} hepatocytes in β1-Integrin$^{fl/fl}$ livers 14 days after DDC induced liver injury. **b** and **c**. Liver tissue analysis of β1-Integrin$^{fl/fl}$ mice at day 14 and 42 recovery post DDC injury; quantifying PCNA expression and nucleus size in both tdTom^{pos} and tdTom^{neg} hepatocytes (HNF4α^{pos}). Paired T-test, ** P=<0.01, *** P=0.005; N=7 biological replicates. **d**. Serial sections of β1-Integrin$^{fl/fl}$ liver 14 days after DDC induced liver injury, tdTom^{neg} hepatocytes are β1-Integrin positive (white arrowheads). Scale bars: 100μM.

Whole liver RNA sequencing at day 7 of recovery

To identify potential factors and signalling pathways that may have a role in regulating non-hepatocyte derived regeneration I performed whole liver RNA-Seq on DDC treated β1-Integrin$^{fl/fl}$ and β1-Integrin^{WT} livers at day-7 of recovery, when new tdTom^{neg} hepatocytes began to appear. Whole liver RNA from β1-Integrin$^{fl/fl}$ and β1-Integrin^{WT} livers at DDC peak injury was extracted and sequenced to determine if the β1-Integrin$^{fl/fl}$ and β1-Integrin^{WT} livers responded differently to DDC induced liver injury. Subsequent bioinformatics were performed by Dr Jonathan Manning of the Centre for Regenerative Medicine's bioinformatic services.

Principle component analysis of the RNA-Seq data from all 4 groups showed samples from each group clustered together. The global gene expression between β1-Integrin$^{fl/fl}$ and β1-Integrin^{WT} livers at peak injury did not vary largely in comparison to day-7 of recovery (Figure 4.14a). Gene set analysis using the MSigDB Hallmark Gene set and a false discovery rate (FDR) threshold of 0.05 identified 34 gene sets differentially expressed between the β1-Integrin$^{fl/fl}$ and β1-Integrin^{WT} livers at day-7 of recovery (Figure 4.14b). 15 of these gene sets could be broadly categorised under inflammation and injury response (Table 4.1), all of which were increased in the β1-Integrin$^{fl/fl}$ liver. 5 Gene sets associated with liver function had a decreased expression in the β1-Integrin$^{fl/fl}$ liver compared the β1-Integrin^{WT} (Table 4.2). 10 signalling gene sets were also upregulated in the β1-Integrin$^{fl/fl}$ liver (Table 4.3), within this group of signalling gene sets were the Notch signalling pathway and the Wnt/β-Catenin signalling pathway.

In the β1-Integrin$^{fl/fl}$ liver there was increased expression of genes in the 'myogenesis' and 'epithelial mesenchymal transition' gene sets, which correlates strongly with the prominent DR observed at the day-7 of recovery time point (Figure 4.5).

Figure 4.14 – Whole liver RNA-Seq reveals gross differences between regenerating β1-Integrin^{WT} and β1-Integrin$^{fl/fl}$ livers

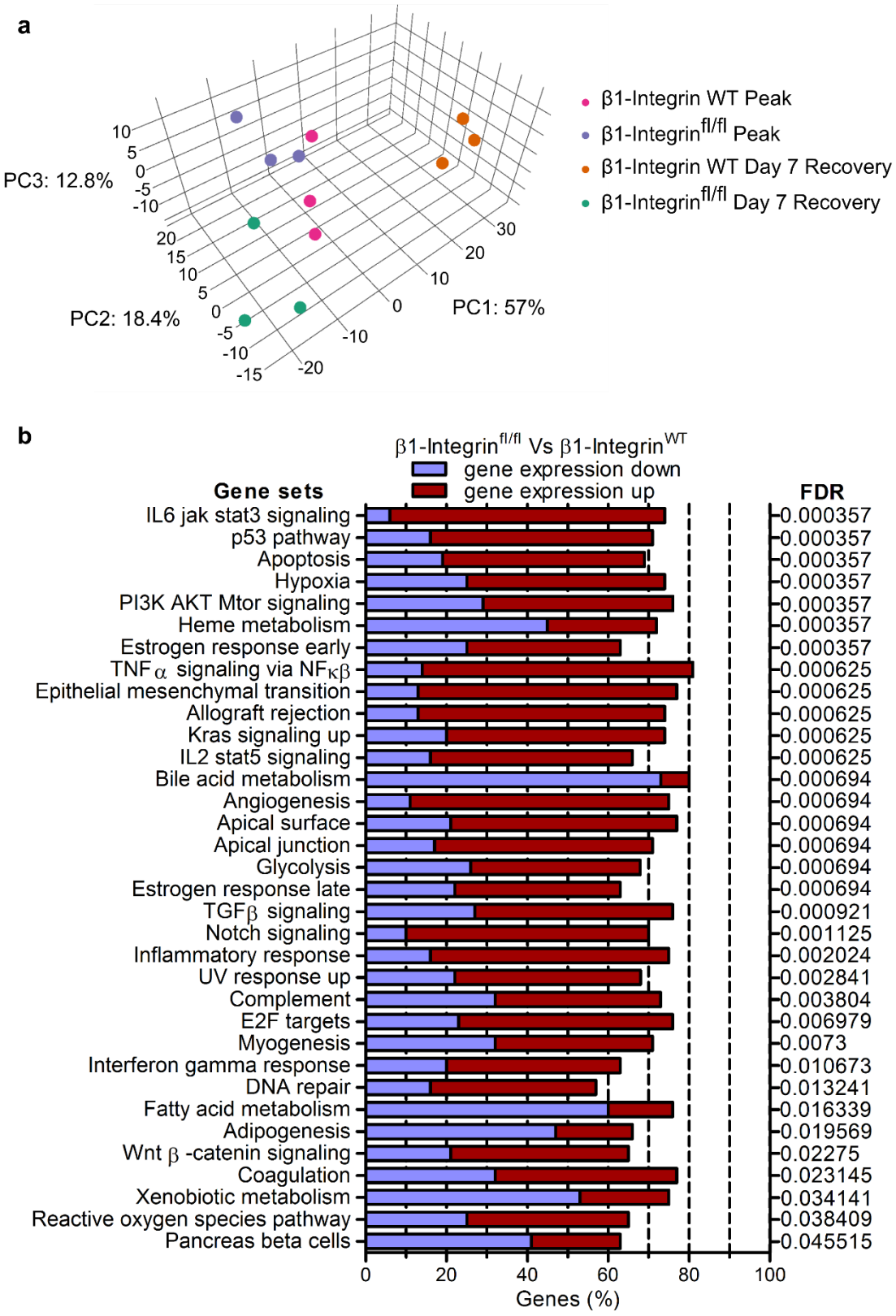

Figure 4.14: Whole liver RNA-Seq after DDC diet induced liver injury and regeneration. **a**. 3D Principle component analysis between 4 groups; β1-Integrin^{WT} peak injury (7days of DDC), β1-Integrin$^{fl/fl}$ peak injury, β1-Integrin^{WT} day 7 of recovery and β1-Integrin$^{fl/fl}$ day 7 of recovery. **b**. MSigDB Hallmark Gene set analysis β1-Integrin$^{fl/fl}$ livers vs β1-Integrin^{WT} livers after 7 days of recovery. Gene sets with a false discovery rate (FDR) below 0.05 are displayed. N=3 biological replicates.

Table 4.1 – Gene sets associated with inflammation and injury response differentially expressed in β1-Integrin$^{fl/fl}$ livers compared to β1-Integrin^{WT} livers at day 7 of recovery

Gene set	p value	Significant Genes (fold change ± >3.5) compared to β1-Integrin^{WT}
IL6 JAK STAT3 signaling	0.0001	*Csf2rb2 Il1b Cd14 Tnf Cd44 Tgfb1 Cxcl10 Jun Ltb Socs3 Il1r2 Tnfrsf12a Ccr1 Cd9 Tlr2 Il3ra Pf4 Cxcl2*
p53 pathway	0.0001	*Cdkn1a Krt17 Tgfb1 Atf3 Hbegf Inhbb Jun Lif Upp1 Ier3 Klf4 Fos Ralgds Procr Ier5 St14 S100a4 Nupr1 Phlda3 Tax1bp3 Def6 Btg2 Vdr Sphk1 Dram1 Prmt2 Cdkn2b Ndrg1*
Apoptosis	0.0001	*Cdkn1a Il1b Cd14 Tnf Cd44 Plat Emp1 Atf3 Clu Gna15 Jun Pak1 Ier3 Gadd45b Pea15a Tnfrsf12a Btg2 Timp1 Lgals3 Egr3 Krt18 Rhob Gstm2*
TNFα signaling via NFKβ	0.0002	*Icam1 Cdkn1a Il1b Tnf Cd44 Dusp4 Cyr61 Tnfrsf9 Cxcl10 Areg Atf3 Hbegf Fut4 Nr4a1 Jun Lif Nfkb2 Olr1 Ccl5 Ccl12 Ier3 Socs3 Bcl2a1b Klf4 Dusp5 Fos Tnfaip3 Relb Tnfaip6 Junb Gadd45b Fjx1 Ier5 Maff Clcf1 Pmepa1 Spsb1 Egr2 Tlr2 F2rl1 Gpr183 Tnip1 Fosb Btg2 Nfkbie Egr3 Sphk1 Dram1 Plaur Icosl Panx1 Tnc Plau Egr1 Serpine1 Rhob Gfpt2 Slc2a6 Cxcl5 Cxcl1 Cxcl2 Tubb2a*
Allograft rejection	0.0002	*Icam1 Il1b Tnf Ncf4 Tgfb1 Cd3e Flna Inhbb Lif Ltb Ccl2 Ccl5 Ccl12 Cd74 Cd8b1 Mmp9 Fgr H2-DMa Cd7 Thy1 Map4k1 Ccl22 Ccl11 Cd247 Itgb2 Ccr1 Elane Tlr2 Timp1 Capg Eif3j2 Hcls1 Il2rb Icosl Nos2 H2-DMb1 H2-DMb2 Pf4 H2-Aa Cd8a*
IL2 STAT5 signaling	0.0002	*Cd44 Emp1 Tnfrsf9 Cxcl10 Etv4 Lif Ltb Rhoh Tgm2 Eomes Ckap4 Ncs1 Gadd45b Il1r2 Maff Serpinb6a Capg Cst7 Plscr1 Il2rb Il3ra Ndrg1 Cdc6 Rhob Aplp1 Glipr2 Adam19*
Angiogenesis	0.0003	*Thbd Olr1 Prg2 Fstl1 S100a4 Col5a2 Timp1 Col3a1 Pf4 Cxcl5*
Inflammatory response	0.0009	*Icam1 Cdkn1a Il1b Cd14 Scn1b Emp3 Tnfrsf9 Cxcl10 Hbegf Gna15 Lif Olr1 Ccl5 Ccl12 Ccl17 Cx3cl1 Has2 Tpbg Tnfaip6 Ccl22 Gpr132 Osm Adora2b Ptafr C5ar1 Slc7a1 Tlr2 Sema4d Gpr183 Btg2 Timp1 Sphk1 Il2rb Plaur Icosl Serpine1 Cxcl5 Cmklr1 Ffar2*
UV response up	0.0013	*Icam1 Amd2 Atf3 Nr4a1 Fos Tyro3 Junb Htr7 Fosb Btg2 Cdkn2b Rhob Cxcl1*
Complement	0.0018	*Itgam Plat Clu Col4a2 Fcnb Ltf Olr1 S100a9 Ccl5 Dusp5 Pla2g7 Tnfaip3 Maff Anxa5 Timp1 Lgals3 Csrp1 Plscr1 Plaur Serpine1 Pdgfb*
E2F targets	0.0034	*Lig1 Cdkn1a Mcm3 Mcm2 Plk1 Cdkn3 Stmn1 Mcm6 Mcm5 Hn1 Racgap1 Cdca3 Kif18b Mthfd2 Kif2c Cdca8 Kif22 Melk Espl1 Mxd3 Birc5 Cdc20 Aurkb Asf1b Cdk1 Tubb5 Ccnb2 Tacc3*
Interferon γ response	0.0056	*Icam1 Ciita Cdkn1a Csf2rb2 Cxcl10 Ccl5 Ccl12 Upp1 Socs3 Cd74 H2-DMa Tnfaip3 Tnfaip6 Itgb7 Mthfd2 Plscr1 Il2rb Xaf1 H2-Aa Cmklr1*
DNA repair	0.0072	*Lig1 Hcls1*
Coagulation	0.0144	*Thbd Plat Clu Itga2 Olr1 Mmp9 Maff Cd9 Fbn1 Sparc Thbs1 Capn5 Timp1 Csrp1 Mmp11 Plau Serpine1 Pdgfb Pf4*
ROS pathway	0.0254	*Lsp1 Junb Mpo*

Table 4.1: MSigDB Hallmark Gene set analysis. FDR = false discovery rate and ROS = reactive oxygen species.

Table 4.2 – Gene sets associated with liver function differentially expressed in β1-Integrin$^{fl/fl}$ livers compared to β1-Integrin^{WT} livers at day 7 of recovery

Gene set	p value	Significant Genes (fold change ± >3.5) compared to β1-Integrin^{WT}
Heme metabolism	0.0001	*Alas2 Top1 Selenbp2 Cir1 Aldh6a1 Klf1 Ell2 Dcun1d1 Car1 Myl4 Fn3k Kdm7a Nr3c1 Daam1 Osbp2 Usp15 Hist2h4*
Bile acid metabolism	0.0003	*Dio1 Abcd3 Cyp8b1 Idi1 Cyp7b1 Klf1 Slc27a5 Pnpla8 Abca1 Cyp7a1 Acsl1 Scp2 Slc27a2 Nudt12 Akr1d1 Sult1b1 Abca6 Hsd3b2*
Fatty acid metabolism	0.0092	*Dld Idi1 Tdo2 Hibch Adh7 Acsl1 Aadat Hsp90aa1 Acsm3 Cyp4a32 Cyp4a12a Cyp4a12b*
Adipogenesis	0.0114	*Dld Chuk Dbt Lifr Omd Hibch Elovl6 Abca1 Scp2*
Xenobiotic metabolism	0.0219	*Ptgds Tdo2 Angptl3 Ces1d Ttpa Adh7 Papss2 Cyp2e1 Hsd11b1*

Table 4.2: MSigDB Hallmark Gene set analysis. FDR = false discovery rate

Table 4.3 – Signalling gene sets differentially expressed in β1-Integrin$^{fl/fl}$ livers compared to β1-Integrin^{WT} livers at day 7 of recovery

Gene set	p value	Significant Genes (fold change ± >3.5) compared to β1-Integrin^{WT}
IL6 JAK STAT3 signaling	0.0001	*Csf2rb2 Il1b Cd14 Tnf Cd44 Tgfb1 Cxcl10 Jun Ltb Socs3 Il1r2 Tnfrsf12a Ccr1 Cd9 Tlr2 Il3ra Pf4 Cxcl2*
PI3K AKT mTOR signaling	0.0001	*Cdkn1a Cxcr4 Sla Cdk1*
Heme metabolism	0.0001	*Alas2 Top1 Selenbp2 Cir1 Aldh6a1 Klf1 Ell2 Dcun1d1 Car1 Myl4 Fn3k Kdm7a Nr3c1 Daam1 Osbp2 Usp15 Hist2h4*
Estrogen response early	0.0001	*Cd44 Areg Inhbb Wisp2 Klf4 Elf3 Tgm2 Hr Fos Tpbg Rab31 Cldn7 Olfml3 Syt12 Slc1a4 Egr3 Myof Slc24a3 Adcy1 Sult2b1 Tubb2b Krt18 Krt8*
TNFα signaling via NFKβ	0.0002	*Icam1 Cdkn1a Il1b Tnf Cd44 Dusp4 Cyr61 Tnfrsf9 Cxcl10 Areg Atf3 Hbegf Fut4 Nr4a1 Jun Lif Nfkb2 Olr1 Ccl5 Ccl12 Ier3 Socs3 Bcl2a1b Klf4 Dusp5 Fos Tnfaip3 Relb Tnfaip6 Junb Gadd45b Fjx1 Ier5 Maff Clcf1 Pmepa1 Spsb1 Egr2 Tlr2 F2rl1 Gpr183 Tnip1 Fosb Btg2 Nfkbie Egr3 Sphk1 Dram1 Plaur Icosl Panx1 Tnc Plau Egr1 Serpine1 Rhob Gfpt2 Slc2a6 Cxcl5 Cxcl1 Cxcl2 Tubb2a*
IL2 STAT5 signaling	0.0002	*Cd44 Emp1 Tnfrsf9 Cxcl10 Etv4 Lif Ltb Rhoh Tgm2 Eomes Ckap4 Ncs1 Gadd45b Il1r2 Maff Serpinb6a Capg Cst7 Plscr1 Il2rb Il3ra Ndrg1 Cdc6 Rhob Aplp1 Glipr2 Adam19*
KRAS signaling up	0.0002	*Il1b Plat Scn1b Emp1 Cxcl10 Hbegf Etv4 Itga2 Kcnn4 Lif Slpi Il1rl2 Klf4 Mmp9 Spon1 Tnfaip3 Laptm5 Map4k1 Tmem158 Lat2 F13a1 Itgb2 Cxcr4 Wnt7a F2rl1 Ace Mmp11 Cpe Plaur Plau Aldh1a3 Aldh1a2 Gfpt2 Adam8 Serpina3c Cmklr1*
Estrogen response late	0.0003	*Cd44 Areg Ltf S100a9 Wisp2 Klf4 Cxcl14 Hr Fos Tpbg Rab31 Gjb3 St14 Cd9 Slc1a4 Cdc20 Ckb Egr3 Kif20a Myof Gins2 Slc24a3 Chst8 Cpe Sult2b1 Cdc6 Ptger3 Serpina3c*
TGFβ signaling	0.0004	*Ltbp2 Tgfb1 Id1 Rab31 Junb Pmepa1 Thbs1 Serpine1*
Notch signaling	0.0005	*Lfng*
WNT β-catenin signaling	0.0137	Significant Genes (fold change ± >2) compared to β1-IntegrinWT
		Trp53 Jag2 Hey1 Nkd1 Fzd1

Table 4.3: MSigDB Hallmark Gene set analysis. FDR = false discovery rate.

Wnt expression increased early in recovering β1-Integrin$^{fl/fl}$ livers

Gene set analysis can be used to interpret whole genome data that has been generated from RNA-Seq. This method utilises established sets of genes associated with a given biological process or cell signalling pathway and compares them to genes expressed in the various experimental groups. Differentially expressed genes that are significantly increased in a group are identified, revealing any active processes or signalling pathways present in the experiment. Using the conservatively curated 'MSigDB Hallmark gene set'[290] the WNT-β-Catenin signalling pathway was identified as being upregulated in β1-Integrin$^{fl/fl}$ livers at day 7 of recovery. No WNT genes from this set had a large increase, i.e. >3.5-fold change, in expression. Therefore, I used the MSigDB canonical gene set, which has been curated by WNT specialists, to specifically analyse the WNT pathway in RNA-Seq data from DDC treated livers at day 7 of recovery.

Gene set enrichment analysis of β1-Integrin$^{fl/fl}$ liver compared to β1-Integrin^{WT} liver at day 7 of recovery revealed an enrichment for upregulated WNT signalling genes (Figure 4.15a). 30 WNT genes from the β1-Integrin$^{fl/fl}$ liver had a >2-fold change in expression compared to β1-Integrin^{WT} liver. Wnt ligand genes: *Wnt7a*, *Wnt11*, *Wnt7b*, *Wnt10a*, *Wnt4*, *Wnt 9a* and *Wnt2* were all upregulated in the β1-Integrin$^{fl/fl}$ liver, along with WNT modulators: *Sfrp1*, *Frzb*, *Sfrp4*, *Nkd1*. *Wif1* and *Apc* express proteins that supress WNT signalling, both were downregulated in the β1-Integrin$^{fl/fl}$ liver. 6 WNT signalling receptors; *Fzd3*, *Fzd2*, *Fzd1*, *Fzd4*, *Fzd8* and *Lrp6* were also differentially expressed in the β1-Integrin$^{fl/fl}$ liver (Figure 4.15b).

Whole liver qPCR was used to validate the RNA-Seq data and investigate *Wnt* (*Wnt9b*, *Wnt7b*, *Wnt11*, *Wnt7a* and *Wnt10a*) expression at other recovery time points. *Wnt* expression was equal between the β1-Integrin$^{fl/fl}$ and β1-Integrin^{WT} livers before injury and during DDC diet treatment. *Wnt* expression remained low in the β1-Integrin^{WT} liver, sharply contrasting the β1-Integrin$^{fl/fl}$ liver, where *Wnt* expression had a 2-4-fold increase (Figure 4.15c).

Figure 4.15 – Whole liver *Wnt* expression increased in the early phase of recovery when β1-Integrin is ablated

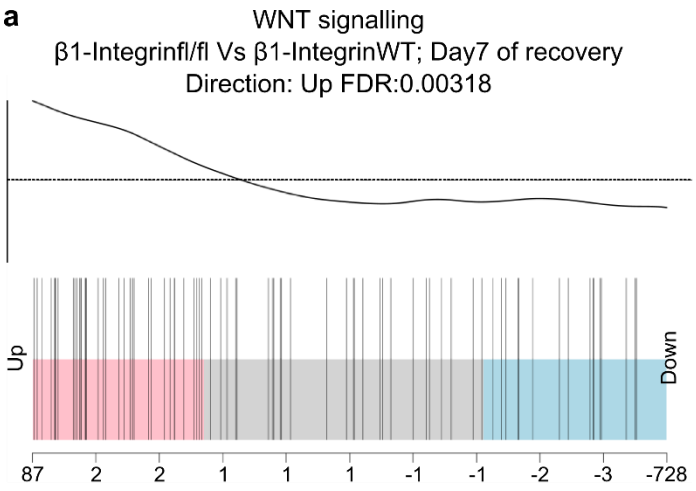

b

Gene	Fold change	q value
Wnt7a	12.76	0.0000000003
Sfrp1	7.05	0.0000000843
Wnt11	5.46	0.0000327770
Jun	4.13	0.0000000000
Fzd3	3.79	0.0000063652
Wnt7b	3.76	0.0000570360
Wnt10a	3.74	0.0106480000
Frzb	3.59	0.0000015169
Fosl1	2.94	0.0004530600
Wnt4	2.89	0.0007780900
Fzd2	2.83	0.0020738000
Sfrp4	2.76	0.0072990000
Nkd1	2.72	0.0000623450
Wnt9a	2.71	0.0001010700
Fzd1	2.61	0.0001564200
Wisp1	2.59	0.0112220000
Actb	2.58	0.0000066673
Ccnd1	2.32	0.0005426800
Wnt2	2.22	0.0652000000
Rhou	2.19	0.0000056778
Ccnd2	2	0.0017006000
Tle2	-2.05	0.0033883000
Fzd4	-2.4	0.0000019475
Dixdc1	-2.47	0.0003520000
Fzd8	-2.48	0.0000009507
Lrp6	-2.61	0.0010651000
Wnt2b	-2.65	0.0330880000
Wif1	-3.45	0.0000057044
Daam1	-3.89	0.0000099869
Apc	-4	0.0003469200

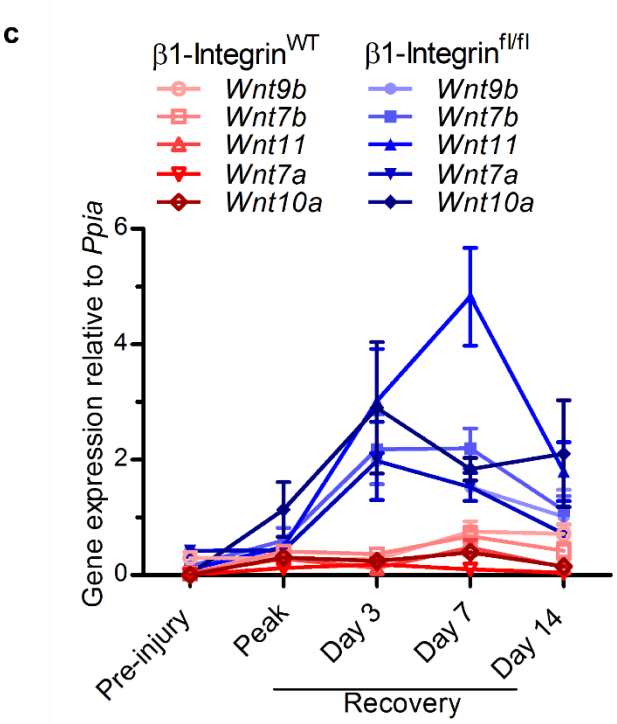

Figure 4.15: **a**. MSigDB canonical gene set analysis, WNT signalling barcode plot; there is an enrichment for upregulated genes associated with the WNT pathway after DDC induced liver injury and 7 days of recovery. FDR = false discovery rate. **b**. Gene list from the 'MSigDB canonical gene set: WNT signalling genes that have >2-fold change in expression in the β1-Integrin$^{fl/fl}$ liver compared to β1-Integrin^{WT}. N=3 biological replicates **c**. Whole liver qPCR for major WNT lignads identified in RNA-Seq analysis, data are mean ± s.e.m; N= 4 biological replicates per condition.

Discussion

Hepatotoxic induced liver injury resulted in strikingly different regenerative responses from the β1-Integrin$^{fl/fl}$ and β1-Integrin^{WT} livers. When both genotypes were treated with DDC diet, liver injury was induced. The β1-Integrin^{WT} livers regenerated via self-duplication of the tdTom labelled hepatocyte epithelium. This method of regeneration resulted in liver recovery 7 days after returning to normal diet, demonstrated by normal LFTs, body weight, and the absence of necrosis and p21 positive hepatocytes (Figure 4.16a). In contrast, the β1-Integrin$^{fl/fl}$ livers had a prolonged recovery; LFTs, body weight and the amount of p21^{pos} hepatocytes did not return to normal (control) levels until day 14 of recovery. Tissue damage continued in the β1-Integrin$^{fl/fl}$ livers, with a large necrotic event occurring around day 3 of recovery. During this second phase of liver damage, a biliary derived, invasive, DR began to infiltrate the parenchyma (Figure 4.16b). Although tdTom^{pos} β1-Integrin$^{fl/fl}$ hepatocytes expressed proliferation markers they failed to completely regenerate the liver; as an alternative, a periportal, non-hepatocyte derived source responded, regenerating the hepatocyte epithelium.

At day-14 of recovery in the β1-Integrin$^{fl/fl}$ liver, regardless of the type of injury, the hepatocyte epithelium was comprised from two distinct populations of hepatocytes. These populations were distinguishable by the fluorescent marker tdTomato. tdTom^{pos} hepatocytes were biased towards a pericentral location and originated from pre-injury hepatocytes that were β1-Integrin deficient. Small, proliferative, tdTom^{neg}, β1-Integrin^{pos} hepatocytes appeared after injury at a periportal location. The periportal distribution of the tdTom^{neg} hepatocytes along with the timing of their appearance, during an atypical DR, suggests that the tdTom^{neg} hepatocytes may have a biliary origin.

During recovery β1-Integrin$^{fl/fl}$ livers eventually stopped displaying markers of hepatocyte injury, with serum LFTs, HMGB1 staining and histological necrosis scoring returning to normal by day-14 of recovery. However, other parameters that were enhanced after DDC induced injury such as the elevated amount of CK19^{pos} cells and liver fibrosis remained abnormally high. Indeed, the degree of fibrosis developed further with striking fibrous septa present throughout the parenchyma by day 42 of recovery. This incomplete recovery can be explained by the composition of the

hepatocyte epithelium, which after day 14 of recovery contained new tdTom^{neg} hepatocytes and the remaining tdTom^{pos}, β1-Integrin deficient, hepatocytes. These defective hepatocytes were likely stimulating fibrosis and the continued presence of atypical ductal cells. Further to this point, the residual atypical ductal cells that were still present in the parenchyma after day 14 of recovery were predominantly distributed amongst the tdTom^{pos}, β1-Integrin deficient, hepatocytes.

Figure 4.16 – Distinct regenerative responses between the β1-Integrin$^{fl/fl}$ and β1-Integrin^{WT} livers

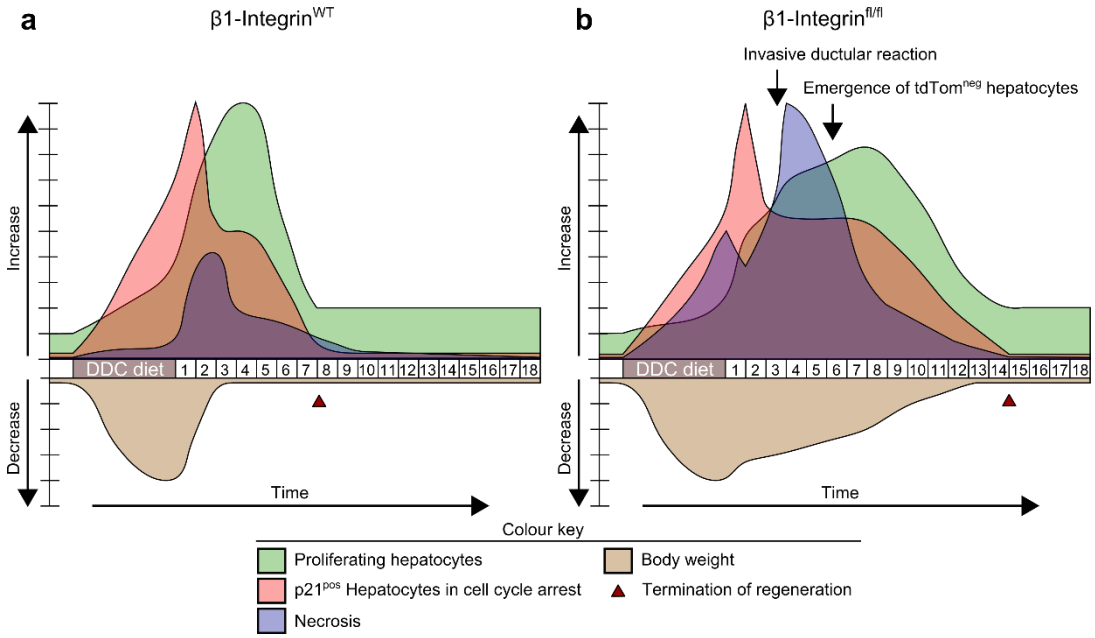

Figure 4.16: Frequency polygons displaying changes to key features observed throughout DDC induced liver injury and recovery. **a**. Frequency polygon for the β1-Integrin^{WT} liver and normal regeneration after DDC treatment. **b**. Frequency polygon for the β1-Integrin$^{fl/fl}$ liver where regeneration occurs later from a non-hepatocyte source.

Another feature observed at peak injury and the early phases of recovery (until day 7) in the β1-Integrin$^{fl/fl}$ liver was hepatocyte ductal-metaplasia. Previously labelled tdTom hepatocytes no longer expressed mature hepatocyte markers such as CYP2D and HNF4α and acquired a morphology similar to the invasive CK19^{pos} biliary ductal

cells. Although these ductal like hepatocytes expressed the biliary marker SOX9, they did not express CK19, and so did not fully convert to biliary epithelial cells. Considering the presence of these ductal like hepatocytes two features strike me. One being their transient appearance during the height of liver injury, suggesting that this might be a pro-survival mechanism, previously hypothesised by Tarlow et al[75]. This pro-survival mechanism could be through either preservation of the ductal-metaplastic cell or enhanced regeneration of the liver by ductal-metaplastic hepatocytes. Font Bugarda et al discovered a regenerative hybrid hepatocyte, which express the ductal marker, SOX9, and can regenerate the hepatocyte epithelium under certain conditions[166]. The second point worth considering is the location of these ductal like hepatocytes, which is at the interface between the biliary epithelium and its respective niche. This raises the question; can hepatocyte identity be manipulated by the ductular reaction and its accompanying niche[43]? Notch signalling and YAP, a component of the Hippo pathway, have both been linked to hepatocyte metaplasia[74,230]. Stromal stimulated notch signalling regulates biliary fate in disease[52,300] and development[201–203], and promotes biliary cell expansion during DR[56]. Furthermore, artificial, overexpression of the 'notch intracellular domain' in hepatocytes reprograms them towards a biliary fate[74]. It is therefore plausible that notch signalling, which is promoting biliary expansion in the DR, may have off target effects that induce neighbouring hepatocytes to undergo ductal-metaplasia. Doxycycline inducible activated-YAP has also been shown to reprogram hepatocytes to a biliary fate[230], it is unknown how Hippo signalling functions during liver regeneration and how it might be related to the DR.

Whole liver RNA-Seq was used to assay for potential factors and signalling pathways involved with the non-hepatocyte derived regeneration detected in β1-Integrin$^{fl/fl}$ livers at day-7 of recovery. Two previously reported important developmental signalling pathways[52], Notch and Wnt/β-Catenin were identified. The Wnt ligands *Wnt11*, *Wnt7b* and *Wnt9b* had increased gene expression at early time points in the recovering β1 Integrin$^{fl/fl}$ livers. These ligands have been linked to cholangiocarcinoma[301] and hepatic development[214,217] and descriptive work by Hu et al revealed many of these *Wnt* ligands are expressed around the DR[302]. WNT responsive cells have an important role in liver regeneration[9,86], particularly in HPC differentiation to hepatocytes[52].

However, non-canonical WNT signalling may also have a role in regulating the DR as 6 non-canonical *Wnt* genes: *Wnt11*, *Wnt4*, Wnt7b, *Jun*, *Rhou*, *Daam1* were highly expressed. These genes are commonly associated with WNT Planar cell polarity (PCP) pathway[303,304] and may have a role in orchestrating the formation and direction of the DR.

To summarise DDC diet caused liver damage to both the β1-Integrin^{WT} and β1-Integrin$^{fl/fl}$ groups. Parameters associated with liver injury rapidly returned to normal in the β1-Integrin^{WT} group, where no indicators of liver damage could be detected after day-7 of recovery. Mice from the β1-Integrin$^{fl/fl}$ group had a delayed return to health, with markers of liver injury not returning to normal until day-14 of recovery. Analysis of tdTomato labelled hepatocytes after liver injury showed that there was a non-hepatocyte source of regeneration in the β1-Integrin ablated liver. The early periportal location of the tdTom^{neg} hepatocytes and the accompanying ductular reaction suggested that the source of these new, non-hepatocyte derived, hepatocytes could be from the biliary epithelium. To investigate the origin of the new tdTom^{neg} hepatocytes I will lineage trace biliary epithelial cells in a setting where hepatocytes are β1-Integrin deficient.

Chapter 5

Biliary ductular cells regenerate the liver when hepatocyte regeneration is impaired by β1-Integrin loss

Introduction

Impaired hepatocyte regeneration caused by ablation of hepatocyte β1-Integrin resulted in regeneration from a non-hepatocyte origin. I hypothesised that the source of these new hepatocytes was the biliary derived DR. To test this hypothesis, labelled BECs were lineage traced in parallel with hepatocyte *Itgb1* suppression.

BEC lineage tracing utilised a tamoxifen inducible Cre transgene specifically expressed in the biliary epithelium to activate tdTom (see chapter 2, Figure 2.1b). In combination with the BEC lineage tracing, a Cre/*Loxp* independent system was developed to target hepatocyte β1-Integrin expression and recapitulate the phenotype observed in the AAV8^{Cre}-β1-Integrin$^{fl/fl}$ model. Interfering RNA (RNAi) molecules packaged in to lipid coated nanoparticles have been shown to specifically suppress *Itgb1* expression in hepatocytes *in vivo*[263,266]. I decided to utilise this system in combination with the DDC and MCD injury models (Figure 5.1) to lineage trace the biliary epithelium in a setting where regenerating hepatocytes are impaired by deficient β1-Integrin expression.

Figure 5.1 – Experimental timeline describing the strategy to lineage trace biliary epithelial cells during nanoparticle-RNAi mediated suppression of *Itgb1*

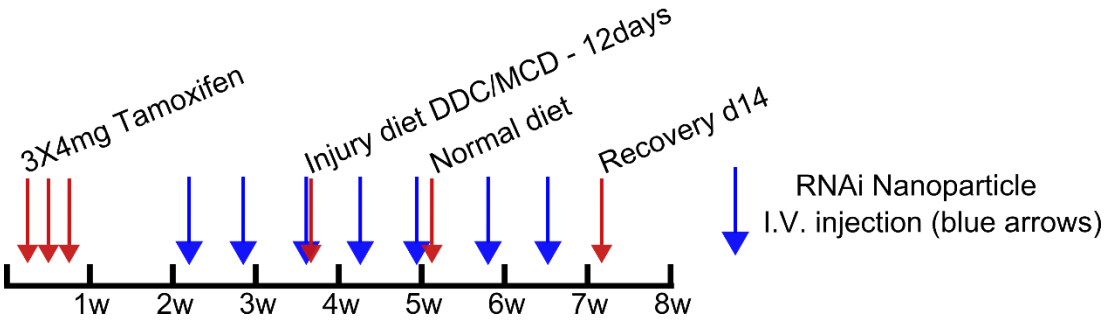

Along with determining the origin of the non-hepatocyte derived regeneration it is also important to compare the new tdTom^{neg} hepatocyte population with, regular, hepatocytes that have regenerated by cell division. Through comparisons of global gene expression, I can determine if the new tdTom^{neg} hepatocyte population have the same phenotype as regular hepatocytes. This experiment was done in collaboration

with Dr. Wei-Yu Lu, Centre for Regenerative Medicine; who had also developed a model to lineage trace CK19^{pos} BECs in to hepatocytes by inducing cell cycle arrest in the hepatocyte epithelium using an AAV8-TBG-p21 virus with the *K19^{CreERT} ^{LSL}TdTomato* mouse[284]. We therefore, designed an experiment that used the MCD diet to stimulate liver regeneration and isolated hepatocytes from the regenerated livers. From a C57Bl/6 genotype we harvested hepatocytes that had regenerated through self-duplication and cholangiocytes (BEC) as a comparative control. The other two populations consisted of the BEC derived tdTom^{pos} hepatocytes (BDhepatocytes) from Dr Wei-Yu Lu's AAV8-p21 model and the tdTom^{neg} hepatocytes from the AAV8^{cre}-β1-Integrin$^{fl/fl}$ model. This allowed for a direct comparison between BEC derived and non-hepatocyte derived hepatocytes in relation to normal hepatocytes and BECs.

Firstly, this chapter aims to ascertain the cellular source of regeneration when hepatocyte regeneration is impaired by loss of β1-Integrin through biliary epithelial lineage tracing. Secondly, this chapter will describe how biliary derived and non-hepatocyte derived hepatocytes compare to control hepatocytes and biliary ductular cells using whole genome RNA-Sequencing.

Results

Validation of the nanoparticle formulated RNAi and the inducible *K19$^{CreERT\ LSL}$tdTomato* transgene

To lineage trace BECs a *K19$^{CreERT\ LSL}$tdTomato* transgene was activated by administering three 4mg doses of tamoxifen via intraperitoneal injection over 5 days (Figure. 5.1), the liver was harvested 19 days later to confirm the specificity of the labelling system. Tamoxifen induced tdTom expression specifically in HNF1β^{pos} BECs (Figure 5.2a, magenta arrowheads) and could not be detected in any other liver cell type prior to MCD or DDC induced liver injury.

To suppress hepatocyte β1-Integrin expression 9 days after the last tamoxifen injection, two doses of 0.5mg/kg RNAi nanoparticles were administered intravenously (IV) at 5 day intervals. 10 days after the first RNAi nanoparticle injection there was a visible reduction in hepatocyte β1-Integrin, at protein level (Figure 5.2b). In comparison, the control, anti-luciferase RNAi, which targets the absent luciferase gene, maintained hepatocyte β1-Integrin expression.

Together, this data demonstrates that the *K19$^{CreERT\ LSL}$tdTomato* transgene in combination with RNAi nanoparticles enables BEC lineage tracing and simultaneous hepatocyte β1-Integrin suppression.

Figure 5.2 – *K19Tom*$^{CreERT\ LSL}$*tdTomato* labels HNF1β^{pos} BECs and RNAi nanoparticles knock down hepatocyte β1-Integrin expression

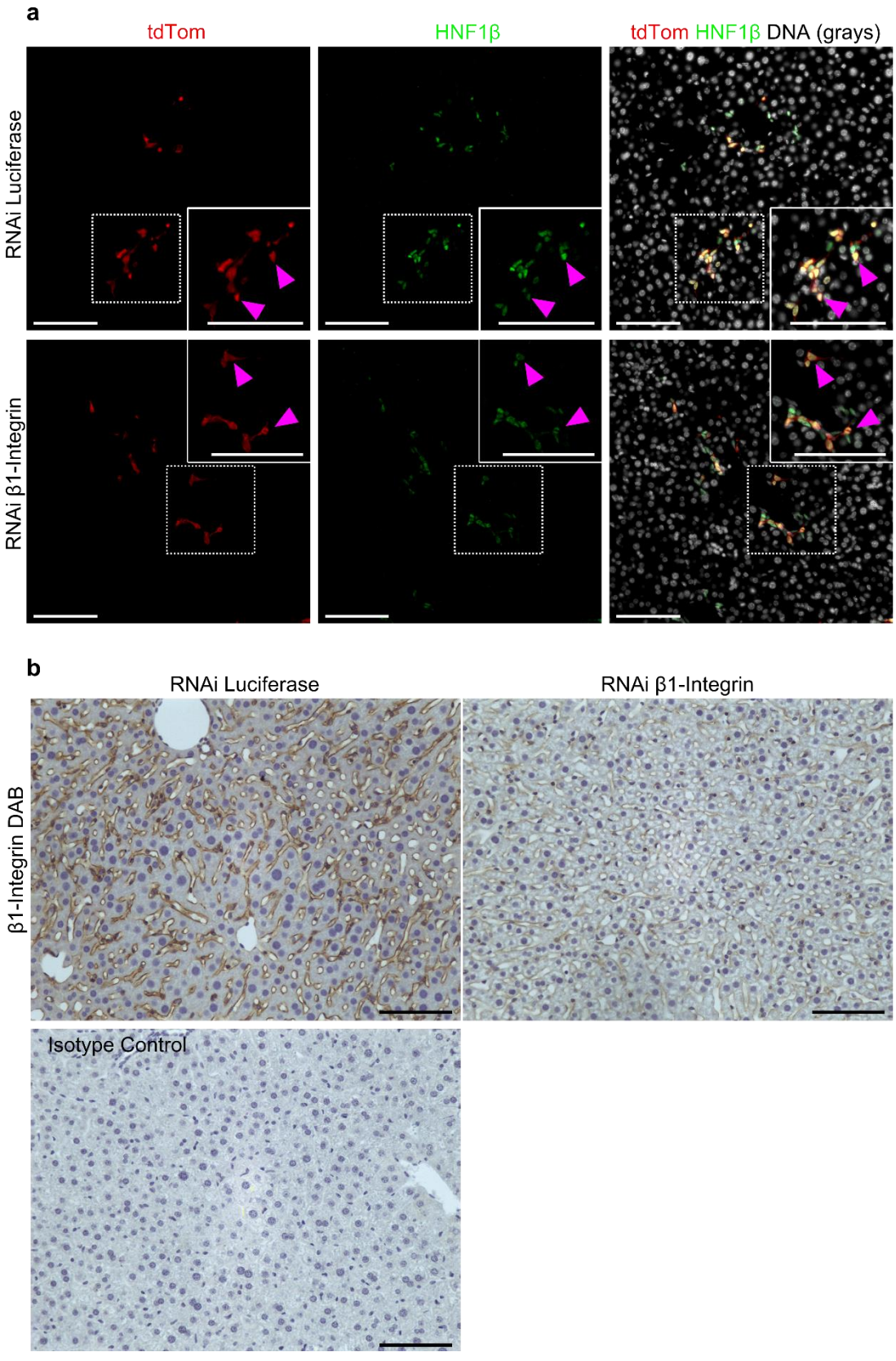

Figure 5.2: *K19$^{CreERT\ LSL}$tdTomato* livers treated with 3X4mg doses of tamoxifen and two 0.5mg/kg, IV, doses of either anti-luciferase or anti-β1-Integrin RNAi nanoparticles. **a**. tdTom/HNF1β dual immuno-fluorescence confocal images, HNF1β^{pos} BECs are labelled tdTom^{pos} – magenta arrowheads. **b**. β1-Integrin immunohistochemistry, images were captured with identical microscope settings. Isotype control refers to sample treated with rabbit IgG, which replaced the rabbit anti-Itgb1 antibody. Scale bars: 100μM.

Conventional murine liver injury models do not induce biliary derived regeneration

K19$^{CreERT\ LSL}$tdTomato induced labelling of BECs does not result in the emergence of tdTom^{pos} hepatocytes after liver injury caused by commonly used mouse hepatoxic injury diets: DDC, MCD and choline deficient ethionine supplemented (CDE) diet (toxic injury diet that models steatosis, DR, fibrosis and inflammation) (Figure 5.3).

Figure 5.3 – Traditional murine HPC inducing liver injury models do not result in BEC derived hepatocyte regeneration

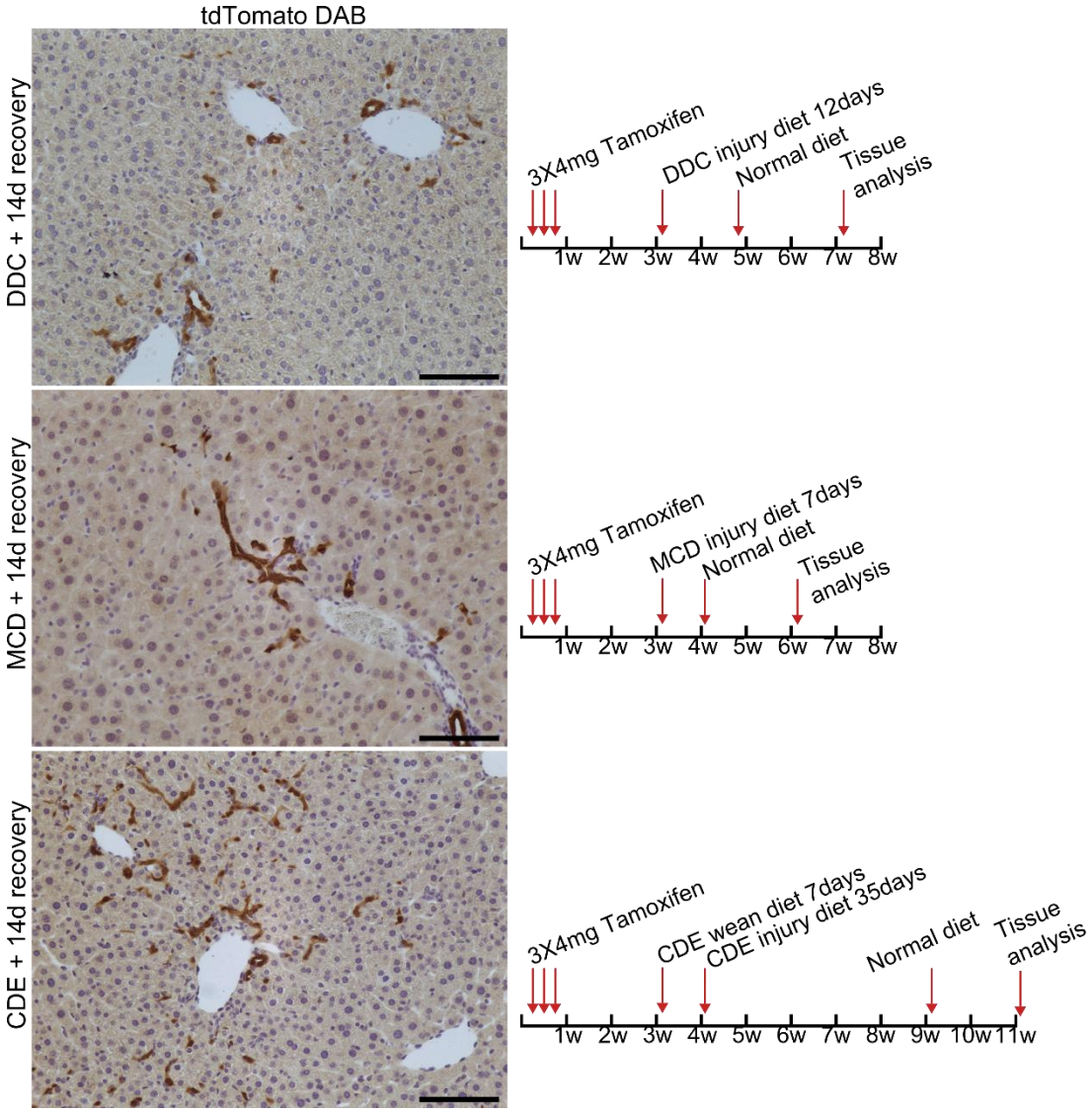

Figure 5.3: tdTomato immunohistochemistry of *K19*$^{CreERT\ LSL}$*tdTomato* livers that were injured using the DDC, MCD and CDE hepatoxic liver injury diets. Corresponding experimental timelines are displayed adjacent to images of each injury model. Scale bars: 100µM.

Itgb1 knock down in hepatocytes provokes biliary derived regeneration of the hepatocyte epithelium

Lipidoid-based nanoparticles specifically target hepatocytes suppressing *Itgb1* expression for 5days[263,266], resulting in significant β1-Integrin decreases at a protein level after 10 days (Figure 5.2b). I therefore, began the liver injury diets 10 days after the first nanoparticle injection. To induce liver injury and stimulate hepatocyte regeneration, nanoparticle treated *K19*$^{CreERT\ LSL}$*tdTomato* mice where given either MCD or DDC diet for 12 days (Figure 5.1).

Livers treated with the anti-β1-Integrin RNAi had small patches of tdTom^{pos}/HNF4α^{pos} hepatocytes adjacent to the PT (Figure 5.4). In contrast, no tdTom^{pos} hepatocytes were detected in the anti-luciferase RNAi treated livers. New tdTom^{pos} hepatocytes were adjacent to panCK^{pos}/tdTom^{pos} BEC, there periportal location was confirmed by their E-Cadherin expression.

Figure 5.4 – Hepatocyte *Itgb1* suppression combined with liver injury induces biliary derived hepatocyte regeneration

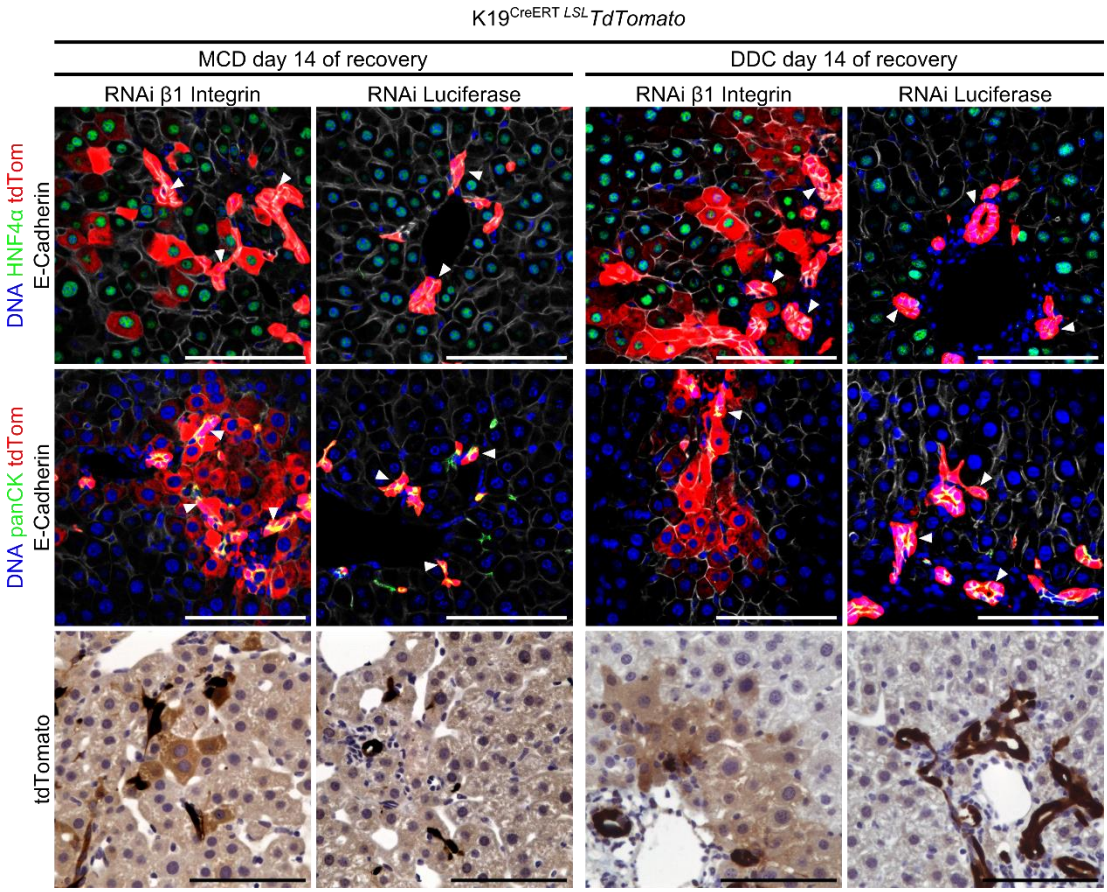

Figure 5.4: HNF4α/tdTom/E-Cadherin and panCK/tdTom/E-Cadherin immunofluorescence and anti-RFP immunohistochemistry reveals biliary to hepatocyte lineage tracing in RNAi β1-Integrin treated liver. RNAi β1-Integrin = samples that received nanoparticles containing interfering RNA against *Itgb1*. RNAi luciferase = control samples that received nanoparticles containing interfering RNA against the absent luciferase gene. Scale bars: 100µM.

Transcriptome comparison between hepatocyte derived hepatocytes and ductal derived hepatocytes

To compare distinct hepatocyte populations that have regenerated from alternative sources, livers were injured with MCD diet and hepatocytes were isolated using fluorescence activated cell sorting (FACS) (Figure 5.5a). Prior to FACS hepatocytes were purified using a Percoll gradient. Purified, living, hepatocytes were then selected using the gating strategy in Figure 5.5b, $tdTom^{pos}$ or $tdTom^{neg}$ hepatocytes were selected using gates established from control, C57BL/6, hepatocytes. Validation, using cytospins and immunofluorescence, revealed cells isolated by FACS were $HNF4\alpha^{pos}$, and were either $tdTom^{pos}$ or $tdTom^{neg}$ depending on the population that was selected (Figure 5.5c).

100,000 cells from each population were collected during FACS, sorted cells were lysed and extracted RNA was sequenced by the Wellcome Trust Clinical Research Facility at the Institute of Genetics and Molecular Medicine. Analysis of the global transcriptional state for each cell population revealed biliary derived hepatocytes (BDhepatocytes) from AAV8-p21 treated livers and $tdTom^{neg}$ hepatocytes from the β1-$integrin^{fl/fl}$ model were highly similar to hepatocytes and distinct from ductal cells (Figure 5.6 a and b). BDhepatocytes from the AAV8-p21 model clustered more closely with control hepatocytes than the $tdTom^{neg}$ hepatocytes from the β1-$integrin^{fl/fl}$ model. Selected genes associated with the hepatocyte and biliary phenotype, and WNT and notch signalling in the liver were analysed between the different populations. Control hepatocytes and BDhepatocytes had a clear hepatocyte gene expression profile, while the $tdTom^{neg}$ cell gene expression profile was mixed, expressing both hepatocyte and biliary genes (Figure 5.7b). Both WNT and notch signalling appeared upregulated in the cholangiocytes and $tdTom^{neg}$ hepatocytes when compared to control and BDhepatocytes (Figure 5.7b). Differences seen between the $tdTom^{neg}$ hepatocytes, the BDhepatocytes and the control hepatocytes were also detected with a 'phase 1 drug metabolism enzymes' qPCR array (Figure 5.7c), confirming the results from the RNA-Seq experiment.

Differences between the $tdTom^{neg}$ hepatocytes from the β1-$integrin^{fl/fl}$ model and the BD hepatocytes from the AAV8-p21 model were predominantly seen in: inflammatory

response, cell cycle, cell adhesion, negative regulation of apoptotic process, and oxidation-reduction process gene sets (Table 5.1).

The FACS and RNA-Seq experiments were part of collaborative work performed in conjunction with Dr Wei-Yu Lu. Bioinformatics and analysis of the RNA-Seq data was carried out by Dr John Thomson at the MRC Human Genetics Unit.

Figure 5.5 – Strategy to Isolate hepatocytes for whole transcriptome analysis

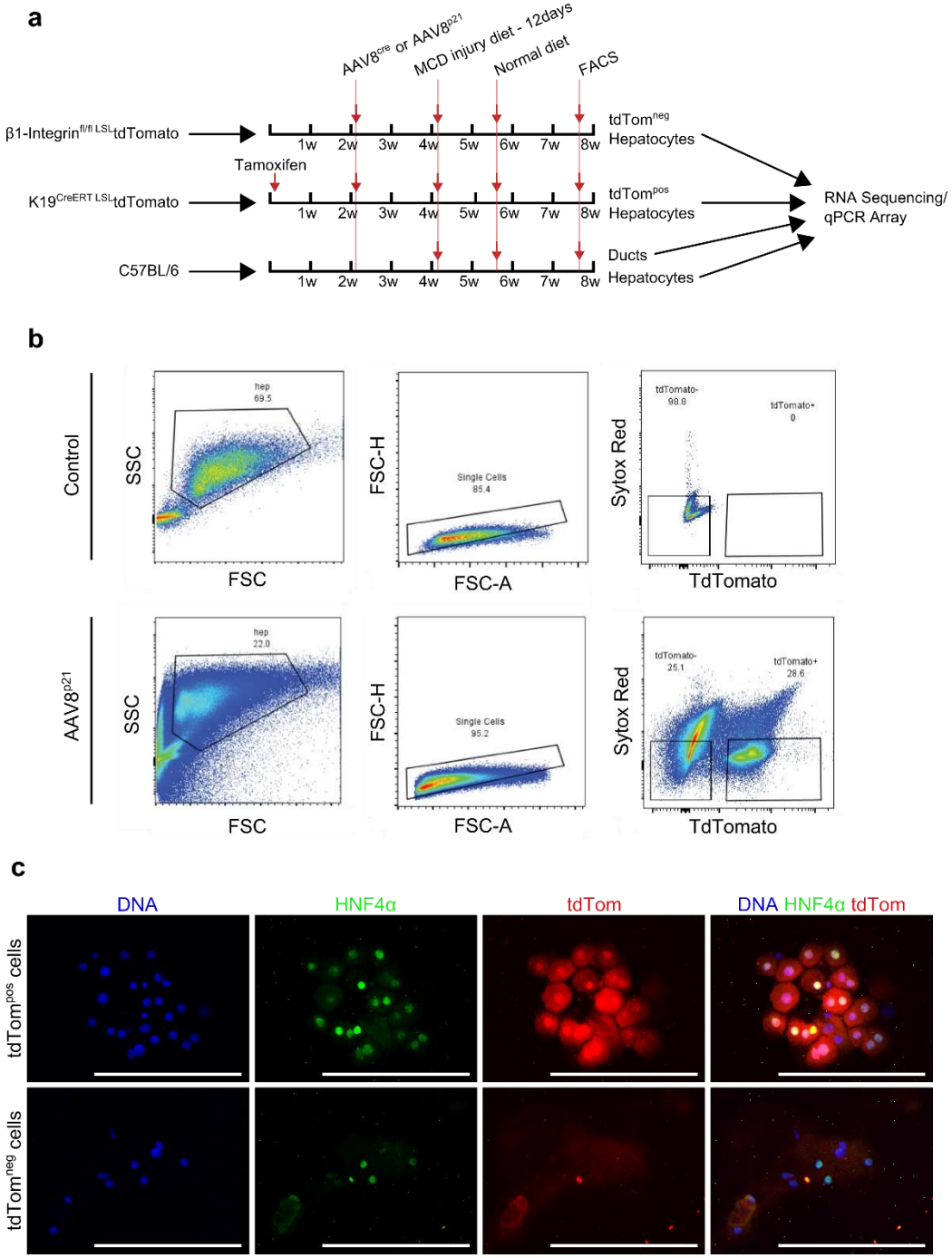

Figure 5.5: a. Schematic to isolate cells from three different mice genotypes that have received MCD induced liver injury for RNA-Seq analysis. **b**. FACS gating strategy to identify tdTom^{pos} and tdTom^{neg} hepatocytes. **c**. Cell cytospins and tdTom/HNF4α immunofluorescence of FACS samples to verify correct gating strategy. Scale bars: 100µM.

Figure 5.6 – Global transcriptome expression profiles from hepatocytes that have regenerated from distinct sources

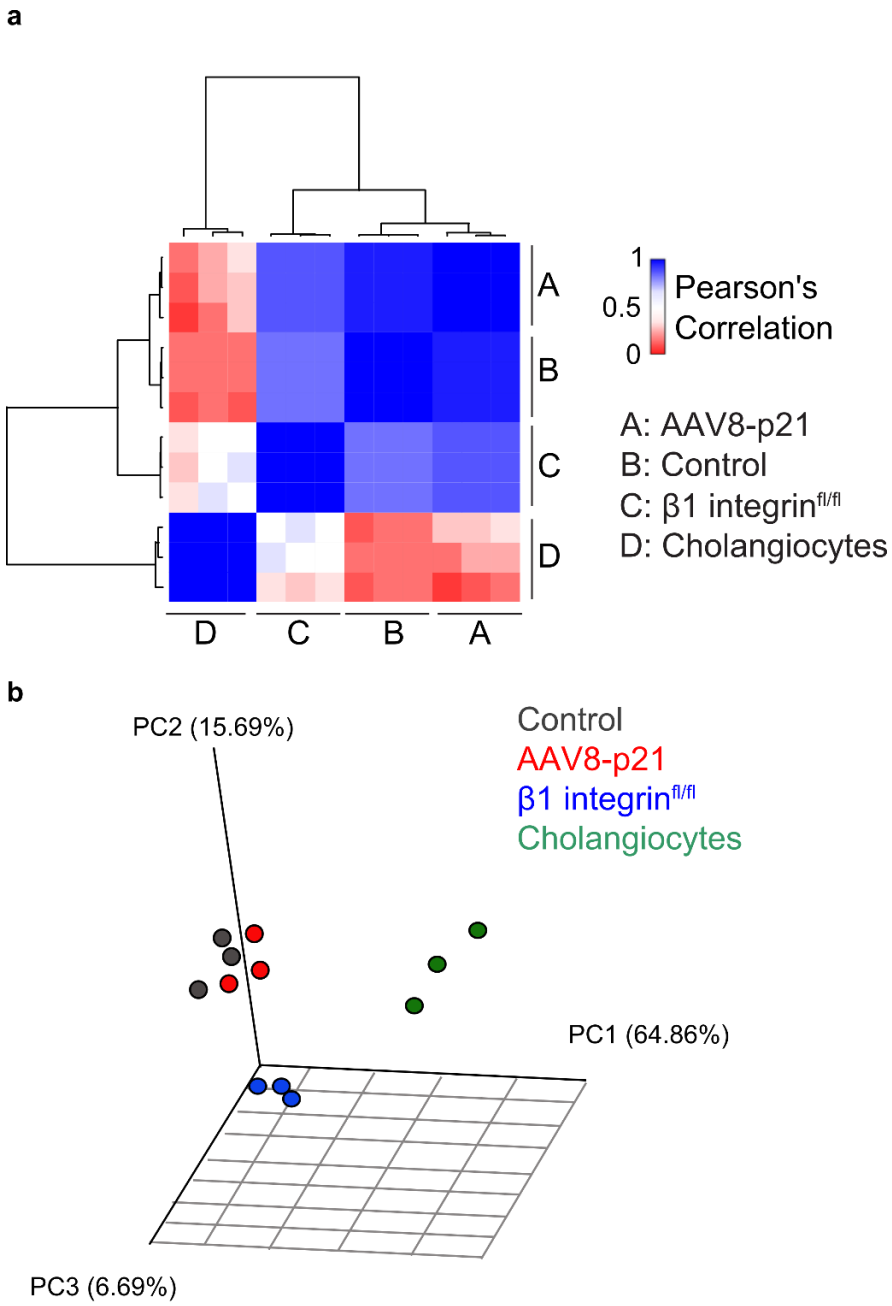

Figure 5.6: **a**. Pearson's correlation matrix comparing non-hepatocyte derived, tdTom^{neg}, hepatocytes (C) to BEC derived tdTom^{pos} hepatocytes (A) and control BEC (D) and hepatocytes (B). **b**. 3D principal component analysis comparing non-hepatocyte derived, tdTom^{neg}, hepatocytes (blue) to BEC derived tdTom^{pos} hepatocytes (red) and control BEC (green) and hepatocytes (black). Control-hepatocytes from C57BL/6. N=3 biological replicates per condition.

Figure 5.7 – Drug metabolism qPCR array and select genes from RNA-Seq reveal differences between tdTom^{neg} hepatocytes from the β1-Integrin$^{fl/fl}$ model and biliary derived hepatocytes from the AAV8^{p21} model

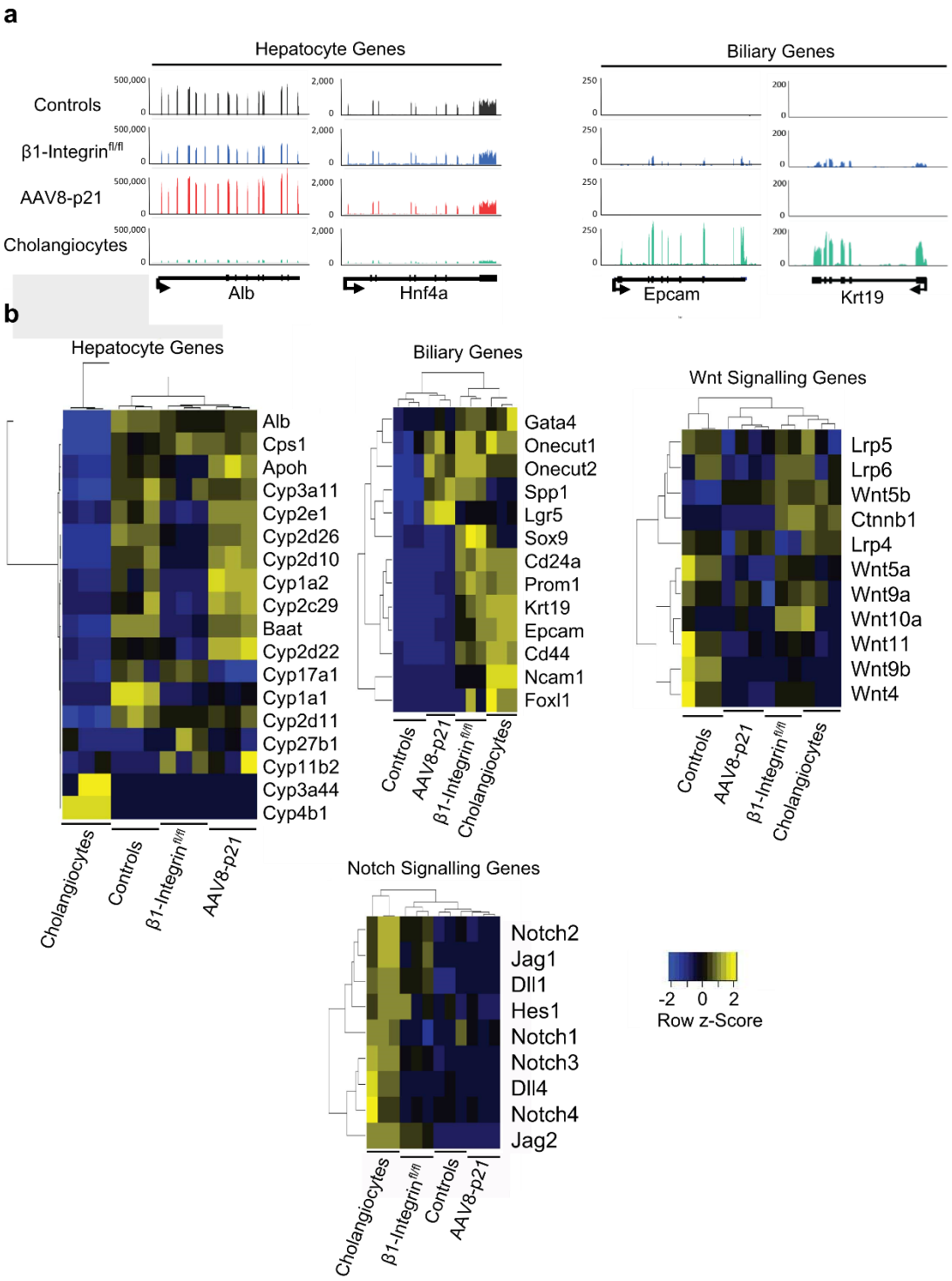

Figure 5.7 – continued

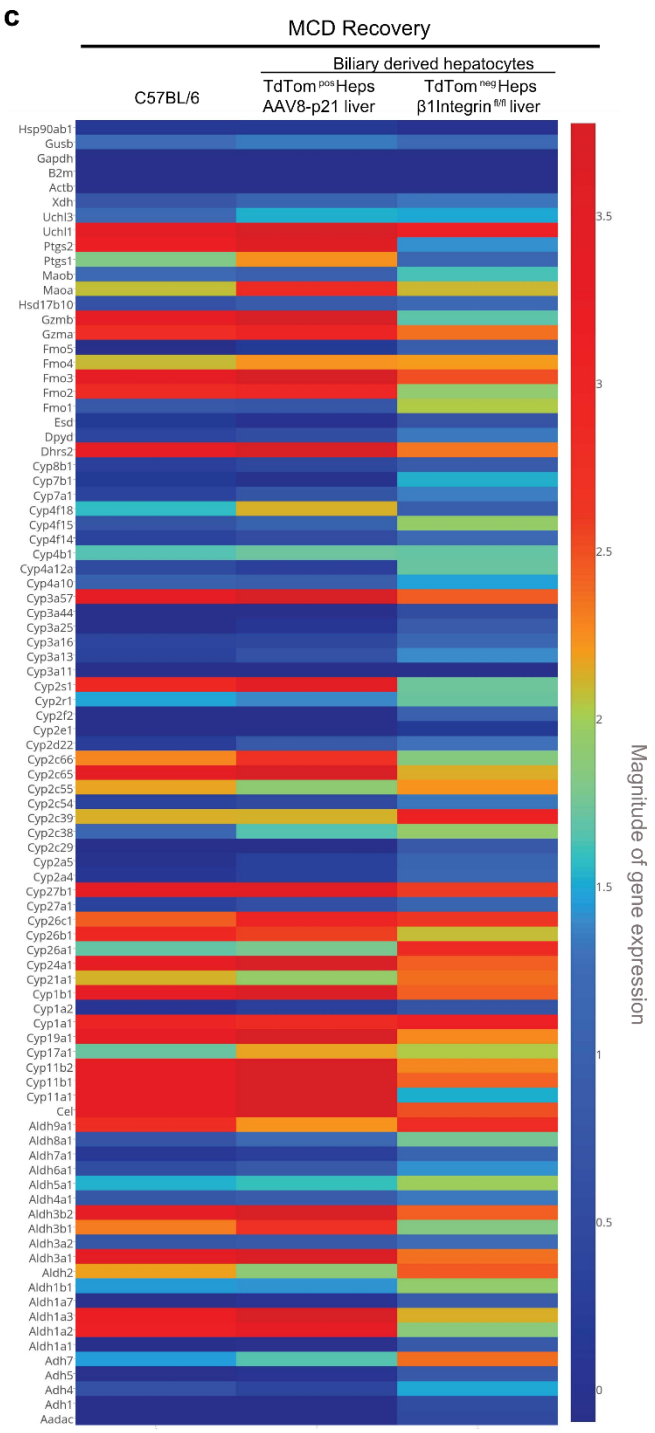

Figure 5.7: **a**. Visual examples of average RNA-Seq transcriptional reads in sample groups across select loci. **b**. RNA-seq generated Z-score heatmaps with hierarchical clustering across specific gene sets. Heatmaps display gene expression levels normalized to each gene. **c**. qPCR array for phase 1 drug metabolism enzymes. Controls-hepatocytes are from C57BL/6 mice. N=3 biological replicates per condition.

Table 5.1 – Gene set analysis comparing tdTom^{neg} hepatocytes from the β1-Integrin$^{fl/fl}$ model and biliary derived hepatocytes from the AAV8^{p21} model

Gene set	p value	Significant Genes
Inflammatory response	0.0000000039	*Axl, Clec7a, Cd14, Cd5l, Elf3, Aif1, Relb, Ccl2,Ccl6, Ccr2, Ccrl2, Cxcl10, Cxcl2, Cela1, Csf1r, Cyba, Cybb, Hck, Ly86, Ncf1, Nfkb2, Nfkbiz, Spp1, Tlr2, Tnfaip3*
Cell cycle	0.0000016	*Nek2, Racgap1, Src, Ajuba, Mki67, Aurka, Aurkb, Birc5, Cdca3, Ccna2, Ccnb1, Ccnb2, Ccnd1, Cdk1, Cdkn1a, Cdkn2c, Ect2, Esco2, Kif11, Mcm3, Mcm5, Mcm6, Nedd9, Ncapd2, Prc1, Rgs2, Smpd3, Ube2c, Uhrf1*
Cell adhesion	0.0000023	*Cd24a, Cd44, Cd63, Cd9, Ephb4, Src, Adgre5, Ajuba, Cadm4, Cx3cr1, Ctgf, Itga5, Itga6, Itgax, Itgb2, Lama5, Mfge8, Myh10, Nedd9, Nid1, Spp1, Sorbs3, Tgfbi, Tnfrsf12a, Vcam1*
Negative regulation of apoptotic process	0.00001	*Axl, Bcl2a1b, Cd44, Cd74, Nat8, Nckap1l, Src, Sox9, Tsc22d1, Aif1, Asns, Aurka, Birc5, Csf1r, Cdk1, Cdkn1a, Fabp1, Flna, Gstp1, Hck, Ier3, Map4k4, Plac8, Rgn, Spp1, Ucp2*
Oxidation-reduction process	0.001	*Sdr9c7, Adh4, Akr1c14, Blvrb, Cyp2a12, Cyp2c29, Cyp2c50, Cyp2c54, Cyp2e1, Cyp2u1, Cyp2c37, Cyp4a12a, Cyp7b1, Cyp8b1, Cyba, Cybb, Dhrs9, Fam213a, Gpx7, Hsd3b5, Hsd11b1, Rrm2, Sord, Scd2*

Table 5.1: Top 5 gene ontology (GO) terms, analysis of differentially expressed genes between hepatocytes from β1-Integrein$^{fl/fl}$ and AAV8-p21 livers.

Discussion

Impaired hepatocyte regeneration, mediated by β1-Integrin ablation, resulted in liver regeneration from a biliary origin. When hepatocyte regeneration is not impaired, as seen in the in the AAV8^{cre}-β1-Integrin^{WT} model and anti-luciferase RNAi treated livers, there is no biliary contribution to hepatocyte regeneration.

The two-step approach to both label BECs and knock down hepatocyte β1-Integrin expression caused small periportal patches of tdTom^{pos} hepatocytes to appear after hepatoxic diet induced liver injury. The prolonged, RNAi mediated, method to suppress β1-Integrin expression was not as robust as the AAV8^{cre}-β1-Integrin$^{fl/fl}$ model. Seven IV tail vein injections over a 35-day period leads to collapsed veins in the mouse tail and did occasionally result in a failed injection at the later time points, disrupting the phenotype and producing variability between each sample. Another limitation of the RNAi method was that it caused partial β1-Integrin ablation unlike the AAV8^{Cre}-β1-Integrin$^{fl/fl}$ model where all hepatocyte β1-Integrin expression was lost, which could explain the observed, moderate, phenotype. Also, the *K19$^{CreERT\ LSL}$tdTomato* transgene has a 40% labelling efficiency in the biliary epithelium[284], therefore, the degree of BEC to hepatocyte differentiation may be higher than detected. For these reasons, direct comparisons of hepatocyte regeneration between the AAV8^{cre}-β1-Integrin$^{fl/fl}$ model and the nanoparticle-*K19$^{CreERT\ LSL}$tdTomato* model are not ideal. However, the nanoparticle-*K19$^{CreERT\ LSL}$tdTomato* model does provide evidence, as a proof of principle, that hepatocyte β1-Integrin loss results in BEC derived regeneration of the hepatocyte compartment. One can therefore infer that in the AAV8^{cre}-β1-Integrin$^{fl/fl}$ model tdTom^{neg} hepatocytes are biliary derived.

Transcriptional analysis of regenerated hepatocytes revealed that BDhepatocytes from the AAV8-p21 model and tdTom^{neg} hepatocytes from the AAV8^{cre}-β1-Integrin$^{fl/fl}$ model were closely related to hepatocytes and distinct from BECs. However, with stricter clustering it was apparent that tdTom^{neg} hepatocytes were different to the control and BDhepatocytes. The tdTom^{neg} hepatocytes maintained expression of some BEC markers and had an increase in notch associated genes, which have been previously shown to induce a biliary phenotype[74,158]. Further to this, the top 5 GO terms identified between the tdTom^{neg} hepatocytes and BDhepatocytes such as

inflammatory response, cell cycle, and negative regulation of apoptotic process, are associated with liver injury. The fact that liver injury is not completely resolved in the β1-Integrin$^{fl/fl}$ model, as discussed in chapter 4, because of the continued presence of defective, β1-Integrin deficient, hepatocytes may account for the transcriptomic differences seen between the tdTom^{neg} hepatocytes and the control/BDhepatocytes. Another, explanation for the differences between BDhepatocytes from the AAV8-p21 model and tdTom^{neg} hepatocytes from the AAV8^{cre}-β1-Integrin$^{fl/fl}$ model could come from the isolation protocol. During FACS, hepatocytes were selected by their size, no cell surface markers were used to specifically select hepatocytes. It is therefore possible some contamination occurred and the tdTom^{neg} cell population was not completely pure.

Another interesting difference between the control hepatocytes and the tdTom^{neg} and the BDhepatocytes, identified through hierarchical clustering, were alterations in *Wnt* signalling. Explanations for this difference could be attributed to the spatial distribution of the various hepatocyte types along the PT-CV axis. The BDhepatocytes and the tdTom^{neg} hepatocytes were predominantly arranged around the PT in zone 1, a WNT low compartment of the liver[8,305]. In contrast the control hepatocytes would have been composed from a random collection of hepatocytes from all 3 liver zones, which may account for the differences.

To conclude, the origin of tdTom^{neg} hepatocytes in the AAV8^{cre}-β1-Integrin$^{fl/fl}$ model was from the biliary epithelium; confirmed by BEC lineage tracing with concurrent, RNAi mediated, hepatocyte *Itgb1* suppression. tdTom^{neg} hepatocytes that regenerate the liver in the AAV8^{cre}-β1-Integrin$^{fl/fl}$ model transcriptionally cluster relatively close to control hepatocytes but do continue to display some BEC characteristics, possibly induced by the continued presence of liver injury.

Chapter 6

Conclusions and future perspectives

Liver disease, a growing health risk in the UK[15], can evolve to liver cirrhosis or liver cancer, for which the only effective treatment is a liver transplant. A scarcity of liver organ donors however impedes and prevents patient treatment. Therefore, therapeutic alternatives are required to treat the growing incidents of liver cirrhosis. Enhancing endogenous liver regeneration is an attractive approach to treating liver disease, as it avoids complications that arise from cell and tissue transplantation therapies, particularly the use of immunosuppressant medicines. During human chronic liver disease, the hepatocyte compartment can no longer regenerate efficiently because of increased levels of parenchymal cell cycle arrest and senescence[34,36,306]. Concurrently, a periportal DR of unknown epithelial origin arises[37,42,61] and can hypothetically regenerate the hepatocyte epithelium[70]. To determine the regenerative potential of the DR and identify the types of epithelial cells and molecular signalling systems regulating DR mediated regeneration we need a suitable murine lineage tracing model.

Investigations of DR derived hepatocyte regeneration using mouse lineage tracing models have challenged the postulated regenerative potential of the DR[56,156,157,159]. A new theory, suggests that the DR is composed from both BECs and hepatocytes undergoing ductal metaplasia. The reversion of metaplastic hepatocytes back to a hepatocyte phenotype imitates biliary derived regeneration of the hepatocyte compartment[75], and actual biliary derived regeneration is minimal, less than 2%[150,156]. However, commonly used mouse liver injury models do not recapitulate human liver disease as they do not cause hepatocyte senescence or impair hepatocyte mediated regeneration[87,156].

The purpose of this PhD thesis therefore, was to determine if cells in the biliary epithelium can regenerate the hepatocyte epithelium. I hypothesised that impairing hepatocyte regeneration, via ablation of β1-Integrin, will induce biliary derived regeneration of the hepatocyte compartment. Using two independent lineage tracing techniques, I have ascertained that a non-hepatocyte source of regeneration from the biliary epithelium can regenerate hepatocytes, when a β1-Integrin deficient hepatocyte epithelium is injured and fails to regenerate. These findings support data from human liver pathology studies[42] and PH-AAF experiments in rat[44,171], which link HPC and DR derived regeneration with an impaired hepatocyte regenerative response.

The first aim of this thesis was to impair hepatocyte regeneration and lineage trace the hepatocyte compartment. Using: AAV8.TBG.Cre to induce a robust genetic recombination efficiency, a *ROSA26*^{LSL}*tdTomato* reporter, and conditional *Itgb1*$^{fl/fl}$ alleles that enable specific ablation of β1-Integrin; I lineage traced hepatocytes and simultaneously impaired hepatocyte regeneration. This experimental model revealed an essential requirement for hepatocyte β1-Integrin expression during homeostasis. The β1-Integrin$^{fl/fl}$ livers displayed markers of chronic liver injury and hepatocytes were regenerated from a non-hepatocyte source. Further analysis of the hepatocyte β1-Integrin$^{fl/fl}$ phenotype revealed a delayed regenerative response after hepatotoxic insult. Recovery of β1-Integrin$^{fl/fl}$ livers coincided with an infiltrating, expanding, DR and the emergence of periportal, non-hepatocyte derived, hepatocytes, which regenerated 25% of the parenchyma. Although hepatocyte ductal metaplasia occurred at peak injury and early in recovery, they were not the source of regeneration as the new hepatocytes were tdTomato negative.

To ascertain the origin of non-hepatocyte derived regeneration in the β1-Integrin$^{fl/fl}$ liver and address aim two of this thesis, BECs were lineage traced in a setting where hepatocyte *Itgb1* expression was knocked down. A *K19*$^{CreERT\ LSL}$*TdTomato* transgene was used to lineage trace BECs and lipid coated RNAi nanoparticles were employed to target hepatocyte β1-Integrin expression. Hepatocyte β1-Integrin knockdown and liver injury induced BEC differentiation to a hepatocyte fate, supporting the theory that new hepatocytes produced in the AAV8^{Cre}-β1-Integrin$^{fl/fl}$ experiments were biliary derived.

Whole genome comparisons between non-hepatocyte derived hepatocytes (tdTom^{neg} hepatocytes) from the AAV8^{Cre}-β1-Integrin$^{fl/fl}$ model, BDhepatocytes, control BECs and control hepatocytes showed tdTom^{neg} and BDhepatocytes were more like hepatocytes on a transcriptomic level than BECs. Furthermore, tdTom^{neg} hepatocytes had a hepatocyte morphology and expressed mature hepatocyte markers at a protein level. Together, these findings demonstrate that non-hepatocyte derived regeneration from a biliary origin produces functional hepatocytes. Although, underlying inflammation and fibrosis caused by remaining β1-Integrin deficient hepatocytes in the AAV8^{Cre}-β1-Integrin$^{fl/fl}$ model may explain why the tdTom^{neg} hepatocytes were, to a small degree, different to control hepatocytes and BDhepatocytes.

Developmental pathways; Hippo, Wnt, Notch, have all been shown to regulate cell fate in the liver[52,74,230]. However, it is unknown how these signalling pathways integrate with a scenario where hepatocyte regeneration is impaired and biliary derived regeneration takes over. The next big question that follows this thesis should ask: how does an environment where hepatocyte regeneration is impaired signal to BECs in the ducts to induce hepatocytic differentiation? The signalling axes regulating this process may be direct, between the defective hepatocytes and the BECs, or may be working indirectly, via the niche that surrounds BECs and DR (Figure6.1).

Figure 6.1 – What is the signalling axis between hepatocytes that cannot regenerate and the biliary derived HPC that differentiates to a hepatocyte fate?

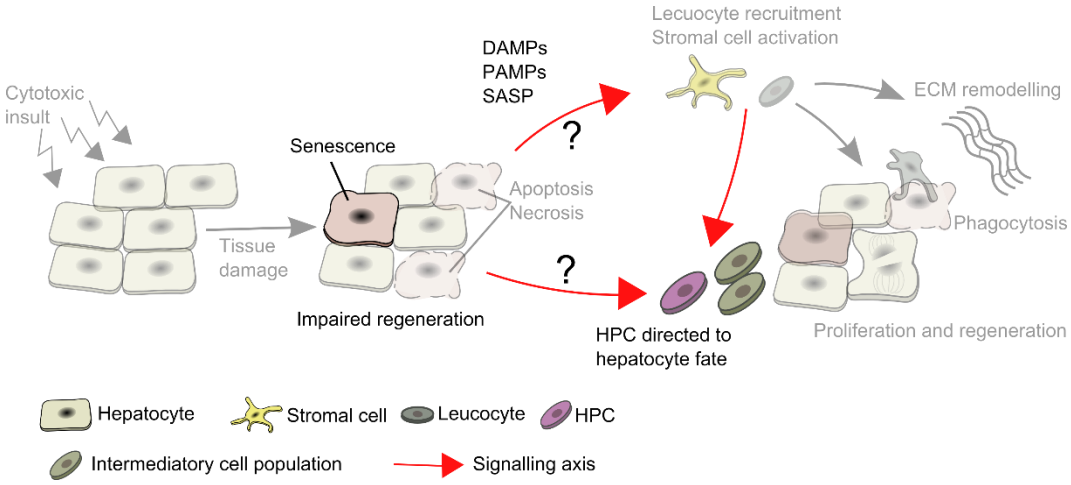

Figure 6.1: Schematic highlighting unknown mechanisms regulating hepatic progenitor cell (HPC) mediated regeneration when the hepatocyte epithelium cannot regenerate.

One prominent candidate that may influence BEC fate is the hepatocyte derived senescence associated secretory phenotype (SASP), as many senescent hepatocytes are present in human liver disease[35,36]. The SASP has been shown to promote cell plasticity and promote regeneration in the epidermis and liver[307]. Also, recent *in vivo* cell re-programming experiments have described enhanced pluripotent

reprogramming in cells exposed to the SASP of neighbouring senescent cells[308,309]. IL-6 activity was identified as a component that improved re-programming; interestingly, IL-6 signalling was a top hit in the gene set analysis of whole liver RNA-Seq from recovering β1-Integrin$^{fl/fl}$ livers. How IL-6, or the SASP in general, promote re-programming is currently unknown. Chromatin rearrangement towards an open chromatin state have been shown to facilitate cell re-programming *in vitro*[310,311]. It would be worth investigating whether a permissive SASP increases chromatin openness in the BECs and DR during liver disease. One could hypothesise that high levels of senescent hepatocytes produce a SASP that primes BECs for hepatocytic differentiation. To test this hypothesis, BECs could be isolated from senescent livers and then sequenced using ATAC-Seq, to reveal any changes in open chromatin and identify the altered locations on the BEC genome when compared to BECs from a control (non-senescent) liver. Another, simpler experiment, could involve either co-cultures with senescent hepatocytes and non-senescent BEC, or culturing BECs with conditioned medium from senescent hepatocytes, to identify any direct effects senescent hepatocytes have on BECs.

Systemic regulation of liver size and mass was previously mentioned as an important factor in liver growth[133,134]. Regulatory pathways that control liver size have been thought to act predominantly on the hepatocyte epithelium[135,312]. However, one could raise the question; if the hepatocyte epithelium fails to respond to these accumulating 'hepatostat' signals, do the BECs in the DR respond by differentiating in to new hepatocytes?

In relation to hepatostat signalling, recent work has identified a form of quorum sensing in the epidermis which directs regeneration according to the degree of damage. Quorum sensing was originally identified in bacteria and is a system where stimuli and response is coupled to population density[313]. In the epidermis, regeneration via a CCL2-macrophage- TNFα axis was only stimulated at a specific threshold of damage[314]. Perhaps a similar mechanism exists in the liver, where a certain threshold of senescent hepatocytes are needed to activate BEC derived regeneration.

The Hippo pathway can regulate organ size[141] and cell fate in the liver, overactivation of YAP in hepatocytes re-programmes them to a biliary fate[230]. Normally, YAP

expression is bimodal, BECs display strong nuclear YAP expression in contrast to the hepatocytes that express YAP at lower levels[230]. The activation of YAP is dependent on bile salt concentration in the liver[312,315], potentially explaining the bimodal expression between the two liver epithelia. Although, the ECM and physical stimulus[142] can also regulate the Hippo pathway, therefore multiple factors may be controlling the Hippo pathway in the liver. Indeed, the ECM surrounding hepatocytes is distinct to the ECM around BECs, the latter, for example is rich in laminins[44]. Also, Hippo signalling during hepatic development modulates enhancers that influences HNF4α and FOXA2 binding[206]. One could therefore hypothesise that loss of either the ECM or bile rich environment at the bile ducts reduces YAP activation in the BEC promoting hepatocytic differentiation. Data from Yimlamai et al supports this theory; in an artificial model where YAP expression could be controlled via a doxycycline sensitive transgene Yimlamai et al showed that hepatocytes with high YAP become BECs. Removal of doxycycline, resulted in loss of YAP activation and 20% of the converted BECs reverting back to hepatocytes[230]. However, the 20% reversion may be caused by incomplete hepatocyte re-programming and not caused by changes in YAP expression. An experimental, transgenic, model that enables YAP modulation in the biliary epithelium would determine the validity of this hypothesis.

Whole liver qPCR and RNA-Seq identified an increase in Wnt signalling during the emergence of $tdTom^{neg}$ hepatocytes in the $\beta1\text{-}Integrin^{fl/fl}$ model. Many of the identified *Wnt* ligands are expressed around the DR[302], although little is known about the functional roles of these *Wnt* ligands in liver regeneration. Canonical WNT/β-Catenin signalling is involved in hepatocyte differentiation and zonal specification[5,7,8], therefore some of the *Wnt* genes may have a role in promoting BEC differentiation to an hepatocyte fate. However, some of the identified *Wnt* genes are also involved in the non-canonical PCP pathway, suggesting WNT signalling may be carrying out multiple functions during DR derived liver regeneration such as: promoting proliferation, directing cell fate and organising BEC polarity in the DR.

In the introduction, I highlighted the many mechanisms that regulate cell fate during hepatic development. Future investigations should aim to determine if, or, how developmental signals might integrate in to the paradigm of biliary derived HPC

regeneration. For example, endothelial cells are essential for hepatic organogenesis[184] and are also a constituent of the adult HPC niche[46], yet no one has investigated if endothelial cells have a role in HPC mediated regeneration. Epigenetic changes probably have an important role in HPC mediated regeneration, as research in the neonate has revealed. Neonatal downregulation of the microRNA, Mir122, by the BEC transcription factor GRHL2 restricts biliary derived HPC differentiation in to hepatocytes[227]. Reversal of this regulatory mechanism, when hepatocyte regeneration is impaired, may be one mechanism that facilitates HPC regeneration. Finally, developmental studies have carefully dissected out the regulatory transcription factors that control hepatic fate[5]. Of particular relevance are the pioneer transcription factors Foxa1/2, which establish new gene programmes that induce hepatic differentiation[186,191]. Pioneer transcription factors regulate cell fate during regeneration and cancer formation[316–319]. Therefore, future work should consider which pioneer transcription factors are involved with HPC differentiation and how they are influenced by impaired hepatocyte regeneration.

The biliary epithelium can regenerate hepatocytes in a mammalian model of impaired hepatocyte regeneration. However, questions remain, can all BECs regenerate the hepatocyte epithelium? Or is there a specialised subset of BECs that can behave as HPCs? Or is it solely, the proposed HPC that resides in the Canal of Hering between the biliary ductules and the hepatocyte epithelium? BECs are heterogeneous, a subset of BECs, express high levels of CD133[87], ST14 (suppression of tumorigenicity 14)[320], or are EpCAM positive and upregulate LGR5[86,89]; these populations can form colonies and self-renew *in vitro* and can, competitively, repopulate the liver after transplantation.

In vivo studies of the intrahepatic biliary network have revealed significant biliary remodelling in response to liver injury[321]. Fate tracing of CD133 positive BECs using 3D imaging showed that BEC growth was stochastic, meaning there was no stem cell hierarchy, BECs could enter or terminate a growth phase suggesting the proliferating BEC sub-population was not fixed[322]. Together, *in vitro* and *in vivo* investigations of BECs have revealed heterogeneity, and the presence of a proliferative subpopulation

of cells. It is unknown if BEC heterogeneity is fixed regarding changes in cell fate, there appears to be a degree of plasticity regarding proliferative BEC subpopulations, as BECs can enter or exit a proliferative state. It is possible a similar degree of plasticity occurs when BECs become primed to differentiate in to hepatocytes.

The dynamics of biliary epithelial mediated regeneration is still unknown; future works should determine if the bulk of hepatocyte regeneration comes from biliary differentiation; or the production of small clusters of healthy biliary derived hepatocytes that proliferate, amplifying their population size to regenerate the liver. In the human, hepatocyte clusters adjacent to the DR have increased HGF and EGF activity[323], suggesting new biliary derived hepatocytes are stimulated further to expand their population size. The proliferation dynamics of the, new, $tdTom^{neg}$ hepatocytes in the $AAV8^{Cre}$-$\beta1\text{-}Integrin^{fl/fl}$ model could be determined using nucleotide analogues BrdU and EdU to sequentially label proliferating cells. Identifying any cells that are continuously dividing as they would be dual positive for BrdU and EdU.

This PhD thesis failed to fully describe the mechanisms involved in hepatocyte $\beta1\text{-}Integrin^{fl/fl}$ mediated pathogenesis. The literature indicates that there could be multiple effects produced by deleting β1-Integrin from hepatocytes. Further work is required to explain the exact mechanism causing liver damage, particularly in a setting where there are no hepatotoxins. Defining the $\beta1\text{-}Integrin^{fl/fl}$ mediated pathophysiology is important as it would reveal how different this mouse liver injury model is to chronic liver disease in the human. A greater understanding of the pathophysiology may also reveal or provide clues to which factors and processes in the liver micro-environment induce biliary epithelial duct cells to become hepatocytes.

The $\beta1\text{-}Integrin^{fl/fl}$ phenotype induced fibrosis and a reduction in the number of labelled hepatocytes. Further experiments over a longer period, 6-12months, should be performed to determine if all the $tdTom^{pos}/\beta1\text{-}Integrin^{fl/fl}$ hepatocytes are completely replaced by the biliary derived $tdTom^{neg}$ hepatocytes. Furthermore, the $\beta1\text{-}Integrin^{fl/fl}$ model of chronic liver disease should be investigated to determine if the chronic injury environment evolves into liver cancer. There is no obvious oncogene inducing mechanism from the loss of β1-Integrin and based upon previous studies

investigating cell growth in the liver, loss of β1-Integrin should have a negative impact on cancer formation[266]. However, the theory that an environment of chronic injury can induce liver cancer could be investigated with this model as it excludes the added complications of introducing a transgenic oncogene or carcinogenic molecule that mutates DNA. Also, the tdTomato labelling would lineage trace tumour origin, to determine if biliary derived ($tdTom^{neg}$ cells) or hepatocytes ($tdTom^{pos}$) contribute to tumorigenicity; recent data suggests malignant HCC predominantly arises from hepatocytes and not biliary derived DR[324].

This thesis has clarified the regenerative potential of the DR, demonstrating that in a setting of impaired hepatocyte regeneration BECs can produce new hepatocytes. This correlates with human liver pathology, where DRs producing new hepatocyte buds increases as the hepatocyte compartment becomes senescent. Now we know impaired hepatocyte regeneration is an essential pre-requisite for biliary derived regeneration, we can begin to investigate regulatory processes that control changes in liver cell fate. This work will advance our understanding of liver regeneration and may produce therapeutic targets that promote DR derived regeneration and hepatocytic differentiation.

References

1. Lefkowitch, J. H. in *Sherlock's Diseases of the Liver and Biliary System, 12th Edition* 1–19 (2011).
2. Overeem, A. W., Bryant, D. M. & van IJzendoorn, S. C. D. Mechanisms of apical-basal axis orientation and epithelial lumen positioning. *Trends Cell Biol.* **25,** 476–485 (2015).
3. Treyer, Aleksandr; Musch, A. Hepatocyte Polarity. *Compr Physiol* **3,** 243–287 (2013).
4. Shin, D., Pal, S. & Monga, S. Cellular and Molecular Basis of Liver Development. *Compr Physiol* **3,** 799–815 (2013).
5. Gordillo, M., Evans, T. & Gouon-Evans, V. Orchestrating liver development. *Development* **142,** 2094–2108 (2015).
6. Jungermann, K. & Kietzmann, T. Oxygen: modulator of metabolic zonation and disease of the liver. *Hepatology* **31,** 255–260 (2000).
7. Benhamouche, S. *et al.* Apc Tumor Suppressor Gene Is the 'Zonation-Keeper' of Mouse Liver. *Dev. Cell* **10,** 759–770 (2006).
8. Burke, Z. D. *et al.* Liver Zonation Occurs Through a B -Catenin–Dependent, c-Myc–Independent Mechanism. *Gastroenterology* **136,** 2316–2324.e3 (2009).
9. Planas-Paz, L. *et al.* The RSPO–LGR4/5–ZNRF3/RNF43 module controls liver zonation and size. *Nat. Cell Biol.* **18,** 467–479 (2016).
10. Rocha, A. S. *et al.* The Angiocrine Factor Rspondin3 Is a Key Determinant of Liver Zonation. *Cell Rep.* **13,** 1757–1764 (2015).
11. Halpern, K. B. *et al.* Single-cell spatial reconstruction reveals global division of labour in the mammalian liver. *Nature* **542,** 352–356 (2017).
12. Colnot, s . Perret, C. in *Molecular pathology of liver diseases* 7–16 (2011).

13. Mokdad, A. A. *et al.* Liver cirrhosis mortality in 187 countries between 1980 and 2010: a systematic analysis. *BMC Med.* **12,** 145 (2014).

14. Ratib, S., West, J., Crooks, C. J. & Fleming, K. M. Diagnosis of Liver Cirrhosis in England, a Cohort Study, 1998-2009: A Comparison With Cancer. *Am. J. Gastroenterol.* **109,** 190–198 (2014).

15. Williams, R. *et al.* Addressing liver disease in the UK: A blueprint for attaining excellence in health care and reducing premature mortality from lifestyle issues of excess consumption of alcohol, obesity, and viral hepatitis. *Lancet* **384,** 1953–1997 (2014).

16. Lucey, M. R., Mathurin, P. & Morgan, T. R. Alcoholic Hepatitis. *N Engl J Med* **360,** 2758–69 (2009).

17. Ezzati, M. & Riboli, E. Behavioral and Dietary Risk Factors for Noncommunicable Diseases. *N. Engl. J. Med.* **369,** 954–964 (2013).

18. Mathurin, P. & Deltenre, P. Effect of binge drinking on the liver: An alarming public health issue? *Gut* **58,** 613–617 (2009).

19. Lok, A. S. F. in *Sherlock's Diseases of the Liver and Biliary System, 12th Edition* 367–392 (2011).

20. Dusheiko, G. in *Sherlock's Diseases of the Liver and Biliary System, 12th Edition* 406–426 (2011).

21. Jones, R., Dunning, J. & Nelson, M. HIV and hepatitis C co-infection. *Int. J.* **59,** 1082–1087 (2005).

22. Rizzetto, M. *et al.* Transmission of the Hepatitis B Virus-Associated Delta Antigen to Chimpanzees. *J. Infect. Dis.* **141,** 590–602 (1980).

23. Karayiannis, P. & Thomas, H. C. in *Sherlock's Diseases of the Liver and Biliary System, 12th Edition* 353–366 (2011).

24. Stewart, S. & Day, C. in *Sherlock's Diseases of the Liver and Biliary System, 12th*

Edition (2011).

25. Wanless, I. R. & Lentz, J. S. Fatty liver hepatitis (steatohepatitis) and obesity: an autopsy study with analysis of risk factors. *Hepatology* **12,** 1106–1110 (1990).
26. Caldwell, S. H. & Argo, C. K. in *Sherlock's Diseases of the Liver and Biliary System, 12th Edition* 546–567 (2011).
27. Hirschfi, G. M. & Heathcote, E. J. in *Sherlock's Diseases of the Liver and Biliary System, 12th Edition* 452–477 (2011).
28. Adams, P. in *Sherlock's Diseases of the Liver and Biliary System, 12th Edition* 521–533 (2011).
29. Bassendine, M. F. in *Sherlock's Diseases of the Liver and Biliary System, 12th Edition* (2011).
30. Rushbrook, S. & Chapman, R. W. in *Sherlock's Diseases of the Liver and Biliary System, 12th Edition* 342–352 (2011).
31. Koti, R. S. & Davidson, B. R. in *Sherlock's Diseases of the Liver and Biliary System, 12th Edition* 294–311 (2011).
32. Pellicoro, A., Ramachandran, P., Iredale, J. P. & Fallowfield, J. A. Liver fibrosis and repair: immune regulation of wound healing in a solid organ. *Nat. Rev. Immunol.* **14,** 181–194 (2014).
33. Wiemann, S. U. *et al.* Hepatocyte telomere shortening and senescence are general markers of human liver cirrhosis. *FASEB J.* **16,** 935–942 (2002).
34. Marshall, A. *et al.* Relation between hepatocyte G1 arrest, impaired hepatic regeneration, and fibrosis in chronic hepatitis C virus infection. *Gastroenterology* **128,** 33–42 (2005).
35. Aravinthan, A. *et al.* Hepatocyte senescence predicts progression in non-alcohol-related fatty liver disease. *J. Hepatol.* **58,** 549–556 (2013).
36. Aravinthan, A. *et al.* Hepatocyte Expression of the Senescence Marker p21 Is Linked

to Fibrosis and an Adverse Liver-Related Outcome in Alcohol-Related Liver Disease. *PLoS One* **8,** 1–8 (2013).

37. Lowes, K. N., Brennan, B. a, Yeoh, G. C. & Olynyk, J. K. Oval cell numbers in human chronic liver diseases are directly related to disease severity. *Am. J. Pathol.* **154,** 537–541 (1999).

38. Yang, S. *et al.* Oval Cells Compensate for Damage and Replicative Senescence of Mature Hepatocytes in Mice with Fatty Liver Disease. *Hepatology* **39,** 403–411 (2004).

39. Roskams, T. *et al.* Oxidative stress and oval cell accumulation in mice and humans with alcoholic and nonalcoholic fatty liver disease. *Am. J. Pathol.* **163,** 1301–11 (2003).

40. Falkowski, O. *et al.* Regeneration of hepatocyte 'buds' in cirrhosis from intrabiliary stem cells. *J. Hepatol.* **39,** 357–364 (2003).

41. Roskams, T. a. *et al.* Nomenclature of the finer branches of the biliary tree: Canals, ductules, and ductular reactions in human livers. *Hepatology* **39,** 1739–1745 (2004).

42. Clouston, A. D. *et al.* Fibrosis correlates with a ductular reaction in hepatitis C: Roles of impaired replication, progenitor cells and steatosis. *Hepatology* **41,** 809–818 (2005).

43. Gouw, A. S. H., Clouston, A. D. & Theise, N. D. Ductular reactions in human liver: Diversity at the interface. *Hepatology* **54,** 1853–1863 (2011).

44. Paku, S., Schnur, J., Nagy, P. & Thorgeirsson, S. S. Origin and structural evolution of the early proliferating oval cells in rat liver. *Am. J. Pathol.* **158,** 1313–23 (2001).

45. Stueck, A. E. & Wanless, I. R. Hepatocyte buds derived from progenitor cells repopulate regions of parenchymal extinction in human cirrhosis. *Hepatology* **61,** 1696–1707 (2015).

46. Lorenzini, S. *et al.* Characterisation of a stereotypical cellular and extracellular adult

liver progenitor cell niche in rodents and diseased human liver. *Gut* **59,** 645–654 (2010).

47. Boulter, L., Lu, W. Y. & Forbes, S. J. Differentiation of progenitors in the liver: A matter of local choice. *J. Clin. Invest.* **123,** 1867–1873 (2013).

48. Viebahn, C. S. *et al.* Invading macrophages play a major role in the liver progenitor cell response to chronic liver injury. *J. Hepatol.* **53,** 500–507 (2010).

49. Bird, T. G. T. *et al.* Bone marrow injection stimulates hepatic ductular reactions in the absence of injury via macrophage-mediated TWEAK signaling. *Proc. Natl. Acad. Sci.* **110,** 6542–6547 (2013).

50. Yeoh, G. C. T. *et al.* Opposing roles of gp130-mediated STAT-3 and ERK-1/2 signaling in liver progenitor cell migration and proliferation. *Hepatology* **45,** 486–494 (2007).

51. Znoyko, I., Sohara, N., Spicer, S. S., Trojanowska, M. & Reuben, A. Expression of oncostatin M and its receptors in normal and cirrhotic human liver. *J. Hepatol.* **43,** 893–900 (2005).

52. Boulter, L. *et al.* Macrophage-derived Wnt opposes Notch signaling to specify hepatic progenitor cell fate in chronic liver disease. *Nat. Med.* **18,** 572–579 (2012).

53. Pintilie, D. G. *et al.* Hepatic stellate cells' involvement in progenitor-mediated liver regeneration. *Lab. Investig.* **90,** 1199–1208 (2010).

54. Takase, H. M. *et al.* FGF7 is a functional niche signal required for stimulation of adult liver progenitor cells that support liver regeneration. *Genes Dev.* **27,** 169–181 (2013).

55. Kim, K., Chen, C., Alpini, G. & Lau, L. F. CCN1 induces hepatic ductular reaction through integrin αv β 5 mediated activation of NF- κ B. *J. Clin. Invest.* **125,** 1886–1900 (2015).

56. Jörs, S. *et al.* Lineage fate of ductular reactions in liver injury and carcinogenesis. *J.*

Clin. Invest. **125,** 2445–2457 (2015).

57. Xie, G. *et al.* Cross-talk between Notch and Hedgehog regulates hepatic stellate cell fate in mice. *Hepatology* **58,** 1801–1813 (2013).

58. Kallis, Y. N. *et al.* Remodelling of extracellular matrix is a requirement for the hepatic progenitor cell response. *Gut* **60,** 525–533 (2011).

59. Hsieh, W.-C. *et al.* Galectin-3 regulates hepatic progenitor cell expansion during liver injury. *Gut* **64,** 312–321 (2014).

60. Tsuchiya, A. *et al.* PolySia-NCAM modulates the formation of ductular reactions in liver injury. *Hepatology* **60,** 1727–1740 (2014).

61. Richardson, M. M. *et al.* Progressive Fibrosis in Nonalcoholic Steatohepatitis: Association With Altered Regeneration and a Ductular Reaction. *Gastroenterology* **133,** 80–90 (2007).

62. Williams, M. J., Clouston, A. D. & Forbes, S. J. Links between hepatic fibrosis, ductular reaction, and progenitor cell expansion. *Gastroenterology* **146,** 349–356 (2014).

63. Knight, B., Lim, R., Yeoh, G. C. & Olynyk, J. K. Interferon-γ exacerbates liver damage, the hepatic progenitor cell response and fibrosis in a mouse model of chronic liver injury. *J. Hepatol.* **47,** 826–833 (2007).

64. Mederacke, I. *et al.* Fate tracing reveals hepatic stellate cells as dominant contributors to liver fibrosis independent of its aetiology. *Nat. Commun.* **4,** 1–11 (2013).

65. Jung, Y. *et al.* Signals from dying hepatocytes trigger growth of liver progenitors. *Gut* **59,** 655–665 (2010).

66. Hellerbrand, C., Stefanovic, B., Giordano, F., Burchardt, E. R. & Brenner, D. a. The role of TGFbeta1 in initiating hepatic stellate cell activation in vivo. *J. Hepatol.* **30,** 77–87 (1999).

67. Jiang, J. X., Mikami, K., Venugopal, S., Li, Y. & Torok, N. J. Apoptotic body

engulfment by hepatic stellate cells promotes their survival by the JAK/STAT and Akt/NF-KB-dependent pathways. *J. Hepatol.* **51,** 139–148 (2009).

68. Bourbonnais, E. *et al.* Liver fibrosis protects mice from acute hepatocellular injury. *Gastroenterology* **142,** 130–139.e4 (2012).
69. Barry-Hamilton, V. *et al.* Allosteric inhibition of lysyl oxidase-like-2 impedes the development of a pathologic microenvironment. *Nat. Med.* **16,** 1009–17 (2010).
70. Lin, W.-R. *et al.* The histogenesis of regenerative nodules in human liver cirrhosis. *Hepatology* **51,** 1017–1026 (2010).
71. Zhou, H., Rogler, L. E., Teperman, L., Morgan, G. & Rogler, C. E. Identification of hepatocytic and bile ductular cell lineages and candidate stem cells in bipolar ductular reactions in cirrhotic human liver. *Hepatology* **45,** 716–724 (2007).
72. Dezső, K. *et al.* Human liver regeneration in advanced cirrhosis is organized by the portal tree. *J. Hepatol.* **66,** 778–786 (2017).
73. Michalopoulos, G. K., Barua, L. & Bowen, W. C. Transdifferentiation of rat hepatocytes into biliary cells after bile duct ligation and toxic biliary injury. *Hepatology* **41,** 535–544 (2005).
74. Yanger, K. *et al.* Robust cellular reprogramming occurs spontaneously during liver regeneration. *Genes Dev.* **27,** 719–724 (2013).
75. Tarlow, B. D. *et al.* Bipotential Adult Liver Progenitors Are Derived from Chronically Injured Mature Hepatocytes. *Cell Stem Cell* **15,** 605–618 (2014).
76. Mccormick, P. A. in *Sherlock's Diseases of the Liver and Biliary System, 12th Edition* **12th editi,** page 103-120 (2011).
77. Burroughs, A. K. & O'Beirne, J. in *Sherlock's Diseases of the Liver and Biliary System, 12th Edition* 704–730 (2011).
78. Forbes, S. J., Gupta, S. & Dhawan, A. Cell therapy for liver disease: From liver transplantation to cell factory. *J. Hepatol.* **62,** S157–S169 (2015).

79. Overturf, K., Al-Dhalimy, M., Finegold, M. & Grompe, M. The repopulation potential of hepatocyte populations differing in size and prior mitotic expansion. *Am. J. Pathol.* **155,** 2135–43 (1999).

80. Azuma, H. *et al.* Robust expansion of human hepatocytes in Fah-/-/Rag2-/-/Il2rg-/- mice. *Nat. Biotechnol.* **25,** 903–10 (2007).

81. Grompe, M. *et al.* Pharmacological correction of neonatal lethal hepatic dysfunction in a murine model of hereditary tyrosinaemia type I. *Nat. Genet.* **10,** 453–460 (1995).

82. Hay, D. C. *et al.* Efficient differentiation of hepatocytes from human embryonic stem cells exhibiting markers recapitulating liver development in vivo. *Stem Cells* **26,** 894–902 (2008).

83. Espejel, S. *et al.* Induced Pluripotent Stem Cell-Derived Hepatocytes Have the Function and Proliferative Capabilities Needed for Liver Regeneration in Mice. *J. Clin. Invest.* **120,** 3120–3126 (2010).

84. Tsuchiya, A. *et al.* Long-term extensive expansion of mouse hepatic stem/progenitor cells in a novel serum-free culture system. *Gastroenterology* **128,** 2089–2104 (2005).

85. Okabe, M. *et al.* Potential hepatic stem cells reside in EpCAM+ cells of normal and injured mouse liver. *Development* **136,** 1951–1960 (2009).

86. Huch, M. *et al.* In vitro expansion of single Lgr5+ liver stem cells induced by Wnt-driven regeneration. *Nature* **494,** 247–50 (2013).

87. Lu, W.-Y. *et al.* Hepatic progenitor cells of biliary origin with liver repopulation capacity. *Nat. Cell Biol.* **17,** 971–983 (2015).

88. Qiu, Q., Hernandez, J. C., Dean, A. M., Rao, P. H. & Darlington, G. J. CD24-Positive Cells from Normal Adult Mouse Liver Are Hepatocyte Progenitor Cells. *Stem Cells Dev.* **20,** 2177–2188 (2011).

89. Huch, M. *et al.* Long-Term Culture of Genome-Stable Bipotent Stem Cells from Adult Human Liver. *Cell* **160,** 299–312 (2015).

90. Katsuda, T. *et al.* Conversion of Terminally Committed Hepatocytes to Culturable Bipotent Progenitor Cells with Regenerative Capacity. *Cell Stem Cell* **20,** 41–55 (2016).

91. Rezvani, M. *et al.* In Vivo Hepatic Reprogramming of Myofibroblasts with AAV Vectors as a Therapeutic Strategy for Liver Fibrosis. *Cell Stem Cell* **18,** 809–816 (2016).

92. Gieseck, R. L. *et al.* Interleukin-13 Activates Distinct Cellular Pathways Leading to Ductular Reaction, Steatosis, and Fibrosis. *Immunity* **45,** 145–158 (2016).

93. Umesono, Y. *et al.* The molecular logic for planarian regeneration along the anterior-posterior axis. *Nature* **500,** 73–6 (2013).

94. Tanaka, E. M. The Molecular and Cellular Choreography of Appendage Regeneration. *Cell* **165,** 1598–1608 (2016).

95. Barker, N. Adult intestinal stem cells: critical drivers of epithelial homeostasis and regeneration. *Nat. Rev. Mol. Cell Biol.* **15,** 19–33 (2014).

96. Gurtner, G., Werner, S., Barrandon, Y. & Langaker, B. Wound repair and regeneration. *Nature* **49,** 35–43 (2008).

97. Barker, N. *et al.* Identification of stem cells in small intestine and colon by marker gene Lgr5. *Nature* **449,** 1003–1007 (2007).

98. Takeo, M. *et al.* Wnt activation in nail epithelium couples nail growth to digit regeneration. *Nature* **499,** 228–232 (2013).

99. Le Grand, F., Jones, A. E., Seale, V., Scime, A. & Rudnicki, M. A. Wnt7a Activates the Planar Cell Polarity Pathway to Drive the Symmetric Expansion of Satellite Stem Cells. *Cell Stem Cell* **4,** 535–547 (2009).

100. Peng, T. *et al.* Hedgehog actively maintains adult lung quiescence and regulates repair and regeneration. *Nature* **526,** 578–582 (2015).

101. Alman, B. a. The role of hedgehog signalling in skeletal health and disease. *Nat. Rev.*

Rheumatol. **1,** 1–9 (2015).

102. Fre, S. *et al.* Notch signals control the fate of immature progenitor cells in the intestine. *Nature* **435,** 964–968 (2005).

103. Aguirre, A., Rubio, M. E. & Gallo, V. Notch and EGFR pathway interaction regulates neural stem cell number and self-renewal. *Nature* **467,** 323–327 (2010).

104. López-Onieva, L., Fernández-Miñán, A. & González-Reyes, A. Jak/Stat signalling in niche support cells regulates dpp transcription to control germline stem cell maintenance in the Drosophila ovary. *Development* **135,** 533–540 (2008).

105. Sugiyama, T., Kohara, H., Noda, M. & Nagasawa, T. Maintenance of the Hematopoietic Stem Cell Pool by CXCL12-CXCR4 Chemokine Signaling in Bone Marrow Stromal Cell Niches. *Immunity* **25,** 977–988 (2006).

106. Ding, B.-S. *et al.* Inductive angiocrine signals from sinusoidal endothelium are required for liver regeneration. *Nature* **468,** 310–315 (2010).

107. Rafii, S., Butler, J. M. & Ding, B.-S. Angiocrine functions of organ-specific endothelial cells. *Nature* **529,** 316–325 (2016).

108. Miron, V. E. *et al.* M2 microglia and macrophages drive oligodendrocyte differentiation during CNS remyelination. *Nat. Neurosci.* **16,** 1211–8 (2013).

109. Godwin, J. W., Pinto, A. R. & Rosenthal, N. A. Macrophages are required for adult salamander limb regeneration. *Proc. Natl. Acad. Sci.* **110,** 9415–20 (2013).

110. Kazanis, I. *et al.* Quiescence and activation of stem and precursor cell populations in the subependymal zone of the mammalian brain are associated with distinct cellular and extracellular matrix signals. *J. Neurosci.* **30,** 9771–9781 (2010).

111. Lukjanenko, L. *et al.* Loss of fibronectin from the aged stem cell niche affects the regenerative capacity of skeletal muscle in mice. *Nat. Med.* **22,** 897–905 (2016).

112. Xin, T., Greco, V. & Myung, P. Review Hardwiring Stem Cell Communication through Tissue Structure. *Cell* **164,** 1212–1225 (2016).

113. Karin, M. & Clevers, H. Reparative inflammation takes charge of tissue regeneration. *Nat. Rev.* **529,** 307–315 (2016).

114. Fuchs, E., Tumbar, T. & Guasch, G. Socializing with the neighbors: Stem cells and their niche. *Cell* **116,** 769–778 (2004).

115. Shin, K. *et al.* Hedgehog/Wnt feedback supports regenerative proliferation of epithelial stem cells in bladder. *Nature* **472,** 110–114 (2011).

116. Lindemans, C. A. *et al.* Interleukin-22 promotes intestinal-stem-cell-mediated epithelial regeneration. *Nature* **528,** 560–564 (2015).

117. Blanpain, C. & Fuchs, E. Stem cell plasticity. Plasticity of epithelial stem cells in tissue regeneration. *Science* **344,** 1242281 (2014).

118. Tata, P. R. *et al.* Dedifferentiation of committed epithelial cells into stem cells in vivo. *Nature* **503,** 218–23 (2013).

119. Rando, T. a. & Chang, H. Y. Aging, rejuvenation, and epigenetic reprogramming: Resetting the aging clock. *Cell* **148,** 46–57 (2012).

120. Carlson, M. E. & Conboy, I. M. Loss of stem cell regenerative capacity within aged niches. *Aging Cell* **6,** 371–382 (2007).

121. Signer, R. a J. & Morrison, S. J. Mechanisms that regulate stem cell aging and life span. *Cell Stem Cell* **12,** 152–165 (2013).

122. Keyes, B. E. *et al.* Impaired Epidermal to Dendritic T Cell Signaling Slows Wound Repair in Aged Skin. *Cell* **167,** 1323–1338.e14 (2016).

123. Conboy, I. M. *et al.* Rejuvenation of aged progenitor cells by exposure to a young systemic environment. *Nature* **433,** 760–764 (2005).

124. Matsuo, T. *et al.* Control mechanism of the circadian clock for timing of cell division in vivo. *Science* **302,** 255–259 (2003).

125. Mitchell, C. & Willenbring, H. A reproducible and well-tolerated method for 2/3 partial hepatectomy in mice. *Nat. Protoc.* **3,** 1167–1170 (2008).

126. Michalopoulos, G. K. and & DeFrances, M. C. Liver Regeneration. *Science* **276,** 60–66 (1997).

127. Wang, B., Zhao, L., Fish, M., Logan, C. Y. & Nusse, R. Self-renewing diploid Axin2+ cells fuel homeostatic renewal of the liver. *Nature* **524,** 180–185 (2015).

128. Mascré, G. *et al.* Distinct contribution of stem and progenitor cells to epidermal maintenance. *Nature* **489,** 257–262 (2012).

129. Kang, L.-I., Mars, W. M. & Michalopoulos, G. K. Signals and cells involved in regulating liver regeneration. *Cells* **1,** 1261–92 (2012).

130. Miyaoka, Y. *et al.* Hypertrophy and Unconventional Cell Division of Hepatocytes Underlie Liver Regeneration. *Curr. Biol.* **22,** 1166–1175 (2012).

131. Gentric, G. & Desdouets, C. Polyploidization in liver tissue. *Am. J. Pathol.* **184,** 322–331 (2014).

132. Huang, J. & Rudnick, D. a. Elucidating the metabolic regulation of liver regeneration. *Am. J. Pathol.* **184,** 309–321 (2014).

133. Van Thiel, D. H. *et al.* Rapid growth of an intact human liver transplanted into a recipient larger than the donor. *Gastroenterology* **93,** 1414–1419 (1987).

134. Francavilla, A. *et al.* Small for size liver transplanted into larger recipient: A model of hepatic regeneration. *Hepatology* **19,** 210–216 (1994).

135. Michalopoulos, G. K. Liver regeneration after partial hepatectomy: critical analysis of mechanistic dilemmas. *Am. J. Pathol.* **176,** 2–13 (2010).

136. Gkretsi, V. *et al.* Liver-specific ablation of integrin-linked kinase in mice results in abnormal histology, enhanced cell proliferation, and hepatomegaly. *Hepatology* **48,** 1932–1941 (2008).

137. Apte, U. *et al.* Enhanced liver regeneration following changes induced by hepatocyte-specific genetic ablation of integrin-linked kinase. *Hepatology* **50,** 844–851 (2009).

138. Cano-Gauci, D. F. *et al.* Glypican-3-deficient mice exhibit developmental overgrowth

and some of the abnormalities typical of Simpson-Golabi-Behmel syndrome. *J. Cell Biol.* **146,** 255–264 (1999).

139. Liu, B. *et al.* Investigation of the role of glypican 3 in liver regeneration and hepatocyte proliferation. *Am. J. Pathol.* **175,** 717–724 (2009).

140. Dong, J. *et al.* Elucidation of a Universal Size-Control Mechanism in Drosophila and Mammals. *Cell* **130,** 1120–1133 (2007).

141. Camargo, F. D. *et al.* YAP1 Increases Organ Size and Expands Undifferentiated Progenitor Cells. *Curr. Biol.* **17,** 2054–2060 (2007).

142. Halder, G., Dupont, S. & Piccolo, S. Transduction of mechanical and cytoskeletal cues by YAP and TAZ. *Nat. Rev. Mol. Cell Biol.* **13,** 591–600 (2012).

143. Michalopoulos, G. K. & Khan, Z. Liver stem cells: Experimental findings and implications for human liver disease. *Gastroenterology* **149,** 876–882 (2015).

144. Mauro, A. Satellite Cell of Skeletal Muscle Fibers. *J. Biophys. Biochem. Cytol.* **9,** 493–495 (1961).

145. Aziz, A., Sebastian, S. & Dilworth, J. J. The Origin and Fate of Muscle Satellite Cells. *Stem Cell Rev. Reports* **8,** 609–622 (2012).

146. Cotsarelis, G., Sun, T. T. & Lavker, R. M. Label-retaining cells reside in the bulge area of pilosebaceous unit: Implications for follicular stem cells, hair cycle, and skin carcinogenesis. *Cell* **61,** 1329–1337 (1990).

147. Means, A. L., Xu, Y., Zhao, A., Ray, K. C. & Gu, G. A CK19CreERT Knockin Mouse Line Allows for Conditional DNA Recombination in Epithelial Cells in Multiple Endodermal Organs. *Genesis* **46,** 318–323 (2008).

148. Furuyama, K. *et al.* Continuous cell supply from a Sox9-expressing progenitor zone in adult liver, exocrine pancreas and intestine. *Nat. Genet.* **43,** 34–41 (2011).

149. Español-Suñer, R. *et al.* Liver progenitor cells yield functional hepatocytes in response to chronic liver injury in mice. *Gastroenterology* **143,** 1564–1575.e7 (2012).

150. Rodrigo-Torres, D. *et al.* The biliary epithelium gives rise to liver progenitor cells. *Hepatology* **60,** 1367–1377 (2014).

151. Carpentier, R. *et al.* Embryonic ductal plate cells give rise to cholangiocytes, periportal hepatocytes, and adult liver progenitor cells. *Gastroenterology* **141,** 1432–1438.e4 (2011).

152. Wang, X. *et al.* Osteopontin induces ductular reaction contributing to liver fibrosis. *Gut* **63,** 1805–1818 (2014).

153. Tarlow, B. D., Finegold, M. J. & Grompe, M. Clonal tracing of Sox9+ liver progenitors in mouse oval cell injury. *Hepatology* **60,** 278–289 (2014).

154. Shin, S. *et al.* Foxl1-Cre-marked adult hepatic progenitors have clonogenic and bilineage differentiation potential. *Genes Dev.* **25,** 1185–1192 (2011).

155. Shin, S., Upadhyay, N., Greenbaum, L. E. & Kaestner, K. H. Ablation of Foxl1-Cre-labeled hepatic progenitor cells and their descendants impairs recovery of mice from liver injury. *Gastroenterology* **148,** 192–202.e3 (2015).

156. Yanger, K. *et al.* Adult Hepatocytes Are Generated by Self-Duplication Rather than Stem Cell Differentiation. *Cell Stem Cell* **19,** 340–349 (2014).

157. Malato, Y. *et al.* Fate tracing of mature hepatocytes in mouse liver homeostasis and regeneration. *J. Clin. Invest.* **121,** 4850–4860 (2011).

158. Sekiya, S. & Suzuki, A. Hepatocytes, rather than cholangiocytes, can be the major source of primitive ductules in the chronically injured mouse liver. *Am. J. Pathol.* **184,** 1468–1478 (2014).

159. Schaub, J. R., Malato, Y., Gormond, C. & Willenbring, H. Evidence against a Stem Cell Origin of New Hepatocytes in a Common Mouse Model of Chronic Liver Injury. *CellReports* **8,** 933–939 (2014).

160. Wang, Y. *et al.* Genetic tracing of hepatocytes in liver homeostasis, injury, and regeneration. *J. Biol. Chem.* **292,** 8594–8604 (2017).

161. He, L. *et al.* Enhancing the precision of genetic lineage tracing using dual recombinases. *Nat. Med.* (2017). doi:10.1038/nm.4437

162. Jho, E. *et al.* Wnt/beta-catenin/Tcf signaling induces the transcription of Axin2, a negative regulator of the signaling pathway. *Mol. Cell. Biol.* **22,** 1172–83 (2002).

163. van Amerongen, R., Bowman, A. N. & Nusse, R. Developmental Stage and Time Dictate the Fate of Wnt/β-Catenin-Responsive Stem Cells in the Mammary Gland. *Cell Stem Cell* **11,** 387–400 (2012).

164. Minear, S. *et al.* Wnt proteins promote bone regeneration. *Sci. Transl. Med.* **2,** 29ra30 (2010).

165. Tsai, J. M. *et al.* Localized hepatic lobular regeneration by central-vein-associated lineage-restricted progenitors. *Proc. Natl. Acad. Sci.* **114,** 3654–3659 (2017).

166. Font-Burgada, J. *et al.* Hybrid Periportal Hepatocytes Regenerate the Injured Liver without Giving Rise to Cancer. *Cell* **162,** 766–779 (2015).

167. Kuwahara, R. *et al.* The hepatic stem cell niche: Identification by label-retaining cell assay. *Hepatology* **47,** 1994–2002 (2008).

168. Pu, W. *et al.* Mfsd2a+ hepatocytes repopulate the liver during injury and regeneration. *Nat. Commun.* **7,** 13369 (2016).

169. Bralet, M. P., Branchereau, S., Brechot, C. & Ferry, N. Cell lineage study in the liver using retroviral mediated gene transfer. Evidence against the streaming of hepatocytes in normal liver. *Am. J. Pathol.* **144,** 896–905 (1994).

170. Trautwein, C. *et al.* 2-acetaminofluorene blocks cell cycle progression after hepatectomy by p21 induction and lack of cyclin E expression. *Oncogene* **18,** 6443–6453 (1999).

171. Evarts, R. P. *et al.* In Vivo Differentiation of Rat Liver Oval Cells into Hepatocytes. *Cancer Res.* **49,** 1541–1547 (1989).

172. Pi, L., Oh, S.-H., Shupe, T. & Petersen, B. E. Role of Connective Tissue Growth

Factor in Oval Cell Response During Liver Regeneration After 2-AAF/PHx in Rats. *Gastroenterology* **128,** 2077–2088 (2005).

173. Petersen, B. E., Zajac, V. F. & Michalopoulos, G. K. Hepatic oval cell activation in response to injury following chemically induced periportal or pericentral damage in rats. *Hepatology* **27,** 1030–1038 (1998).

174. Debaun, J. R., Rowley, J. Y., Miller, E. C. & Miller, J. A. Sulfotransferase Activation of N-Hydroxy-2-acetylaminofluorene in Rodent Livers Susceptible and Resistant to this Carcinogen. *Proc Soc Exp Biol Med* **129,** 268–273 (1967).

175. Kaji, K. *et al.* DNMT1 is a required genomic regulator for murine liver histogenesis and regeneration. *Hepatology* **64,** 582–598 (2016).

176. Li, D. *et al.* Hepatic loss of survivin impairs postnatal liver development and promotes expansion of hepatic progenitor cells in mice. *Hepatology* **58,** 2109–21 (2013).

177. Curado, S., Stainier, D. & Anderson., R. Nitroreductase-mediated cell/tissue ablation in zebrafish: a spatially and temporally controlled ablation method with applications in developmental and regeneration studies. *Nat. Protoc.* **3,** 948–954 (2008).

178. Choi, T. Y., Ninov, N., Stainier, D. Y. R. & Shin, D. Extensive conversion of hepatic biliary epithelial cells to hepatocytes after near total loss of hepatocytes in zebrafish. *Gastroenterology* **146,** 776–788 (2014).

179. He, J., Lu, H., Zou, Q. & Luo, L. Regeneration of liver after extreme hepatocyte loss occurs mainly via biliary transdifferentiation in zebrafish. *Gastroenterology* **146,** 789–800.e8 (2014).

180. Choi, T.-Y. *et al.* Bone morphogenetic protein signaling governs biliary-driven liver regeneration in zebrafish through tbx2b and id2a. *Hepatology* **66,** 1616–1630 (2017).

181. Rossi, J. M., Dunn, N. R., Hogan, B. L. M. & Zaret, K. S. Distinct mesodermal signals, including BMPs from the septum, transversum mesenchyme, are required in

combination for hepatogenesis from the endoderm. *Genes Dev.* **15,** 1998–2009 (2001).

182. Bort, R., Signore, M., Tremblay, K., Barbera, J. P. M. & Zaret, K. S. Hex homeobox gene controls the transition of the endoderm to a pseudostratified, cell emergent epithelium for liver bud development. *Dev. Biol.* **290,** 44–56 (2006).

183. Si-Tayeb, K., Lemaigre, F. P. & Duncan, S. a. Organogenesis and Development of the Liver. *Dev. Cell* **18,** 175–189 (2010).

184. Matsumoto, K., Yoshitomi, H., Rossant, J. & Zaret, K. S. Liver Organogenesis Promoted by Endothelial Cells Prior to Vascular Function. *Science* **294,** 559–563 (2001).

185. Zaret, K. S. *From Endoderm to Liver Bud: Paradigms of Cell Type Specification and Tissue Morphogenesis*. *Current Topics in Developmental Biology* **117,** (Elsevier Inc., 2016).

186. Lee, C. S., Friedman, J. R., Fulmer, J. T. & Kaestner, K. H. The initiation of liver development is dependent on Foxa transcription factors. *Nature* **435,** 944–947 (2005).

187. Bossard, P. & Zaret, K. S. GATA transcription factors as potentiators of gut endoderm differentiation. *Development* **125,** 4909–4917 (1998).

188. Zhao, R. *et al.* GATA6 is essential for embryonic development of the liver but dispensable for early heart formation. *Mol. Cell. Biol.* **25,** 2622–31 (2005).

189. Watt, A. J., Zhao, R., Li, J. & Duncan, S. a. Development of the mammalian liver and ventral pancreas is dependent on GATA4. *BMC Dev. Biol.* **7,** 37 (2007).

190. Lokmane, L. *et al.* Crucial role of vHNF1 in vertebrate hepatic specification. *Development* **135,** 2777–86 (2008).

191. Sekiya, T., Muthurajan, U. M., Luger, K., Tulin, A. V. & Zaret, K. S. Nucleosome-binding affinity as a primary determinant of the nuclear mobility of the pioneer transcription factor FoxA. *Genes Dev.* **23,** 804–809 (2009).

192. Gualdi, R. *et al.* Hepatic specification of the gut endoderm in vitro: Cell signaling and transcriptional control. *Genes Dev.* **10,** 1670–1682 (1996).

193. Parviz, F. *et al.* Hepatocyte nuclear factor 4alpha controls the development of a hepatic epithelium and liver morphogenesis. *Nat. Genet.* **34,** 292–296 (2003).

194. Margagliotti, S. *et al.* The Onecut transcription factors HNF-6/OC-1 and OC-2 regulate early liver expansion by controlling hepatoblast migration. *Dev. Biol.* **311,** 579–589 (2007).

195. Lüdtke, T. H. W., Christoffels, V. M., Petry, M. & Kispert, A. Tbx3 promotes liver bud expansion during mouse development by suppression of cholangiocyte differentiation. *Hepatology* **49,** 969–978 (2009).

196. Yamasaki, H. *et al.* Suppression of C/EBPalpha expression in periportal hepatoblasts may stimulate biliary cell differentiation through increased Hnf6 and Hnf1b expression. *Development* **133,** 4233–4243 (2006).

197. Alpern, D. *et al.* TAF4, a subunit of transcription factor II D, directs promoter occupancy of nuclear receptor HNF4A during post-natal hepatocyte differentiation. *Elife* **3,** 1–23 (2014).

198. Kyrmizi, I. *et al.* Plasticity and expanding complexity of the hepatic transcription factor network during liver development. *Genes Dev.* **20,** 2293–2305 (2006).

199. Sosa-Pineda, B., Wigle, J. T. & Oliver, G. Hepatocyte migration during liver development requires Prox1. *Nat. Genet.* **25,** 254–255 (2000).

200. Seth, A. *et al.* Prox1 ablation in hepatic progenitors causes defective hepatocyte specification and increases biliary cell commitment. *Development* **141,** 538–47 (2014).

201. Zong, Y. *et al.* Notch signaling controls liver development by regulating biliary differentiation. *Development* **136,** 1727–1739 (2009).

202. Kodama, Y., Hijikata, M., Kageyama, R., Shimotohno, K. & Chiba, T. The role of

notch signaling in the development of intrahepatic bile ducts. *Gastroenterology* **127,** 1775–1786 (2004).

203. Hofmann, J. J. *et al.* Jagged1 in the portal vein mesenchyme regulates intrahepatic bile duct development: insights into Alagille syndrome. *Development* **137,** 4061–4072 (2010).

204. Clotman, F. *et al.* Control of liver cell fate decision by a gradient of TGF β signaling modulated by Onecut transcription factors. *Genes Dev.* **19,** 1849–1854 (2005).

205. Takayama, K. *et al.* CCAAT/enhancer binding protein-mediated regulation of TGFβ receptor 2 expression determines the hepatoblast fate decision. *Development* **141,** 91–100 (2014).

206. Alder, O. *et al.* Hippo signaling influences HNF4A and FOXA2 enhancer switching during hepatocyte differentiation. *Cell Rep.* **9,** 261–271 (2014).

207. Yimlamai, D. *et al.* Hippo pathway activity influences liver cell fate. *Cell* **157,** 1324–1338 (2014).

208. Poncy, A. *et al.* Transcription factors SOX4 and SOX9 cooperatively control development of bile ducts. *Dev. Biol.* **404,** 136–148 (2015).

209. Antoniou, A. *et al.* Intrahepatic bile ducts develop according to a new mode of tubulogenesis regulated by the transcription factor SOX9. *Gastroenterology* **136,** 2325–33 (2009).

210. Hunter, M. P. *et al.* The homeobox gene Hhex is essential for proper hepatoblast differentiation and bile duct morphogenesis. *Dev. Biol.* **308,** 355–367 (2007).

211. Glaser, S. *et al.* Differential transcriptional characteristics of small and large biliary epithelial cells derived from small and large bile ducts. *Am. J. Physiol. Gastrointest. Liver Physiol.* **299,** G769–G777 (2010).

212. Clotman, F. *et al.* The onecut transcription factor HNF6 is required for normal development of the biliary tract. *Development* **129,** 1819–28 (2002).

213. Lickert, H. *et al.* Formation of multiple hearts in mice following deletion of ??-catenin in the embryonic endoderm. *Dev. Cell* **3,** 171–181 (2002).

214. Li, Y. *et al.* Sfrp5 coordinates foregut specification and morphogenesis by antagonizing both canonical and noncanonical Wnt11 signaling. *Genes Dev.* **22,** 3050–3063 (2008).

215. Ober, E. a, Verkade, H., Field, H. a & Stainier, D. Y. R. Mesodermal Wnt2b signalling positively regulates liver specification. *Nature* **442,** 688–691 (2006).

216. Lu, H., Ma, J., Yang, Y., Shi, W. & Luo, L. EpCAM Is an Endoderm-Specific Wnt Derepressor that Licenses Hepatic Development. *Dev. Cell* **24,** 543–553 (2013).

217. Matsumoto, K., Miki, R., Nakayama, M., Tatsumi, N. & Yokouchi, Y. Wnt9a secreted from the walls of hepatic sinusoids is essential for morphogenesis, proliferation, and glycogen accumulation of chick hepatic epithelium. *Dev. Biol.* **319,** 234–47 (2008).

218. Tan, X. *et al.* B-Catenin Deletion in Hepatoblasts Disrupts Hepatic Morphogenesis and Survival During Mouse Development. *Hepatology* **47,** 1667–1679 (2008).

219. Kiyohashi, K. *et al.* Wnt5a signaling mediates biliary differentiation of fetal hepatic stem/progenitor cells in mice. *Hepatology* **57,** 2502–2513 (2013).

220. Cordi, S. *et al.* Role of β-catenin in development of bile ducts. *Differentiation.* **91,** 42–9 (2016).

221. Suzuki, A., Iwama, A., Miyashita, H., Nakauchi, H. & Taniguchi, H. Role for growth factors and extracellular matrix in controlling differentiation of prospectively isolated hepatic stem cells. *Development* **130,** 2513–2524 (2003).

222. Hay, D. C. *et al.* Highly efficient differentiation of hESCs to functional hepatic endoderm requires ActivinA and Wnt3a signaling. *Proc. Natl. Acad. Sci.* **105,** 12301–6 (2008).

223. Sullivan, G. J. *et al.* Generation of functional human hepatic endoderm from human

induced pluripotent stem cells. *Hepatology* **51,** 329–35 (2010).

224. Touboul, T. *et al.* Generation of functional hepatocytes from human embryonic stem cells under chemically defined conditions that recapitulate liver development. *Hepatology* **51,** 1754–1765 (2010).

225. Cameron, K. *et al.* Recombinant Laminins Drive the Differentiation and Self-Organization of hESC-Derived Hepatocytes. *Stem Cell Reports* **5,** 1–13 (2015).

226. Tanimizu, N. *et al.* Hepatic biliary epithelial cells acquire epithelial integrity but lose plasticity to differentiate into hepatocytes in vitro during development. *J. Cell Sci.* **126,** 5239–46 (2013).

227. Tanimizu, N., Kobayashi, S., Ichinohe, N. & Mitaka, T. Downregulation of miR122 by grainyhead-like 2 restricts the hepatocytic differentiation potential of adult liver progenitor cells. *Development* **141,** 4448–4456 (2014).

228. Van Hul, N. K. M., Abarca-Quinones, J., Sempoux, C., Horsmans, Y. & Leclercq, I. a. Relation between liver progenitor cell expansion and extracellular matrix deposition in a CDE-induced murine model of chronic liver injury. *Hepatology* **49,** 1625–1635 (2009).

229. Zhao, B. *et al.* Inactivation of YAP oncoprotein by the Hippo pathway is involved in cell contact inhibition and tissue growth control. *Genes Dev.* **21,** 2747–2761 (2007).

230. Yimlamai, D. *et al.* Hippo pathway activity influences liver cell fate. *Cell* **157,** 1324–1338 (2014).

231. Bonnans, C., Chou, J. & Werb, Z. Remodelling the extracellular matrix in development and disease. *Nat. Rev. Mol. Cell Biol.* **15,** 786–801 (2014).

232. Hynes, R. O. & Naba, A. Overview of the matrisome-An inventory of extracellular matrix constituents and functions. *Cold Spring Harb. Perspect. Biol.* **4,** 1–16 (2012).

233. Hynes, R. O. The extracellular matrix: not just pretty fibrils. *Science* **326,** 1216–1219 (2009).

234. Ricard-Blum, S. The Collagen Family. *Cold Spring Harb. Perspect. Biol.* **3,** 1–19 (2011).

235. Domogatskaya, A., Rodin, S. & Tryggvason, K. Functional Diversity of Laminins. *Annu. Rev. Cell Dev. Biol.* **28,** 523–553 (2012).

236. O'Brien, L. E. *et al.* Rac1 orientates epithelial apical polarity through effects on basolateral laminin assembly. *Nat. Cell Biol.* **3,** 831–838 (2001).

237. F. M. Watt; T. S. Huck. Role of the extracellular matrix in regulating stem cell fate. *Nat. Rev. Mol. Cell Biol.* **14,** 467–474 (2013).

238. Engler, A. J., Sen, S., Sweeney, H. L. & Discher, D. E. Matrix Elasticity Directs Stem Cell Lineage Specification. *Cell* **126,** 677–689 (2006).

239. Das, R. K., Gocheva, V., Hammink, R., Zouani, O. F. & Rowan, A. E. Stress-stiffening-mediated stem-cell commitment switch in soft responsive hydrogels. *Nat Mater* **15,** 318–325 (2016).

240. Levental, K. R. *et al.* Matrix Crosslinking Forces Tumor Progression by Enhancing Integrin Signaling. *Cell* **139,** 891–906 (2009).

241. Brizzi, M. F., Tarone, G. & Defilippi, P. Extracellular matrix, integrins, and growth factors as tailors of the stem cell niche. *Curr. Opin. Cell Biol.* **24,** 645–651 (2012).

242. Hynes, R. O. Integrins : Bidirectional , Allosteric Signaling Machines. *Cell* **110,** 673–687 (2002).

243. Geiger, B. & Yamada, K. M. Molecular Architecture and Function of Matrix Adhesions. *Cold Spring Harb Perspect. Biol.* **3,** 1–22 (2011).

244. Winograd-Katz, S. E., Fässler, R., Geiger, B. & Legate, K. R. The integrin adhesome: from genes and proteins to human disease. *Nat. Rev. Mol. Cell Biol.* **15,** 273–288 (2014).

245. Fässler, R. & Meyer, M. Consequences of lack of beta 1 gene expression in mice. *Genes Dev.* 1896–1908 (1995).

246. Petridou, N. I. & Skourides, P. A. A ligand-independent integrin β1 mechanosensory complex guides spindle orientation. *Nat. Commun.* **7,** 1–15 (2016).

247. Bombardelli, L. *et al.* Pancreas-Specific Ablation of B1 Integrin Induces Tissue Degeneration by Disrupting Acinar Cell Polarity. *Gastroenterology* **138,** 2531–2540 (2010).

248. Rognoni, E. *et al.* Kindlin-1 controls Wnt and TGF-β availability to regulate cutaneous stem cell proliferation. *Nat. Med.* **20,** 350–359 (2014).

249. Taddei, I. *et al.* Beta1 integrin deletion from the basal compartment of the mammary epithelium affects stem cells. *Nat. Cell Biol.* **10,** 716–722 (2008).

250. Kren, A. *et al.* Increased tumor cell dissemination and cellular senescence in the absence of beta1-integrin function. *EMBO J.* **26,** 2832–2842 (2007).

251. Hoshino, A. *et al.* Tumour exosome integrins determine organotropic metastasis. *Nature* **527,** 329–335 (2015).

252. Moro, L. *et al.* Integrin-induced Epidermal Growth Factor (EGF) Receptor Activation Requires c-Src and p130Cas and Leads to Phosphorylation of Specific EGF Receptor Tyrosines. *J. Biol. Chem.* **277,** 9405–9414 (2001).

253. Cordes, N., Seidler, J., Durzok, R., Geinitz, H. & Brakebusch, C. B1-Integrin-Mediated Signaling Essentially Contributes To Cell Survival After Radiation-Induced Genotoxic Injury. *Oncogene* **25,** 1378–1390 (2006).

254. Raghavan, S., Bauer, C., Mundschau, G., Li, Q. & Fuchs, E. Conditional ablation of β1 integrin in skin: Severe defects in epidermal proliferation, basement membrane formation, and hair follicle invagination. *J. Cell Biol.* **150,** 1149–1160 (2000).

255. Popov, C. *et al.* Integrins α2β1 and α11β1 regulate the survival of mesenchymal stem cells on collagen I. *Cell Death Dis.* **2,** e186 (2011).

256. Riopel, M. *et al.* Conditional beta1-integrin-deficient mice display impaired pancreatic beta cell function. *J Pathol* **224,** 45–55 (2011).

257. Rozo, M., Li, L. & Fan, C. Targeting β 1-integrin signaling enhances regeneration in aged and dystrophic muscle in mice. *Nat. Med.* **22,** 889–896 (2016).

258. Renner, G. *et al.* Integrin α5β1 and p53 convergent pathways in the control of anti-apoptotic proteins PEA-15 and survivin in high-grade glioma. *Cell Death Differ.* **4,** 640–653 (2015).

259. Shiojiri, N. & Sugiyama, Y. Immunolocalization of extracellular matrix components and integrins during mouse liver development. *Hepatology* **40,** 346–355 (2004).

260. Vestentoft, P. S. *et al.* Molecular constituents of the extracellular matrix in rat liver mounting a hepatic progenitor cell response for tissue repair. *Fibrogenesis Tissue Repair* **6,** 21 (2013).

261. Tanimizu, N., Kikkawa, Y., Mitaka, T. & Miyajima, A. A1- and A5-Containing Laminins Regulate the Development of Bile Ducts Via B1 Integrin Signals. *J. Biol. Chem.* **287,** 28586–28597 (2012).

262. Kikkawa, Y., Mochizuki, Y., Miner, J. H. & Mitaka, T. Transient expression of laminin α1 chain in regenerating murine liver: Restricted localization of laminin chains and nidogen-1. *Exp. Cell Res.* **305,** 99–109 (2005).

263. Speicher, T. *et al.* Knockdown and knockout of β1-integrin in hepatocytes impairs liver regeneration through inhibition of growth factor signalling. *Nat. Commun.* **5,** 3862 (2014).

264. Le Bail, B. *et al.* Extracellular matrix composition and integrin expression in early hepatocarcinogenesis in human cirrhotic liver. *J. Pathol.* **181,** 330–337 (1997).

265. Peng, Z. W. *et al.* Integrin avB6 critically regulates hepatic progenitor cell function and promotes ductular reaction, fibrosis, and tumorigenesis. *Hepatology* **63,** 217–232 (2016).

266. Bogorad, R. L. *et al.* Nanoparticle-formulated siRNA targeting integrins inhibits hepatocellular carcinoma progression in mice. *Nat. Commun.* **5,** 3869 (2014).

267. Issa, R. *et al.* Spontaneous recovery from micronodular cirrhosis: Evidence for incomplete resolution associated with matrix cross-linking. *Gastroenterology* **126,** 1795–1808 (2004).

268. Perepelyuk, M. *et al.* Hepatic stellate cells and portal fibroblasts are the major cellular sources of collagens and lysyl oxidases in normal liver and early after injury. *Am. J. Physiol. Gastrointest. Liver Physiol.* **304,** G605-14 (2013).

269. Klaas, M. *et al.* The alterations in the extracellular matrix composition guide the repair of damaged liver tissue. *Sci. Rep.* **6,** 27398 (2016).

270. Singh, S. *et al.* Liver stiffness is associated with risk of decompensation, liver cancer, and death in patients with chronic liver diseases: A systematic review and meta-analysis. *Clin. Gastroenterol. Hepatol.* **11,** 1573–1584 (2013).

271. Nejjari, M. *et al.* Integrin up-regulation in chronic liver disease: relationship with inflammation and fibrosis in chronic hepatitis C. *J. Pathol.* **195,** 473–481 (2001).

272. Volpes, R., van den Oord, J. J. & Desmet, V. J. Distribution of the VLA family of integrins in normal and pathological human liver tissue. *Gastroenterology* **101,** 200–206 (1991).

273. Quondamatteo, F., Kempkensteffen, C., Miosge, N., Sonnenberg, A. & Herken, R. Ultrastructural localization of integrin subunits a3 and a6 in capillarized sinusoids of the human cirrhotic liver. *Histol. Histopathol.* **19,** 799–806 (2004).

274. Henderson, N. C. *et al.* Targeting of αv integrin identifies a core molecular pathway that regulates fibrosis in several organs. *Nat. Med.* **19,** 1617–24 (2013).

275. Schrader, J. *et al.* Matrix Stiffness Modulates Proliferation, Chemotherapeutic Response and Dormancy in Hepatocellular Carcinoma Cells. *Hepatology* **53,** 1192–1205 (2012).

276. Shiraki, N. *et al.* Efficient differentiation of embryonic stem cells into hepatic cells in vitro using a feeder-free basement membrane substratum. *PLoS One* **6,** 1–10 (2011).

277. Zhang, H. *et al.* Beta 1-integrin protects hepatoma cells from chemotherapy induced apoptosis via a mitogen-activated protein kinase dependent pathway. *Cancer* **95,** 896–906 (2002).

278. Lázaro-Diéguez, F. *et al.* Par 1b links lumen polarity with LGN-NuMA positioning for distinct epithelial cell division phenotypes. *J. Cell Biol.* **203,** 251–264 (2013).

279. Fickert, P. *et al.* Bile acid-induced Mallory body formation in drug-primed mouse liver. *Am. J. Pathol.* **161,** 2019–26 (2002).

280. Fickert, P. *et al.* A New Xenobiotic-Induced Mouse Model of Sclerosing Cholangitis and Biliary Fibrosis. *Am. J. Pathol.* **171,** 525–536 (2007).

281. Liu, Y. *et al.* Animal models of chronic liver diseases. *Am. J. Physiol. Gastrointest. Liver Physiol.* **304,** G449-68 (2013).

282. Guest, R. V. *et al.* Cell lineage tracing reveals a biliary origin of intrahepatic cholangiocarcinoma. *Cancer Res.* **74,** 1005–1010 (2014).

283. Akhurst, B. *et al.* A modified choline-deficient, ethionine-supplemented diet protocol effectively induces oval cells in mouse liver. *Hepatology* **34,** 519–522 (2001).

284. Raven, A. *et al.* Cholangiocytes act as facultative liver stem cells during impaired hepatocyte regeneration. *Nature* **547,** 350–354 (2017).

285. Preibisch, S., Saalfeld, S. & Tomancak, P. Globally optimal stitching of tiled 3D microscopic image acquisitions. *Bioinformatics* **25,** 1463–1465 (2009).

286. Kreamer, B. L. *et al.* Use of a low-speed, iso-density percoll centrifugation method to increase the viability of isolated rat hepatocyte preparations. *Vitr. Cell. Dev. Biol.* **22,** 201–211 (1986).

287. Robinson, M. D. & Oshlack, A. A scaling normalization method for differential expression analysis of RNA-seq data. *Genome Biol* **11,** R25 (2010).

288. Robinson, M. D., McCarthy, D. J. & Smyth, G. K. edgeR: A Bioconductor package for differential expression analysis of digital gene expression data. *Bioinformatics* **26,**

139–140 (2009).

289. Ritchie, M. E. *et al.* Limma powers differential expression analyses for RNA-sequencing and microarray studies. *Nucleic Acids Res.* **43,** e47 (2015).

290. Liberzon, A. *et al.* The Molecular Signatures Database Hallmark Gene Set Collection. *Cell Syst.* **1,** 417–425 (2015).

291. Liberzon, A. *et al.* Molecular signatures database (MSigDB) 3.0. *Bioinformatics* **27,** 1739–1740 (2011).

292. Bult, C. J. *et al.* The Mouse Genome Database (MGD): integrating biology with the genome. *Nucleic Acids Res.* **32,** D476-81 (2004).

293. Wu, D. *et al.* ROAST: Rotation gene set tests for complex microarray experiments. *Bioinformatics* **26,** 2176–2182 (2010).

294. Mazzaccara, C. *et al.* Age-related reference intervals of the main biochemical and hematological parameters in C57BL/6J, 129SV/EV and C3H/HeJ mouse strains. *PLoS One* **3,** 4–10 (2008).

295. Zhou, X. & Hansson, G. K. Effect of Sex and Age on Serum Biochemical Reference Ranges in C57BL / 6J Mice. **54,** 176–178 (2004).

296. Giannini, E. G., Testa, R. & Savarino, V. Liver enzyme alteration: A guide for clinicians. *Cmaj* **172,** 367–379 (2005).

297. Huebener, P. *et al.* The HMGB1/RAGE axis triggers neutrophil-mediated injury amplification following necrosis. *J. Clin. Invest.* **125,** 539–550 (2015).

298. Scaffidi, P., Misteli, T. & Bianchi, M. E. Release of chromatin protein HMGB1 by necrotic cells triggers inflammation. *Nature* **418,** 191–195 (2002).

299. Wang, X. *et al.* The origin and liver repopulating capacity of murine oval cells. *Proc. Natl. Acad. Sci.* **100,** 11881–11888 (2003).

300. Spee, B. *et al.* Characterisation of the liver progenitor cell niche in liver diseases: potential involvement of Wnt and Notch signalling. *Gut* **59,** 247–257 (2010).

301. Boulter, L. *et al.* WNT signaling drives cholangiocarcinoma growth and can be pharmacologically inhibited. *J. Clin. Invest.* **125,** 1269–1285 (2015).

302. Hu, M. *et al.* WntB-Catenin Signaling in Murine Hepatic Transit Amplifying Progenitor Cells. *Gastroenterology* **133,** 1579–1591 (2007).

303. Niehrs, C. The complex world of WNT receptor signalling. *Nat. Rev. Mol. Cell Biol.* **13,** 767–79 (2012).

304. Schlessinger, K. *et al.* Wnt signaling pathways meet Rho GTPases. *Genes Dev.* **23,** 265–277 (2009).

305. Yang, J. *et al.* Beta-catenin signaling in murine liver zonation and regeneration: A Wnt-Wnt situation! *Hepatology* **60,** 964–976 (2014).

306. Lunz, J. G., Tsuji, H., Nozaki, I., Murase, N. & Demetris, A. J. An inhibitor of cyclin-dependent kinase, stress-induced p21 Waf-1/Cip-1, mediates hepatocyte mito-inhibition during the evolution of cirrhosis. *Hepatology* **41,** 1262–1271 (2005).

307. Ritschka, B. *et al.* The senescence-associated secretory phenotype induces cellular plasticity and tissue regeneration. *Genes Dev.* **31,** 1–12 (2017).

308. Mosteiro, L. *et al.* Tissue damage and senescence provide critical signals for cellular reprogramming in vivo. *Science* **354,** aaf4445 (2016).

309. Chiche, A. *et al.* Injury-Induced Senescence Enables In Vivo Reprogramming in Skeletal Muscle. *Cell Stem Cell* **20,** 407–414.e4 (2016).

310. Soufi, A., Donahue, G. & Zaret, K. S. Facilitators and impediments of the pluripotency reprogramming factors' initial engagement with the genome. *Cell* **151,** 994–1004 (2012).

311. Soufi, A. *et al.* Pioneer transcription factors target partial DNA motifs on nucleosomes to initiate reprogramming. *Cell* **161,** 555–568 (2015).

312. Naugler, W. E. *et al.* Fibroblast Growth Factor Signaling Controls Liver Size in Mice With Humanized Livers. *Gastroenterology* **149,** 728–740 (2015).

313. Bassler, B. L. Small talk: Cell-to-cell communication in bacteria. *Cell* **109,** 421–424 (2002).

314. Chen, C. C. *et al.* Organ-level quorum sensing directs regeneration in hair stem cell populations. *Cell* **161,** 277–290 (2015).

315. Anakk, S. *et al.* Bile Acids Activate YAP to Promote Liver Carcinogenesis. *Cell Rep.* **5,** 1060–1069 (2013).

316. Adam, R. C. *et al.* Pioneer factors govern super-enhancer dynamics in stem cell plasticity and lineage choice. *Nature* **521,** 366–370 (2015).

317. Larsimont, J.-C. *et al.* Sox9 Controls Self-Renewal of Oncogene Targeted Cells and Links Tumor Initiation and Invasion. *Cell Stem Cell* **17,** 60–73 (2015).

318. Hnisz, D. *et al.* Super-enhancers in the control of cell identity and disease. *Cell* **155,** 934–47 (2013).

319. Whyte, W. a. *et al.* Master transcription factors and mediator establish super-enhancers at key cell identity genes. *Cell* **153,** 307–319 (2013).

320. Li, B. *et al.* Adult Mouse Liver Contains Two Distinct Populations of Cholangiocytes. *Stem Cell Reports* **9,** 478–489 (2017).

321. Kaneko, K., Kamimoto, K., Miyajima, A. & Itoh, T. Adaptive remodeling of the biliary architecture underlies liver homeostasis. *Hepatology* **61,** 2056–2066 (2015).

322. Kamimoto, K. *et al.* Heterogeneity and stochastic growth regulation of biliary epithelial cells dictate dynamic epithelial tissue remodeling. *Elife* **5,** 1–26 (2016).

323. Hattoum, A., Rubin, E., Orr, A. & Michalopoulos, G. K. Expression of hepatocyte epidermal growth factor receptor, FAS and glypican 3 in EpCAM-positive regenerative clusters of hepatocytes, cholangiocytes, and progenitor cells in human liver failure. *Hum. Pathol.* **44,** 743–749 (2013).

324. Tummala, K. S. *et al.* Hepatocellular Carcinomas Originate Predominantly from Hepatocytes and Benign Lesions from Hepatic Progenitor Cells. *Cell Rep.* **19,** 584–

600 (2017).